Characterization and synthesis of drug carriers based on artificial exosomes dedicated to treatment of the microangiopathic complications of diabetes

Doctoral thesis

Anna Drożdż

Faculty of Physics, Astronomy and Applied Computer Science

Jagiellonian University

supervised by:

prof. Ewa Stępień

Kraków, 2021

Wydział Fizyki, Astronomii i Informatyki Stosowanej

Uniwersytet Jagielloński

Oświadczenie

Ja, niżej podpisana, Anna Drożdż (nr indeksu: 1040786), doktorantka Wydziału Fizyki, Astronomii i Informatyki Stosowanej Uniwersytetu Jagiellońskiego, oświadczam, że przedłożona przeze mnie rozprawa doktorska pt. „*Characterization and synthesis of drug carriers based on artificial exosomes dedicated to treatment of the microangiopathic complications of diabetes*" jest oryginalna i przedstawia wyniki badań wykonanych przeze mnie osobiście, pod kierunkiem prof. Ewy Stępień. Pracę napisałem samodzielnie.

Oświadczam, że moja rozprawa doktorska została opracowana zgodnie z Ustawą o prawie autorskim i prawach pokrewnych z dnia 4 lutego 1994 r. (Dziennik Ustaw 1994 nr 24 poz. 83 wraz z późniejszymi zmianami).

Jestem świadom, że niezgodność niniejszego oświadczenia z prawdą ujawniona w dowolnym czasie, niezależnie od skutków prawnych wynikających z ww. ustawy, może spowodować unieważnienie stopnia nabytego na podstawie tej rozprawy.

…… ……

Kraków, dnia podpis doktoranta

Acknowledgements

When I started my PhD studies I didn't realize how bumpy and difficult the path to the summit would be. It is often said that you should not go hiking alone and that there are some summits, which especially do not like solo climbers. I think that preparing a PhD thesis is definitely one of them. Here, I would like to acknowledge all people who accompanied me on this climb and helped me to succeed.

Firstly, I would like to thank my supervisor prof. Ewa Stępień for introducing me to the field of extracellular vesicles, giving me the opportunity to work in her research group and to conduct independent, interdisciplinary research, as well as her valuable help in the experimental work. Secondly, I would like to thank other Members of the Medical Physics Department at the Institute of Physics, especially dr Katarzyna Dziedzic-Kocurek, dr Andrzej Wróbel, dr Agnieszka Kamińska, dr Martyna Durak-Kozica and dr Ewelina Kubicz for all lively discussions, valuable hints and being some of the most important people during my everyday life at the Faculty. Finally, I would like to thank my fellow PhD students - Monika Szczepanek, Tomasz Kołodziej, Carina Rząca and Dominik Panek for paving the way for science with me, consolation after failed experiments and shared joy from the successful ones.

My scientific path led me not only to the Faculty of Physics, but also to other outstanding science institutes and to the people working there. I would like to thank all my colleagues form the Małopolska Center of Biotechnology, especially dr Tomasz Gromowski, dr Anna Biela, dr Marcin Jaciuk for their support and help in my experiments and for explaining even the most basic things to me. I would like to express my special thanks to dr Michał Bochenek, for the numerous fascinating talks, not only about flow cytometry, but also politics, literature and traveling.

I would like to thank the Members of the Institute of Zoology – prof. Małgorzata Przybyło and dr Magdalena Surman for their trust, the opportunity to get engaged in their projects, and invaluable help in my own research.

During my PhD studies I had a great pleasure to do a research internship in Slovenia, as well as in the Netherlands. I would like to thank my friends from the Joseph Stephan Institute in Ljubljana – Ana and Aleksandr – for their support in my research at the Institute and for becoming more than just colleagues. Thanks to you, during my stay in Slovenia in the middle of the COVID-19 pandemic, I didn't feel lonely even for a minute. I would also like to express my gratitude to Janez Štrancar and Rienk Nieuwland for inviting me to their laboratories and helping me greatly during my stay.

I want to thank my mountain family – AKT Rozdroże and Dinozaury for the wonderful hiking trips that we continue despite graduation, moving to other parts of Poland and the emergence of new responsibilities – as well as Piwko, for always being ready for new adventures.

I also have to mention Gosia Siwek who was my first laboratory partner. Thank you for being a wonderful friend, who is never afraid to share an honest opinion with me and with whom I can share all the joys and sorrows of life.

I would like to thank my parents – Alicja and Andrzej for showing me how beautiful and interesting the world around us is and for never saying “no” even to my craziest ideas. I would like to thank my brother – Jędrek for being a great companion in some of them.

Finally, I would like to thank my beloved husband – Piotr for his unconditional support, permanent optimism, and faith in me greater than my own. Without you this thesis would never have been started or finished. I know that together we will always reach the top, even when it sometimes seems impossible.

Fundings

This work was supported by the National Science Centre (NCN) the grant Preludium 13 (2017/25/N/ST5/00831) to Anna Drożdż, the grant OPUS 4 to prof. Ewa Stępień (2012/07B/NZ5/02510), the OPUS 17 to prof. Ewa Stępień (2019/33/B/NZ3/01004) and the Ministry of Science and Higher Education (7150/E-338/M/2017, 7150/E-338/M/2018, 2019-N17/MNS/000015).

Abstract

This thesis focuses on the development of a new drug delivery system for the treatment of microvascular complications of diabetes, based on artificial exosmoses. Exosomes, which are one of the types of extracellular vesicles, are small (30 - 100 nm), lipid structures secreted by cells into the extracellular matrix, transporting enclosed fragments of DNA, RNA and proteins. Their circulation in body fluids is responsible for a long-distance cell-to-cell communication, which creates an opportunity to use them as a new drug carrier type. Unfortunately, the process of encapsulating therapeutic molecules inside them is extremely difficult, and the methods used so far are characterized by low efficiency.

The main goal of the project, which is the basis of this thesis, was to design a protocol for the synthesis of artificial exosomes, *via* the fusion of extracellular vesicles and liposomes. The FRET (Förster Resonance Energy Transfer) technique was used to monitor this process. Artificial exosomes were characterized in terms of their: morphology (Cryogenic Electron Microscopy - CryoEM), zeta potential (Dynamic Light Scattering - DLS), size and concentration (Nanoparticle Tracking Analysis - NTA), and the presence of typical vesicles' markers (western blot). In addition, encapsulation efficiency was determined and a protocol for decorating artificial exosomes with Del-1 protein, responsible for the internalization of natural exosomes by endothelial cells, was developed. The internalization process was observed using confocal microscopy.

A series of functional tests, performed on the endothelial model of diabetes, confirmed that anti-miR-221-3p encapsulated in the synthesized artificial exosomes can block the activity of miR-221-3p, the overexpression of which correlates with the development of endothelial cell dysfunction (ECD) during the diabetes. Stimulation with artificial exosomes increases the expression of TIMP-3 mRNA (Tissue Inhibitor of Metalloproteinases 3) and decreases the activity of metalloproteinases controlled by TIMP-3 (MMP-2 and MMP-9). Changes induced by artificial exosomes favorably affect the migration of endothelial cells and wound healing processes.

This thesis describes a new drug delivery system for the treatment of endothelial cells dysfunction, which has a beneficial effect on their migration processes. It has been confirmed that fusion between EVs and liposomes can occur, and the most efficient fusion protocol has been established. Additionally, physical, and biological properties aEx have been analyzed. In the functional tests, the values of key cell parameters after stimulation with miR-221-3p-containing artificial exosomes were similar to the ones obtained for physiological controls, there was no positive effect of Del-1 on tested parameters. Obtained results confirmed that this system can be used in the treatment of microvascular complications of diabetes.

Streszczenie

Niniejsza praca poświęcona jest opracowaniu nowego systemu dostarczania leków do leczenia mikronaczyniowych powikłań cukrzycy opartego na sztucznych egzosmozach. Egzosomy, jeden z rodzajów mikropęcherzyków zewnątrzkomórkowych, to niewielkie (30 – 100 nm), lipidowe struktury wydzielane przez komórki do przestrzeni międzykomórkowej, transportujące wewnętrzu fragmenty DNA, RNA i białek. Ich przemieszczanie się w płynach ustrojowych odpowiada za długodystansową komunikację międzykomórkową, co czyni je idealnymi kandydatami na nowe nośniki leków. Niestety, proces zamykania w ich wnętrzu molekuł terapeutycznych jest wyjątkowo trudny, a dotychczas stosowane metody charakteryzują się niską wydajnością.

Głównym celem niniejszej pracy było opracowanie protokołu syntezy sztucznych egzosomów, poprzez fuzję mikropęcherzyków zewnątrzkomórkowych i liposomów. Do monitorowania procesu fuzji wykorzystano metodę FRET (rezonansowy transfer energii Förster'a). Sztuczne egzosomy scharakteryzowano poprzez zbadanie: morfologii (kriogeniczna mikroskopia elektronowa), potencjału zeta (dynamiczne rozpraszanie światła), wielkości oraz koncentracji (śledzenie trajektorii ruchu nanocząstek), a także obecności typowych markerów pęcherzykowych (western blot). Ponadto określono wydajność enkapsulacji oraz opracowano protokół powlekania sztucznych egzosomów białkiem, które odpowiada za internalizację naturalnych mikropęcherzyków przez komórki śródbłonka. Proces internalizacji obserwowano z wykorzystaniem mikroskopii konfokalnej.

Szereg testów funkcjonalnych przeprowadzonych na śródbłonkowym modelu cukrzycy potwierdził, że anty-miR-221-3p zamknięte w sztucznych egzosomach może blokować aktywność miR-221-3p, którego nadekspresja koreluje z rozwojem dysfunkcji śródbłonka w przebiegu cukrzycy. Stymulacja sztucznymi egzosomami powoduje wzrost ekspresji mRNA dla TIMP-3 (tkankowego inhibitora metaloproteinaz 3), a także obniża aktywność metaloproteinaz (MMP-2 i MMP-9) będących pod jego kontrolą. Zmiany indukowane przez stymulację sztucznymi egzosomami korzystnie wpływają na migrację komórek śródbłonka i proces gojenia się ran.

W niniejszej rozprawie opisano nowy, działający system dostarczania leków do komórek śródbłonka, który wywiera korzystny wpływa na ich migrację. Potwierdzono, że fuzja pomiędzy mikropęcherzykami a liposomami może zachodzić oraz stworzono efektywny protokół do procesu prowadzenia fuzji. Ponadto sztuczne egzosomy zostały scharakteryzowane pod kątem właściwości fizycznych i biologicznych. W testach funkcjonalnych wartości badanych parametrów były zbliżone do wyników uzyskanych dla fizjologicznych kontroli. Badania wykazały, że powlekanie sztucznych egzosomów białkiem Del-1 nie wpływa na poprawę analizowanych parametrów. Uzyskane wyniki potwierdzają, że stworzony system może znaleźć zastosowanie w leczeniu mikronaczyniowych powikłań cukrzycy.

List of Author's full-papers

1. **Drożdż A**, Kamińska A, Surman M, Gonet-Surówka A, Jach R, Huras H, et al. Low-vacuum filtration as an alternative extracellular vesicle concentration method: A comparison with ultracentrifugation and differential centrifugation. Pharmaceutics. 2020;12(9):1–17.

   Points of the Ministry of Education and Science (2020): 100 pts
   Impact factor (2020): 6.07

2. Surman M, Kędracka-Krok S, Hoja-Łukowicz D, Jankowska U, **Drożdż A**, Stępień EŁ, et al. Mass Spectrometry-Based Proteomic Characterization of Cutaneous Melanoma Ectosomes Reveals the Presence of Cancer-Related Molecules. Int J Mol Sci. 2020;21(8):2934.

   Points of the Ministry of Education and Science: 140 pts
   Impact factor (2020) : 5.556

3. Hohendorff J, **Drożdż A**, Borys S, Ludwig-Slomczynska AH, Kiec-Wilk B, Stepien EL, et al. Effects of Negative Pressure Wound Therapy on Levels of Angiopoetin-2 and Other Selected Circulating Signaling Molecules in Patients with Diabetic Foot Ulcer. J Diabetes Res. 2019; 2019:1–7.

   Points of the Ministry of Education and Science (2019): 70 pts
   Impact factor (2019) : 2.965

4. Surman M, Hoja-Łukowicz D, Szwed S, Kędracka-Krok S, Jankowska U, Kurtyka M, **Drożdż A**, et al. An Insight into the Proteome of Uveal Melanoma-Derived Ectosomes Reveals the Presence of Potentially Useful Biomarkers. Int J Mol Sci. 2019;20(15).

   Points of the Ministry of Education and Science (2019): 140 pts
   Impact factor (2019) : 4.602

5. Surman M*, **Drożdż A***, Stępień E, Przybyło M. Extracellular Vesicles as Drug Delivery Systems - Methods of Production and Potential Therapeutic Applications. Curr Pharm Des. 2019;25(2):132–54. *equally contributed

   Points of the Ministry of Education and Science (2019): 70 pts
   Impact factor (2019): 2.208

6. Chyrchel B, **Drożdż A**, Długosz D, Stępień E, Surdacki A. Platelet reactivity and circulating platelet-derived microvesicles are differently affected by P2Y 12 receptor antagonists. Int J Med Sci. 2019;16(2):264–75.

   Points of the Ministry of Education and Science (2019): 70 pts
   Impact factor (2019) : 2.523

7. Roman M, Kamińska A, **Drożdż A**, Platt M, Kuźniewski M, Małecki MT, et al. Raman spectral signatures of urinary extracellular vesicles from diabetic patients and hyperglycemic endothelial cells as potential biomarkers in diabetes. Nanomedicine Nanotechnology, Biol Med. 2019;17:137–49.

   Points of the Ministry of Education and Science (2019): 140 pts
   Impact factor (2019) : 5.182

8. Surman M, Hoja-Łukowicz D, Szwed S, **Drożdż A**, Stępień E, Przybyło M. Human melanoma-derived ectosomes are enriched with specific glycan epitopes. Life Sci. 2018;207(March):395–411.

   Points of the Ministry of Education and Science (2018): 25 pts
   Impact factor (2018): 3.448

9. Stępień E, Costa MC, Kurc S, **Drożdż A**, Cortez-Dias N, Enguita FJ. The circulating non-coding RNA landscape for biomarker research: Lessons and prospects from cardiovascular diseases review-article. Acta Pharmacol Sin. 2018;39(7):1085–99.

   Points of the Ministry of Education and Science (2018): 30 pts
   Impact factor (2018): 3.912

10. **Drożdż A**, Stępień E. Circulating Microvesicles in Regenerative Angiogenesis. Curr Trends Biomed Eng Biosci. 2017;3(1):12–4.

    Points of the Ministry of Education and Science (2017): 0 pts
    Impact factor (2017): 0

11. Posadowska U, Brzychczy-Włoch M, **Drożdż A**, Krok-Borkowicz M, Włodarczyk-Biegun M, Dobrzyński P, et al. Injectable hybrid delivery system composed of gellan gum, nanoparticles and gentamicin for the localized treatment of bone infections. Expert Opin Drug Deliv. 2016;13(5).

    Points of the Ministry of Education and Science (2016): 45 pts
    Impact factor (2016): 5.729

List of conference presentations:

1. International Society for Extracellular Vesicles - ISEV Virtual Meeting 2020 (20-22 July 2020)
   Poster presentation: *Hybrid extracellular vesicles - biomimetic tool for drug delivery to repair endothelial cell dysfunction*

2. Sympozjum Sekcji Kardiologii Eksperymentalnej Polskiego Towarzystwa Kardiologicznego, Tomaszowice, Poland (28-30 listopad 2019)
   Poster presentation: *Optimization and characterization of low vacuum filtration procedure — novel method for the isolation of endothelial extracellular vesicles*

3. Nanotech Poland 2018, Poznań, Poland (5 – 8 June 2019)
   Oral presentation : *Influence of the composition of liposomes on their stability and interactions with plasma proteins*

4. International Society for Extracellular Vesicles - ISEV Annual Meeting 2019, Kyoto, Japan
   (24 – 28 April 2019)
   Poster presentation: *Optimization and characterization of low vacuum filtration procedure - novel method for the isolation of extracellular vesicles*

5. Nanotech Poland 2018, Poznań, Poland (6 – 9 June 2018)
   Poster presentation: *Validation and characterization of a new method for the isolation of extracellular vesicles*

6. International Society for Extracellular Vesicles - ISEV Annual Meeting 2018, Barcelona, Spain (2-6 May 2018)
   Poster presentation: *Microvesicles induced in hyperglycemic conditions regulate endothelial cell stiffness and cell shape fluctuations*

7. Eurobiotech 2017, 6th Central European Congress of Life Sciences, Krakow, Poland (11-14 September 2017)
   Poster presentation: *Microvesicles stimulates endothelial cell migration in hyperglycemic conditions*

8. International Society for Extracellular Vesicles - ISEV Annual Meeting 2017 Toronto, Canada (18-21 May 2017)
   Poster presentation: *Hyperglycemia induced microvesicles control endothelial cell migration*

Contents

List of Abbreviations

aEx – artificial exosomes

AGEs – advanced glycation end-products

AGO2 – argonaut 2 protein

AKT – actin protein

APS – Ammonium persulfate

ARF6 – ADP-ribosylation factor 6

Arg – arginine

ASO – antisense oligonucleotides

BSA – bovine serum albumin

cDNA – complementary DNA

CE – cholesteryl ester

Cer – ceramide

CHMP4 – charged multivesicular body protein 4

CHOL – cholesterol,

CI – confluence index

CL – cationic liposomes

Cox – cyclooxygenase

DAG – diacylglycerol

DDS – drug delivery systems

Del-1 – developmental endothelial locus-1

Dll-4 – Delta-like 4 protein

DLS – dynamic light scattering

DOPS – 1,2-dioleoyl-sn-glycero-3-phospho-L-serine

DOTAP – 1,2-dioleoyl-3-trimethylammonium-propane

EC – endothelial cells

ECD – endothelial cell dysfunction

ECM – extracellular matrix

EDTA – ethylenediaminetetraacetic acid

EGF-like – epidermal growth factor–like

ERK – extracellular signal regulated kinases

ESCRT – endosomal sorting complex required for transport

EVs – extracellular vesicles

FAM – carboxyfluorescein

FBS – fetal bovine serum

FDA – Food and Drug Administration

FRET – Förster resonance energy transfer

GAD65 – Glutamic Acid Decarboxylase

Gb3 – globotriaosylceramide

GLUT4 – glucose transporter type 4

hBMSCs – human bone marrow-derived mesenchymal stem cells

HEK293 – human embryonic kidney cells

HexCer – hexosylceramide

HG – hyperglycemia

HIV – human immunodeficiency virus

HMEC-1 – human mammary epithelial cells

HRP – horse radish peroxidase

HUVEC – human umbilical vein endothelial cells

IA-2 – islet antigen 2

IL-6 – interleukin 6

ILV – intraluminal vesicles

IR – infrared

IRec – insulin receptor

LacCer – lactosylceramide

LBPA – lysobisphosphatidic acid

LDL – low density lipoproteins

LDV – laser Doppler velocimetry

lncRNA – long non-coding RNA

LVF – low vacuum filtration method

MAPK – mitogen-activated protein kinase

MCP-1 – monocyte chemoattractant protein 1

miRISC – miRNA-induced silencing complex

miRNA – micro RNA

MLCK – myosin light-chain kinase

MMP – matrix metalloproteinase

MP – micro particles

MPS – mononuclear phagocyte system

MSD – mean square displacement

mTHPC – 5,10,15,20-Tetrakis(3-hydroxyphenyl)chlorin

MVBs – multivesicular bodies

NA – numerical aperture

NADPH – nicotinamide adenine dinucleotide phosphate

NBD – 7-nitro-2-1,3-benzoxadiazol-4-yl

NG – normoglycemia

NO – nitroxide

nSMase – neutral sphingomyelinase

NTA – nanoparticle tracking analysis

PA – phosphatidic acid

PBS – phosphate-buffered saline

PC – phosphatidylcholine

pDNA – plasmide DNA

PE – phosphatidylethanolamine

PEG – polyethylene glycol

PG – phosphatidylglycerol

PI – phosphatidylinositol

piRNA – pico RNA

PS – phosphatidylserine

PS – phosphatidylserine

PVD – polyvinylidene difluoride

qPCR – quantitative Polymerase Chain Reaction

RBP-4 – retinol binding protein 4

RES – reticuloendothelial system

RISC – RNA-associated silencing complex

RLU – relative luminescence units

ROCK I – Rho-associated coiled coil kinase I

ROCK II – Rho-associated coiled coil kinase II

RPLP0 – ribosomal protein lateral stalk subunit P0

SDS-PAGE – sodium dodecyl sulphate–polyacrylamide gel electrophoresis

SEC – size exclusion chromatography

SFM medium – Human Endothelium Serum-Free Medium

siRNA – small interfering RNA

SM – sphingomyelin

SNARE – soluble N-ethylmaleimide-sensitive receptors complex

STAT5 – signal transducer and activator of transcription 5

TBS – Tris-Buffered Saline

TEMED – N,N,N',N'-Tetramethylethylenediamine

TFRC – transferrin receptor 1

TIMP – tissue inhibitor of matrix metalloproteinases

TLR4 – toll-like receptor 4

TNFα – tumor necrosis factor α

TR – transferrin receptor 1

TSG101 – tumor susceptibility gene 101 protein

UV – ultraviolet

VSMCs – vascular smooth muscle cells

YBX1 – Y-box-binding protein 1

1. Theoretical background

In 1971 two independent research teams have, for the first time, described extracellular vesicles (EVs). Their findings have been published in two journals: BBA Biomembranes and British Journal of Hematology. Since then, the number of studies focusing on EVs, microvesicles, ectosomes and exosomes has grown exponentially. EVs has been identified in all body fluids, in very different living organisms. Their engagement in various cellular processes and their role in the pathogenesis of diseases is still broadly investigated and debated. Their undoubtful contribution in coagulation processes was investigated in many studies devoted to cardiovascular biomarkers [1]. However, one of the most interesting features of EVs is their role in cell-to-cell communication. This opens up a possibility of using them, in order to deliver carefully chosen cargo to the dedicated cells, meaning that they could form a new drug delivery system. Unfortunately, despite significant effort of many research teams, this goal remains very hard to achieve.

This thesis is devoted to the development of drug delivery system inspired by natural EVs. The system is based on the fusion particles – artificial exosomes – which are the hybrids of EVs and artificially created liposomes, containing encapsulated cargo. In the thesis the protocol of the synthesis of artificial exosomes is presented. They are then characterized, and their biological activity is carefully tested on the endothelial model of diabetes.

Decision to develop a new drug delivery system for the treatment of endothelial cell dysfunction, caused by high glucose levels, which lead to the microvascular complications of diabetes, was carefully planned. The use such promising new drug carriers to create a treatment to one of the most prevalent diseases of XXI century seems particularly promising. According to the World Health Organization, there are 422 million people suffering from diabetes worldwide [2]. Moreover, the steady increase in the number of diabetes cases over the past few past decades has been observed. It is known that the normalization of blood glucose level is not enough to treat diabetes. Some complications can develop before the clinical manifestation of diabetes, which means they can remain

problematic during the diagnosis and the subsequent improvement of the condition of patients. There is still a great need to design early prognostic tests and new therapies to restore endothelial cell function and to treat injuries in the smallest vessels – leading to macroangiopathic complications – and then to neurological malfunction, sight loss, and renal failure. This treatment is extremely challenging, and it seems that EVs based therapies could be promising solution.

The Author puts in the hands of the reader this thesis, describing a finalized research project, however with the hope that this is just a beginning. Drug delivery systems based on EVs and artificial exosomes could be applied in the future for the treatment of various diseases, due to the great flexibility of the described carrier. Wider introduction of EVs to the therapy could open up a new era of pharmacology.

1.1. Endothelial cell dysfunction as a cause of macroangiopathic complications of diabetes

Diabetes mellitus is a group of metabolic diseases associated with hyperglycemia: high glucose levels in blood. Hyperglycemia can be caused either by a lack of insulin synthesis in the pancreas (type 1 diabetes mellitus - T1DM) or by the resistance of cells to insulin (type 2 diabetes mellitus - T2DM). Over time, high glucose levels in the bloodstream can trigger macrovascular and microvascular complications such as loss of sight (retinopathy), end-stage renal failure (nephropathy), peripheral neuropathy, diabetic cardiomyopathy, or non-healing foot ulcers [3]. Moreover, it has been shown that even very good normalization of glucose levels during diabetes treatment, does not prevent the vascular damage, which is mainly related to the endothelial cell dysfunction (ECD) [4, 5].

In the physiological conditions, endothelial cells (EC) are responsible for the production of nitric oxide (NO), balance control between vasodilatation and vasoconstriction, regulation of platelet aggregation, coagulation, immune function, control of blood volume, and electrolyte content of the intravascular and extravascular spaces [6, 7]. During diabetes, endothelial cells' functions are dysregulated and the number of adverse structural, biochemical and functional changes are observed.

Imbalance between vasodilation and vasoconstriction, decrease in cells' proliferation and migration, impaired wound healing, induction of ischemia and neo-angiogenesis or enhanced apoptosis [8, 9] are typical functional changes observed in ECD. Further damage in the endothelial cells are related to the oxidative stress, triggered by hyperglycemia. It has been shown, that ECD is associated with a decreased NO bioavailability, which is a result of an impaired NO production by the endothelium and/or increased decrement of NO by reactive oxygen species (ROS) [10]. Functional changes are accompanied by the structural alterations. It has been observed that during diabetes, the production of extracellular matrix (ECM) proteins (collagen, fibronectin) is increased, which leads to the thickening of the vascular basement membrane and losing its elasticity [11, 12]. *In vitro* studies have shown, that hyperglycemia triggers various biochemical changes in the endothelial and vascular smooth muscle cells (VSMCs): activation of the polyol pathway, accumulation of advanced glycation end-products (AGEs), activation of the mitogen-activated protein kinase (MAPK) signaling pathways and protein kinase C [9]. Additionally, oxidative stress induced by hyperglycemia, increases the activity of matrix metalloproteinases (MMP-2 and MMP-9) and decreases the activity of the tissue inhibitor of matrix metalloproteinases (TIMP) in vascular cells. This stimulates further remodeling of the ECM, increases vascular permeability and facilitates neo-angiogenesis leading to the development of microangiopathy complications [13].

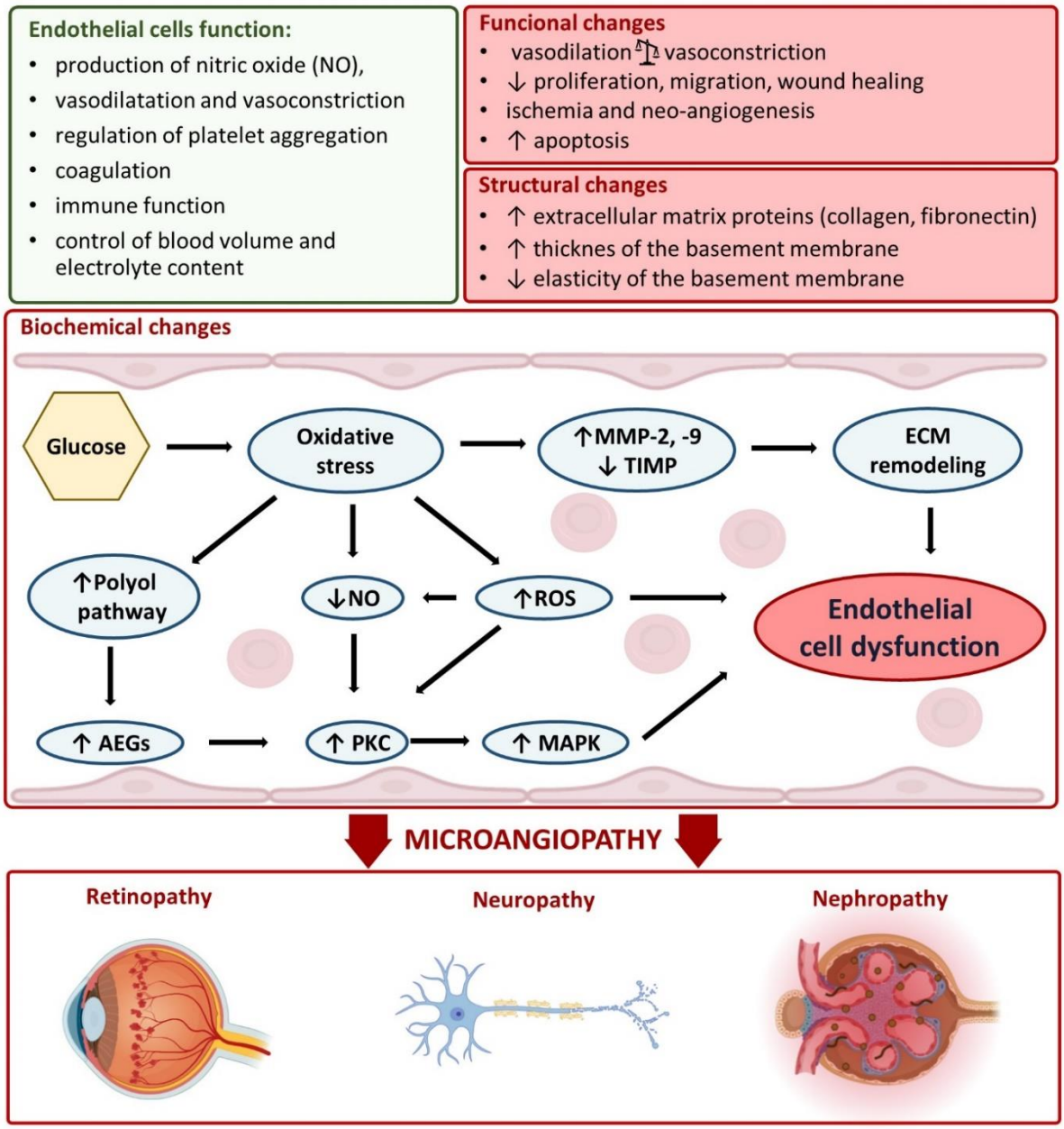

Fig. 1. Endothelial cell dysfunction and their consequences in diabetes. *Created with BioRender.com.*

1.1.1. miRNA in diabetes

MicroRNAs (miRNAs) are the class of small (21-23 nt), noncoding RNA molecules which are responsible for regulation of gene expression. miRNAs are specific gene silencers, functioning through the base pairing to the 3'untranslated regions (UTRs) of target messenger RNAs (mRNAs). miRNAs act by inhibiting translation or by affecting mRNA stability and degradation [14]. It has been show that circulating miRNA can participated in diabetes progression. Term *circulating miRNA* usually refers to the miRNA bound to the protein argonaute 2 (AGO2), combined with RNA-associated silencing complex (RISC), or encapsulated in extracellular vesicles (EVs).

Several reports showed that circulating miRNA could be used as biomarkers of various forms of diabetes. Increase in the level of several miRNAs (miR- 24, miR-30d, miR-34a, miR-126, miR-146 and miR-148a) could be linked to glucose intolerance, disease progression (miR-122, miR-133, miR-210), β-cell injury (miR-375), and inflammation (miR-21-5p) [15, 16, 17]. Additionally, it has been suggested that some miRNAs, such as miR-126 [18], miR-192 and miR-193b [19], can be used as the early pre-diabetes biomarkers allowing for preventive therapy.

Profiling of plasma circulating miRNAs, detected in patients suffering from T2DM, showed that this disease is associated with the decreased concentration of several miRNAs (miR-20b, miR-21, miR-24, miR-15a, miR-126, miR-191, miR-197, miR-223, miR-320, and miR-486) [18]. Additionally, the study showed that high glucose concentrations reduced the miR-126 content of the endothelial apoptotic bodies, which can be linked to the ECD. Garcia-Contreras *et al*. showed, that the changes in the miRNA cargo of exosomes accompanied also T1DM [20]. In exosomes isolated form plasma samples, an upregulation of miR-25-3p and a downregulation of miR-16-5p, miR-302d-3p, miR-378a, miR-570-3p, miR-574-5p, and miR-579 have been detected. Authors suggested, that these miRNAs can be linked to glucose metabolism (hsa-miR-25-3p and miR-16-5p), insulin resistance (miR-302d-3p) or autoimmunity (miR-574-5p). Stępień *et al.* compared the miRNA cargo of circulating ectosomes isolated from T2DM patients with healthy control. They detected increased concentration of several miRNAs involved in angiogenesis and vascular development: miR-

193b-3p, miR-199a-3p, miR-20a-3p, miR-26b-5p, miR-30b-5p, miR-30c-5p, miR-374a-5p, miR-409-3p, and miR-95-3p [21]. One of them – miR-221-3p – seems to be particularly interesting. It has been shown that miR-221-3p could trigger ECD *via* inflammation, pathological angiogenesis, hyperpermeability and apoptosis [22]. It has been shown that the downregulation of miR-221-3p attenuates high glucose-induced suppression in cell migration *in vivo* [23]. Additionally, miR-221-3p regulates the expression of proteins engaged in ECD. Fiorentino *et al*. observed a correlation between the reduced level of TIMP-3 and the elevated level of miR-221-3p in the tissue obtained from the biopsy of the kidneys of diabetic mice and in hyperglycemic mesangial cell cultures [24].

1.2. Characterization of extracellular vesicles

EVs are nano-sized (30 – 4000 nm), lipid bilayer vesicles released by various cells into the extracellular space. They are present in various body fluids such as: blood, urine, saliva, cerebrospinal fluid, milk [25, 26, 27, 28, 29]. Additionally, they can accumulate in cell culture media [30]. The number and characteristics of EVs can vary depending on: the type of the cell, state of the organism (pathological or physiological), and the release mechanism. Based on these criteria, EVs are divided into three basic subgroups: exosomes, ectosomes (microvesicles), and apoptotic bodies.

In recent years, there is a growing interest in EVs research, mostly focusing on their drug delivery potential and perspectives of creating tailored drug delivery systems for different diseases and dedicated for specific patients.

1.2.1. Nomenclature of extracellular vesicles

The population of EVs is highly heterogenic and three main types of EVs can be canonically distinguished: exosomes, microvesicles (also called ectosomes, microparticles), and apoptotic bodies. Different cellular origin, formation mechanism and molecular composition have implications on their biological functions and can also cause several misconceptions in nomenclature. To this moment there is no consensus on the specific markers for EVs' subtypes. Because of that, assigning an EV to a particular biogenesis pathway (exosome with endosomal origin or ectosome derived from plasma membrane)

remains difficult. Therefore, according to the recommendation of the International Society of Extracellular Vesicles [31], if there is no clear evidence of a biogenesis pathway (e.g. the EV is observed during the act of release by live imaging technique), only operational terms to describe different subtypes of EVs should be used. For example: a) size - small EVs, large EVs (with defined size ranges; b) density - low, high (with defined rages); c) biochemical composition (CD63+/CD81+- EVs, Annexin A5-stained EVs, etc.); or d) descriptions of conditions or the cell of origin (podocyte EVs, hypoxic EVs, large oncosomes, apoptotic bodies). It is recommended to clearly define the nomenclature regarding EVs at the beginning of each publication.

Nomenclature in this thesis is based on one of most common characteristics – the formation pathway. Additionally, a) while citing literature references, I decided to use the same nomenclature as the author of the research, b) in my research I use the term "extracellular vesicles" to refer to the vesicles isolated with the low vacuum filtration method, c) hybrid exosomes or artificial exosomes are used to describe the vesicles after fusion with liposomes due to the size of liposomes and size of the vesicles after fusion.

1.3. Biogenesis of extracellular vesicles

Exosomes

Exosomes are released from the parent cells through multivesicular bodies (MVBs) which are formed inside the cell [32]. Classical pathway of exosomes formation starts on the level of plasma membrane, where due to the invagination of particular fragment, an early endosome is formed (Fig.2). Inside the cell, early endosome's membrane invaginates once again and creates MVB, filled with intraluminal vesicles (ILV). Finally, the MVB fuses with a lysosome (causing degradation) or moves along the microtubules (this process is regulated by cholesterol) [33], reaches cell membrane and releases exosomes into extracellular space. Several different molecules involved in MVB trafficking and the final docking of the MVB to the plasma membrane have already been described, including: small GTPases from the Rab family (Rab11, Rab27a, Rab27b, Rab35) [34, 35, 36], cytosolic calcium ions [35], citron

kinase [37], and combination of soluble *N*-ethylmaleimide-sensitive receptors complex (SNARE).

It is important to highlight that during EV formation the membrane asymmetry, typical for membrane of parent cell, disappears [38]. It has been shown that phosphatidylserine, usually present in inner layer of the cell membrane [39], in EVs is located in the outer membrane [40]. Opposite changes were observed for sphingomyelin, which concertation in the outer layer of membrane is decreased [41]. Additionally, exosomes are enriched in glycosphingolipids, sphingomyelin, cholesterol, and phosphatidylserine, in comparison to the parental cells [42].

Currently, several different mechanisms responsible for the exosomal protein sorting have been described. The first one, is endosomal sorting complex required for transport (ESCRT) which activity is crucial for the trafficking of ubiquitinated proteins from endosomes into lysosomes *via* MVBs. Multiple ESCRT proteins such as Alix or TSG101 and ubiquitinated proteins were identified in exosomes [43, 44]. Second mechanism is based on lipids and lipid metabolizing enzymes. It has been shown that inhibition of neutral sphingomyelinase (nSMase) resulted in the reduced secretion of exosomes from Oli-neu cells [45]. Finally, few more mechanism of protein sorting to exosomes such as incorporation into detergent-resistant protein complexes [46], higher-order oligomerization [47], or incorporation of cytosolic proteins into exosomes [48] have been described.

Not only proteins but also lipids are sorted into exosomes, however these processes are not yet well described. One of the lipids involved in the exosomes synthesis is lysobisphosphatidic acid (LBPA). LBPA is a lipid specific for MVB's, which strongly interacts with Alix. Knocking down Alix expression reduces the level of LBPA, triggers the reduction of the number of MVB in cells [49], and decreases the number of ILV in late endosomes.

Besides proteins and lipids, exosomes can also carry nucleic acids, including RNAs (mRNAs or non-coding RNAs such as miRNAs) [50], and DNAs [51]. Probably, sorting of nucleic acids into exosomes is also regulated, but the extend of passive and active sorting still remains unclear. It has been shown that miRNAs are differentially sorted into exosomes depending

on their sequence (due to the presence of specific motifs - EXOmotifs) [52]. It has been suggested that the ESCRTII and the tetraspanin-enriched microdomains [53] could act as RNA-binding subunits. Recently, new possible regulators of miRNA sorting into exosomes have been described: miRNA-induced silencing complex (miRISC) and the protein argonaute 2 (AGO2) [54], KRAS–MEK signaling pathway which also acts through AGO2 [54], major vault protein, and Y-box-binding protein 1 (YBX1) [55].

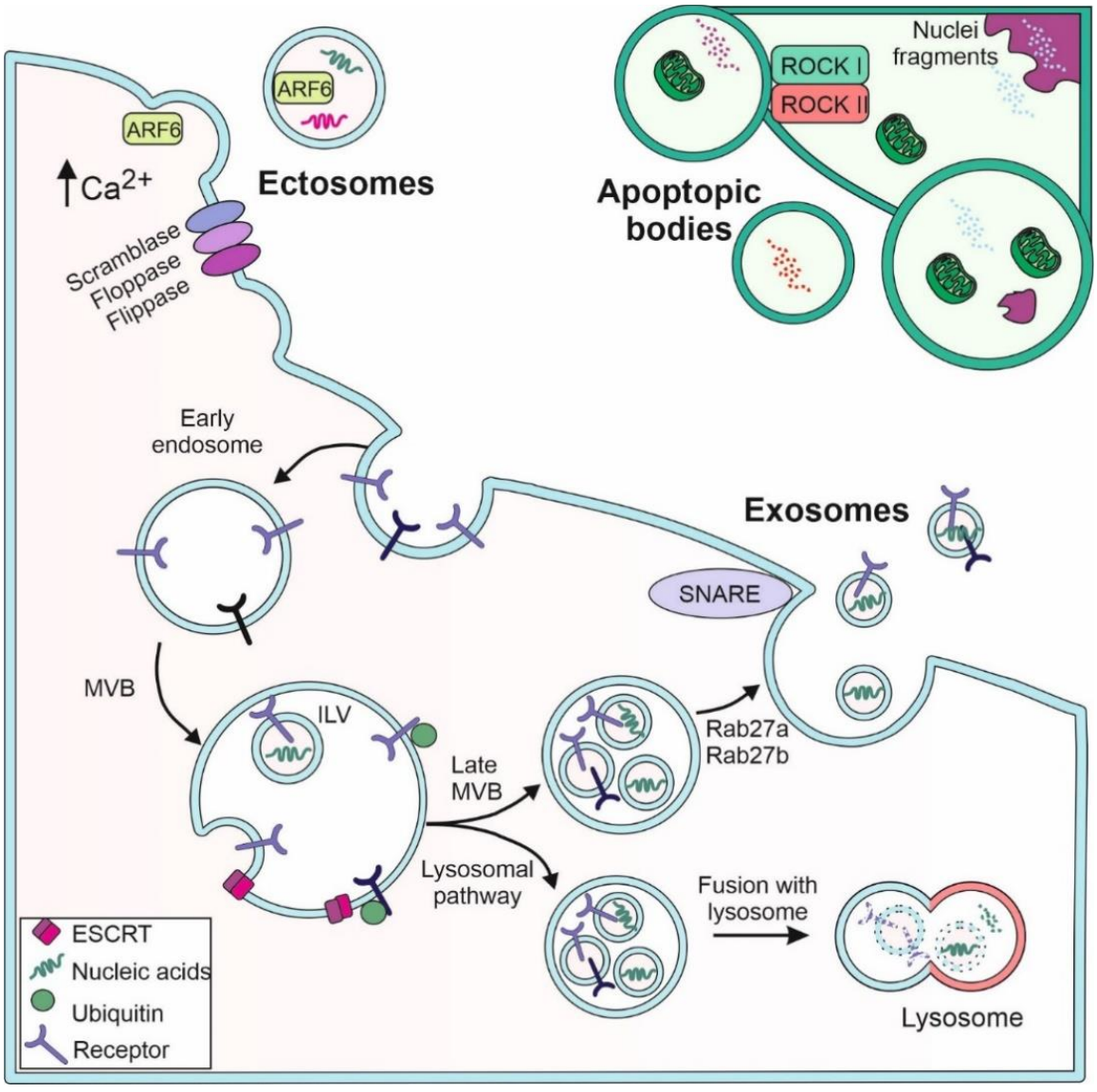

Fig. 2. Extracellular vesicles biogenesis and secretion mechanisms (adapted from [56]).

Microvesicles

Microvesicles are formed on the cell surface, followed by their release into extracellular space. Formation process starts from the outward budding of the cell membrane in the specific region and is followed by the direct shedding and immediate fission of the vesicle from cell membrane. Release of microvesicles requires rearrangements within plasma membrane, including lipid and protein components, and is most often induced by the activation of a given cell by different agonists (such as ATP, growth factors, cytokines [57]). After activation, the intracellular level of Ca^{2+} increases, which influences the activity of enzymes, which are responsible for maintaining phospholipid membrane asymmetry. Firstly, due to activation of floopase and scramblase, which cause phosphatidylserine (PS) and phosphatidylethanolamine (PE) location to the outer leaflet of the cell membrane. Secondly, inhibition of flippase prevents from the reversion of PS and PE to the inner leaflet [58]. Those spatial changes induce bending of the membrane and reorganization of the underlying actin cytoskeleton, by the proteolysis promoted by calcium-activated calpains and gelsolin [59, 60]. Finally, cell membrane is budding to form microvesicles.

RhoA, from Ras protein superfamily of small GTPases, Rho-associated: protein kinase (ROCK), LIM kinase (LIMK) and coffilin (actin-binding protein) are one of the proteins which are engaged in the release of microvesicles from cell surface. RhoA reorganize the structure of actin-myosin filaments, leading to the increased microvesicles secretion by different cancer cell lines [61]. Additionally, in cancer cells, extracellular signal regulated kinases (ERK) and myosin light-chain kinase (MLCK) can be activated by AFR6 (GTP-binding protein). This activation leads to actin polymerization and phosphorylation of myosin light chains, and finally to the release of microvesicles [62]. Another mechanism was described in the enterocyte cells. In the enterocyte brush border, myosin 1a is distributed along the microvillar tips and exerts forces leading the apical membrane to form and release of gut microvesicles [63].

The process of microvesicles cargo loading is not well understood. It has been suggested that macromolecules, such as lipids and other membrane-associated cargoes can be incorporated into the sites of microvesicles budding through their affinity for lipid rafts, or

anchoring to the plasma membrane. Cytosolic components require binding to the inner leaflet of the plasma membrane by plasma membrane anchors, such as palmitoylation, prenylation, myristoylation [64, 65]. In nucleic acids loading, conserved zipcode RNA sequence motifs could be involved [66].

Apoptotic bodies

In contrast to exosomes and microvesicles, the release of apoptotic bodies is not a continuous process but occurs only when a cell undergoes apoptosis. One of the earliest morphological changes during cell apoptosis is a deformation generated by cytoskeleton contractions, followed by membrane blebbing and the increase of hydrostatic pressure within the cell. These changes are controlled by the Rho effector – Rho-associated coiled coil kinase I (ROCK I). Caspase-mediated cleavage of ROCK I results in myosin light chain phosphorylation leading to the membrane blebbing [67, 68]. Alternatively, granzyme B cleaves Rho-associated coiled coil kinase II (ROCK II), which produces a constitutively active enzyme, and increases myosin light chain phosphorylation as well as membrane blebbing [69]. It is worth mentioning, that the release of multiple apoptotic bodies is not a universal feature of cells undergoing apoptosis and some cells do not appear to generate membrane blebs but form a single apoptotic body [70].

Cargo sorting to the apoptotic bodies is a spatial process and depends on the region of the cell within bleb is form. They can be enriched in DNA and histones, when they originate from the plasma membrane, or immature glycoepitopes, when they originate from the endoplasmic reticulum [71].

1.2.2. Biological function of extracellular vesicles

Numerous studies have shown that EVs, carrying bioactive molecules to the distinct cells, have a unique ability to mediate cell-to-cell communication [72, 73, 21]. EVs are engaged in a variety of physiological and pathological processes, like: immune response modulation [74], cell adhesion [75] or tumor progression [76]. Some of these processes, such as coagulation [77] and angiogenesis [78], are directly linked to the vascular and inflammatory

disorders [79], encompassing also microangiopathy. Moreover, in recent years, EVs engagement in tissue regeneration is a subject of great interest, due to the possible application of EVs in regenerative medicine and therapy [80].

Coagulation

EVs contain several macromolecules which are crucial for coagulation and thrombosis – negatively charged PS, exposed in the outer layer of EVs membrane, tissue factor (TF) and urokinase plasminogen activator receptor (uPAR) [81]. PS creates negatively charged surface for the assembly of coagulation cascade enzyme complex. It has been shown, that the lack of a surface exposure of PS, as well as the reduction of platelet-derived EVs plasma level, is manifested as a bleeding disorder called Scot syndrome [82].

Activity of TF, which is delectable on the EVs surface, depends on the condition of the organism. It has been shown that platelet-derived EVs from healthy donors contain TF in inactive form which exhibit coagulation activity after recruitment to the place of injury [83]. In pathological states such as cancer or inflammation EVs contain active form of TF and can be used as a biomarker of hypercoagulability [84]. Additionally, it has been shown that platelet-derived EVs level is elevated in other pathologies associated with an increased risk of thromboembolic events such as atherosclerosis [85], sepsis [86], and pre-eclampsia [87].

It has been shown that leucocyte and endothelial cell derived microvesicles contain uPAR on their surface and therefore can stimulate plasminogen activation [88]. Moreover, it was suggested that in endothelial cell dysfunction uPAR is remove from endothelial cell surface by releasing soluble uPAR – bearing vesicles [89]. This induce prothrombotic activity of endothelial cell which can be linked with an increased risk of vascular complications in patients with diabetes.

Angiogenesis

Angiogenesis is a strictly regulated and multistage process which involves: enzymatic degradation of the vessel's basement membrane, endothelial cells proliferation, migration, and tube formation. In recent years, a numerous studies highlighting EVs involvement in

angiogenesis, have been presented. Depending on the content and surface molecule expression, EVs can either stimulate or inhibit angiogenesis.

EVs carry a set of proteins with confirmed pro-angiogenic activity. It has been shown that EC derived EVs can transfer Delta-like 4 (Dll4) protein and incorporate it into the plasma membrane of recipient cells inhibiting Notch signaling. This results in an increase in vessel density and branching [90]. Additionally, EC derived EVs contain matrix metalloproteinases which degrade compounds of extracellular matrix and facilitate EC invasion and capillary-like structure formation *in vitro* [91].

miRNAs cargo of EVs is also involved in modulating the formation processes of new blood vessels. Studies showed that EVs can transfer functional miR-126-3p and STAT5 into ECs, which leads to cyclin D1 transcription and tridimensional tube-like structure formation [92]. Other authors demonstrated that EC-derived exosomes, containing miR-214, decreased the expression of ataxia telangiectasia mutated protein in recipient cells, preventing senescence, improving cell migration and allowing the formation of blood vessels [93].

In pathological state like diabetic nephropathy or retinopathy EVs can stimulate also pathological neo-angiogenesis. It has been shown that MVs isolated from plasma contain receptor for chemokine RANTES (CCR5). Level of CCR5-bearing MVs correlates with the severity of diabetic retinopathy [94]. Moreover, in another study the same authors showed that in EVs isolated form plasma of diabetic patients levels of cytokines and pro-angiogenic factors such as VEGF, b-FGF, Ang-2 are elevated and could be linked with duration of disease and the outcome of the diabetic treatment [79].

The exosomes containing high amount of PS in outer membrane demonstrate the opposite activity. It has been suggested, that PS interact with CD36 expressed on EC, resulting in ROS production in a NADPH oxidase and Src family kinase dependent manner. This leads to inhibition of EC migration and tube formation [95].

Tissue regeneration

Tissue regeneration is the physiological processes of replacing necrotic cells and tissue by new cells, in order to restore healthy tissue. In the context of regeneration, EVs can act in

paracrine manner, and stimulate repairmen and regeneration. In a kidney injury model, tubular epithelial cells were exposed to hypoxic release exosomes enriched in TGF-β1 mRNA. The study showed that these exosomes can stimulate proliferation, α-smooth muscle actin expression, F-actin expression, and type I collagen production in fibroblasts [96]. Another study highlighted exosomes cardioprotective role in ischemia-reperfusion injury models. It has been shown that exosomes isolated from heathy individuals can reduce infract area by activating TLR4 signaling in a rat infract model [97]. Exosomes are also involved in tissue regeneration in diabetic chronic wounds. Human bone marrow-derived mesenchymal stem cells (hBMSCs) exosomes can stimulate endothelial angiogenesis, proliferation, and migration of fibroblasts through the activation of several signaling pathways including Akt, Erk1/2, and STAT3 [98].

1.2.3. Extracellular vesicles in diabetes

During diabetes (type 1 and type 2) both plasma and urine level of EVs, as well as EVs cargo are altered [99]. The meta-analysis study [100] showed that patients with type 2 diabetes have elevated levels of circulating total-microparticles, platelet-derived microparticles, myocyte-derived microparticles and endothelial-derived microparticles in plasma. It has been shown that microparticles isolated from patients with metabolic syndrome, in contrast to microparticles isolated from healthy donors, induce vascular damage after intravenous administration in mouse model [101]. Additionally, it has been observed that the concentration of urinary EVs correlates with diabetic renal damage and could be used as a prognostic factor [102].

One of the risk factors of type 2 diabetes is obesity. Recent studies showed that insulin resistance in type 2 diabetes could be linked with abnormal adipocytes-derived EVs cargo. EVs can be involved in the down-regulation of glucose transporter type 4 (GLUT4) and malfunction of insulin receptor (IR). It has been observed that adipocyte-derived EVs from obese mice could induce pro-inflammatory macrophage phenotype and cause insulin resistance in the adipose tissue [103]. Moreover, EVs isolated from adipose tissue of obese patients contain pro-inflammatory cytokines (IL-6, MCP-1, RBP-4, and adiponectin) and can

induce insulin resistance in hepatocytes and myocytes [104]. EVs isolated form obese individuals contain high levels of miR-155 and miR-27a and can decrease the number of GLUT4 transporters in the plasma membrane of skeletal muscle and adipose tissue [105, 103]. EVs can also regulate cell response to the oxidative stress. It has been shown that internalization of EVs from individuals with diabetes modulates the expression of genes responsible for oxidative stress management and inhibits oxidative stress response in monocytes [99].

In type 1 diabetes exosomes may be involved in the development of autoimmunity. It has been shown that rat and human pancreatic islets under proinflammatory conditions release exosomes containing autoantigens: GAD65, IA-2, and insulin/proinsulin [106]. Autoantigens outside the cell may activate antigen presenting cells and be presented to the self-reactive T cells, triggering autoimmunity against pancreatic β-cells. Additionally, exomes can be used as an early biomarker of developing type 1 diabetes. *In vitro* experiments have shown that human islets stimulated with inflammatory cytokines release EVs enriched in miR-21-5p. These results were validated on serum samples from children with new-onset type 1 diabetes. Serum EVs miR-21-5p levels was significantly higher in comparison to non-diabetic individuals [107].

1.3. EVs as drug delivery systems

Nanoscale drug delivery systems (DDS) have been used to improve the therapeutic efficacy of chemical and biomolecular drugs for almost fifty years [108]. Unfortunately, a wide range of side effects such as organ toxicity or adverse immunogenic reactions are still registered [109, 110]. Additionally, high reticuloendothelial system (RES) or mononuclear phagocyte system (MPS) clearance, makes it necessary to modify drug surface to reduce it [111, 112]. One of the biggest challenges are interactions of DDS with plasma proteins (nano-bio interactions) initialized immediately after introducing nanodrugs to the circulation system. Nano-bio interaction include: clotting, inflammation and endothelium injury and may lead to unpredictable (beneficial or harmful) alterations of nanodrugs activity. Consequently,

only a small number of nano-based DDS have been approved by the FDA for use in humans [113].

Unlike, synthetic nanodrugs, endogenous EVs have been promising in enhancing drug delivery and therapeutic efficacy. In living organisms, EVs are responsible for the transport of biomolecules enclosed in their lumen to the distinct body compartments. It has been proven that EVs are rich in non-coding RNA, such as miRNA, lncRNA, piRNA, and they can alter the metabolism of recipient cells. Additionally, EVs are able to avoid opsonins (C-reactive proteins), coagulation factors and complement, as well as antibody responses [114]. EVs, due to their naturally biocompatible characteristic: small size allowing for penetration into deep tissue, deformable cytoskeleton, slightly negative zeta potential for long circulation and the presence of multiple adhesive molecules on their surface are perfect nanocarriers for DDS applications.

1.3.1. Drug loading strategies

At the cellular level, EVs are perfect nanocarriers, but therapeutic applications require further modifications, such as drug loading and surface modification for targeting. Currently two different strategies of drug loading into EVs are under development. In the first approach, drug/bioactive molecules are loaded into EVs before isolation. The simplest method to achieve this goal, is by adding the drug to the cell culture media. This method was applied to the production of EVs derived from mesenchymal stromal cells and loaded with paclitaxel [115]. The study demonstrated that after the incubation with cells, paclitaxel is loaded into EVs and those EVs have a strong anti-proliferative activity on the human pancreatic carcinoma cell line CFPAC-1. Cell transfection is mainly used to incorporate small molecules, like miRNA or siRNA, into EVs. Zhang *et al.* [116] transfected human monocytic cell line THP-1 with miR-150 and showed that miR-150 was packaged into EVs. Moreover, EVs isolated from cell culture media were efficiency uptaken by Human Mammary Epithelial Cells (HMEC-1) increasing their migration and decreasing the expression of protooncogene c-Myb.

In the second approach drug/bioactive molecules are loaded into EVs after isolation. The simplest strategy is the incubation of the molecule with isolated EVs, sometimes with an addition of membrane permeabilizers, like saponins [117]. This method has been used by Sun *et al*. [118]. In the study EVs were incubated with curcumin and used to activate myeloid cells *in vitro*. The study showed that target specificity is determined by the exosomes, and the improvement of curcumin activity is achieved by directing curcumin to inflammatory cells, which is associated with strengthened therapeutic effects.

Other two techniques applied to load bioactive drugs into EVs are electroporation and sonication. Tian *et al*. [119] loaded doxorubicin into EVs isolated from mouse immature dendritic cells (imDCs) using electroporation and used those EVs for tumor treatment in tumor-bearing mouse model. The studies have shown that the doxorubicin anticancer activity is enhanced when the drug is loaded into exosomes, in comparison to other delivery systems and it caused significantly less side effects. It is worth mentioning that drug loading during extrusion was also investigated. Unfortunately, it has been observed that extrusion, depending of the conditions can change zeta potential of the EVs and cause cytotoxicity [117].

1.3.2. Engineered vesicles

Engineered vesicles could be distinguished as a separate category of EVs based drug carriers. Engineered vesicles can be created by slicing the vesicles form the cell surface, by cells extrusion, or by the fusion of EVs with liposomes. First approach was developed by Yoon *et al*. [159] who designed a microfluidic system that generates EV-mimetic particles by slicing a cell membrane with 500 nm silicon nitride (Si_xN_y) microblades. In the system, living cells flow through microchannels lined with the blades. The plasma membrane fragments are sliced from the cells and immediately form spherical vesicles with the diameter of 100-300 nm. In this study EV-mimetics were loaded with polystyrene beads which were added to the buffer solution and encapsulated inside vesicles during their self-assembly. The study showed that EV-mimetics can deliver encapsulated beads to the

recipient cells, while free beads were not able to penetrate through the plasma membrane [120].

In second method EV-mimetics are generated by disrupting cells membrane via extrusion. During the extrusion cells pass through several filters with diminishing pore sizes (10, 5, and 1 μm), in the presence of the drug, and form EV-mimetics with encapsulated drug molecules. One of the biggest advantage of this method is a high yield of synthesis. Jang *et al*. synthesized doxorubicin loaded EV-mimetics by the extrusion of U937 and Raw264 cells [121]. They showed that the yield of EV-mimetics production was 100-fold higher than during exosomes isolation and that the structure of the outer cell membrane was preserved. *In vitro* tests showed that doxorubicin-loaded EV-mimetics induced the death of TNF-α-treated human umbilical vein cells (HUVECs) in a dose dependent manner. *In vivo* studies showed that doxorubicin-loaded artificial EVs accumulate in the tumor tissue and reduce tumor growth, without accumulation in the heart of the patients, which is especially sensitive to the doxorubicin side effects. Furthermore, compared to doxorubicin-loaded exosomes, doxorubicin-loaded nanovesicles showed similar antitumor activity *in vitro*.

The third method allows for the synthesis of hybrid exosomes (hEx) through the fusion of EVs with liposomes. This method was described for the first time by Sato *et al*. in 2016 [122]. The authors, using freeze/thawing cycles, fused exosomes isolated from the Raw 264.7 cell culture media with the liposomes of different composition or with PEGylated liposomes. The study showed that fusion efficiency increases with number of freeze/thawing cycles and depends on the liposomes composition. Additionally, fusion efficiency was higher for PEGylated liposomes. Up-take studies showed that that hEx are internalized by HeLa cells and the efficiency of internalization depends on the liposomes lipid composition.

Encapsulation of drugs into liposomes is well established, so the fusion of EVs with liposomes could be applied for delivery of different types of bioactive molecules to various cells. Piffoux et al. [123] showed that hEx can deliver chemotherapeutic compound (mTHPC) with 3 - 4 times higher efficiency, as compared to the free drug, or the drug-loaded liposome precursor.

1.3.3. Targeting

Targeted delivery system should be able to interact selectively with only one type of cells or tissue. It has been shown, that some EVs types have a natural tendency to accumulate in the specific types of cells. Rana *et al*. [124] showed that tetraspanins are responsible for the preferential interaction with specific types of cells. Exosomes isolated from transfected adenocarcinoma cell lines, and expressing the Tspan8–alpha4 complex, are more efficiently up taken by endothelial and pancreas cells, than by lung fibroblast or bone marrow cells both in the *in vitro* and in the *in vivo* studies. Additionally, EVs surface can be decorated with targeting molecules after isolation by a simple incubation with molecule with a known affinity to the EVs surface [125]. A novel method of surface modification employs click chemistry and allows to attach molecules *via* covalent bonds [126]. Copper-catalyzed azide-alkyne cycloaddition is suitable for the bioconjugation of small molecules and macromolecules to the surface of EVs, due to fast reaction times, high specificity, and compatibility in aqueous buffer. This method was applied by Smyth *et al*. to attach fluorescent dye to the EVs surface with good yields. To my best knowledge, there are currently no studies regarding utilizing these methods for attaching targeting molecules to the EVs surface, however, this approach seems promising.

Currently, several drug delivery systems based on EVs have been proposed. While the great potential of these particles in targeted drug delivery has been recognized, this field is still in the early stage of development.

2. Objectives of the thesis

The main objective of the project, described in this thesis, was to synthesize a new drug delivery system based on the artificial exosomes (aEx) for the delivery of anti-miRNA to endothelial cells, in order to restore their physiological characteristics, in the cellular model of diabetes. The project consists of two parts: the first one is devoted to the synthesis and characterization of artificial exosomes, while the second one concerns mostly functional tests and the effects of the drug delivered using aEx on the studied cells.

Following intermediate objectives, grouped into the two categories, related to the two parts of the project, serve as a way of achieving the main objective.

The objectives on the level of synthesis were to:

- confirm that the fusion between liposomes and EVs occurs;
- design the most efficient protocol for the fusion between liposomes and EVs;
- examine the influence of the composition of liposomes and liposomes to EVs ratio on the fusion process;
- characterize aEx in terms of physical (size, concentration, lamellarity, zeta potential and biological characteristics (cytotoxicity and internalization into endothelial cells).

The objectives on the level of the functional tests were to evaluate:

- whether aEx, after internalization by HUVECs, can restore physiological levels of TIMP-3 mRNA, TIMP-3 protein, metalloproteinases and improve wound healing process in the cellular model of diabetes;
- whether the changes induced by aEx are significantly different from those induced by EVs and experimental controls;
- how the decoration of aEx with Del-1 protein modifies the induced effects.

3. Methodology

3.1. Synthesis of the artificial exosomes

Artificial exosomes (aEx) were synthesized by the fusion of EVs isolated form Human Umbilical Vein Endothelial Cell (HUVECs) cell culture media, and liposomes of different composition. Additionally, aEx were loaded with anti-miRNA-221-3p and decorated with Del-1 protein. The process of synthesis consists of several steps: cell culture and EVs isolation, liposomes synthesis with/without miRNA loading (depending on the experiment set-up), fusion, and decoration with Del-1 protein. All of these steps are precisely described in the following subchapters.

3.1.1. Cell culture and extracellular vesicles isolation

HUVECs (cat. No. 200P-05N, Cell Application Inc.) were cultured in the 1: 1 mixture of 199 medium (cat. No. M7653, Sigma Aldrich) and the SFM medium (Human Endothelium Serum-Free Medium, cat. No. 11111044, GIBCO), supplemented with exosomes depleted FBS (10% v/v) (Gibco, cat. No. A2720801), penicillin/streptomycin (cat. No. P0781, BioReagent) at a concentration of 10,000 units/l (penicillin) and 1 mg/l (streptomycin), and 2 mM of L-glutamine (cat. No. 17-605E, BioWhitaker, Lonza). To obtain hyperglycemic culture conditions (HGC), additional glucose was added to the cell culture media in order to obtain the final concentration of 25 mM (cat. No. G7021, Sigma Aldrich).

EVs were isolated using low vacuum filtration method (LVF) [127]. Cell culture media were collected from HUVECs seeded in a 75 cm^2 cell culture flasks after 24h of culturing in fresh media. To remove cell debris, the media were centrifuged subsequently at 400g (10 min) and 3100g (25 min). Afterwards, the debris pellets were discarded, and the supernatants were filtered on dialysis membranes (cat. No. 131486, Spectra/Por Biotech) with MCWO = 1000 kDa. The filtration was facilitated with additionally applied pressure (-0.3 Bar). When the sample volume in the membrane reached 1 ml, 15 ml of water was added and filtered in order to wash away proteins unbound to the EVs. The final volume (around 1 ml) was collected and stored in -80°C for further analysis and experiments (Fig.3.).

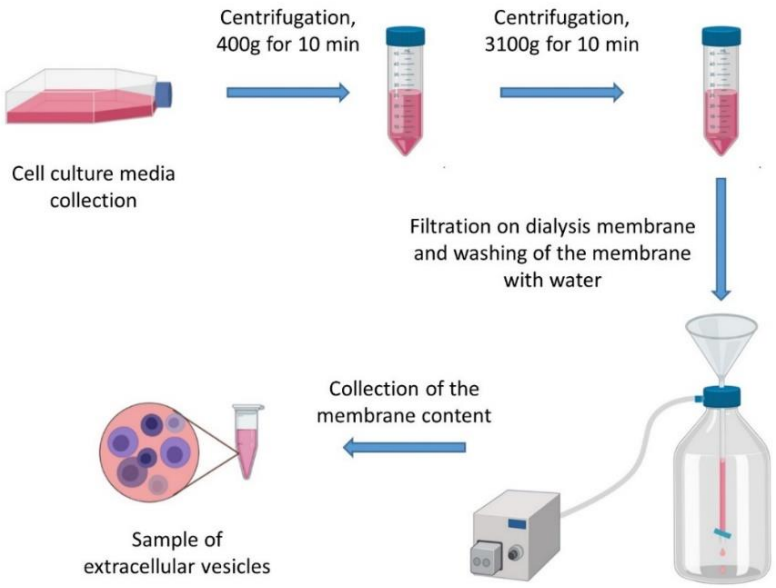

***Fig. 3. A workflow of the extracellular vesicles isolation protocol**. Created with BioRender.com.*

3.1.2. Liposomes synthesis

To mimic the natural EVs composition, lipids were chosen based on their presence in the EVs membrane. Lipidomic analysis of various exosomes showed high content of cholesterol, diglycerides, glycerophospholipids, phospholipids, and sphingolipids [128] as well as bioactive lipids (prostaglandins and leukotrienes) (Tab.1.). For the study, three most abundant lipids: DOPC - phosphatidylcholine (cat. No. 850375C, Avanti Polar Lipids), PS - phosphatidylserine (cat. No. 870336C, Avanti Polar Lipids) and SM - sphingomyelin (cat. No. 860061P, Avanti Polar Lipids) were used (Fig.4.).

Lipids [%]	PC-3 cells [42]	PC-3 cells + HG [129]	B-lymphocytes [130]	Mast cells [38]	Dendritic cells [38]	Reticulocytes [131]	Proteasome [132]	Urine [133]	Platelets [134]
CHOL	43.5	59	42.1	15		47	54.45	63	42.5
SM	16.3	9.1	23.0	12	20	8.4f	21.45	11.7	12.5
PC	15.3	10.8	(20.3)*	28	26	23.5	1.8	2.7	15.9
PS	11.7	6.9	(20.3)*	(16)*	(19)*	5.9	6.25	13.2	10.5
PE	5.8	1.1	(14.6)*	24	26	12.7	0.45	-	3.1
PE O/P	3.3	4.7	(14.6)*					4,6	
DAG	1.5	1.1						0.1	
PC O/P	0.81	0.7							1.4
HexCer	0.76	2.3					14.45	1.9	
Cer	0.32	0.7						0.1	0.4
PG	0.17	0.1							
PA	0.16	0.1	(20.3)*						
PI	0.13	0.3	(20.3)*	(16)*	(19)*	2.4	1.2		5.2
LacCer	0.12	0.7						0.8	
CE	0.08							0.3	4.1
Gb3	0.02							1.1	
LPC									0.79

Tab. 1. Lipid content of exosomes from different cells [133, 135] (%: Percent of total lipid quantified, *Sum of all classes shown in parentheses and having the same numbers). *Abbreviations: CE - cholesteryl ester, CHOL – cholesterol, Cer – ceramide, DAG – diacylglycerol, Gb3 – globotriaosylceramide, HexCer – hexosylceramide, LacCer – lactosylceramide, PA - phosphatidic acid, PC – phosphatidylcholine, PC O/P - PC ethers (alkyl or alkenyl), PE - phosphatidylethanolamine, PE O/P - PE ethers (alkyl or alkenyl); PG - phosphatidylglycerol; PI – phosphatidylinositol, PS – phosphatidylserine, SM – sphingomyelin (Table adapted from [133]).*

In order to improve encapsulation and cargo delivery, positively charged cholesterol derivative – DC-Chol (cat. No. 700001P, Avanti Polar Lipids) was used for liposomes

synthesis (Fig.4). Encapsulation of nucleic acid cargo such as pDNA, siRNA or miRNA is more efficient when cationic liposomes (Cls) are used. Moreover, liposomes composed of DC-Chol and DOPE have been classified as some of the most efficient gene delivery systems [136]. The biggest drawback of CLs is their short circulation lifetime and tendency to aggregate. This can be overcome by PEGylation of CLs surface [137]. Unfortunately, it has been shown that this modification can lead to reduced internalization, nucleic acid endosomal escape, and hence decreased transfection efficiency [138]. Fusion with EVs – natural nucleic acid carriers in living organisms may improve the characteristics of CLs.

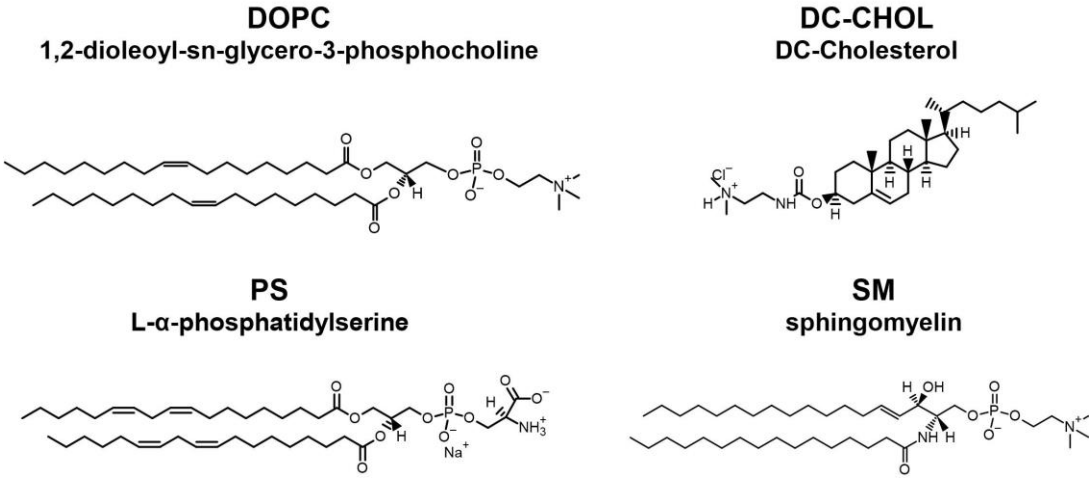

Fig. 4. The chemical structure of lipids used in the study.

Experimental set-up

Liposomes were synthesized using the thin film hydration method followed by repeated freeze/thawing cycles. The reduction of the size of multilamellar liposomes was performed by extrusion with a manual extruder (cat. No. 61000, Avanti Polar Lipids) thorough polycarbonate membranes with a 100 nm diameter pores (cat. No. 800309, Whatman).

To obtain a thin film, organic solutions of lipids and cholesterol in a concentration of 10 µmol/ml were mixed in glass beakers in an appropriate molar ratio (Tab. 2.) and dried under a nitrogen stream. Thin films were kept under vacuum overnight to remove any remaining solvent. Next, the thin films were hydrated with PBS solution for 30 minutes above the phase transition temperature, and vortexed for 2 minutes to obtain liposomes dispersion

in the concertation of 2 µmol/ml. In the next step, liposomes dispersions underwent five freeze/thawing cycles and were extruded ten times through 100 nm pores.

3.1.3. Encapsulation of anti-miRNA in artificial exosomes

As a biologically active particle anti-miR-221-3p was chosen due to the well documented involvement of miR-221-3p in the development of ECD during diabetes, and benefits stemming from blocking the miR-221-3p activity (subsection 2.1.1.). miR-221 is clustered with miR-222 and is located on the short arm of an X chromosome [139]. The sequence of miR-221-3p is: 65 – AGCUACAUUGUCUGCUGGGUUUC – 87 [140]. According to the RNACetral database, miR-221-3p has 844 identified protein targets, including TIMP-3 [141]. Based on that, I am also expecting positive influence of the downregulation of miR-221-3p on metalloproteinases, which are elevated during diabetes. Interestingly there is no data about the role of miR-221-3p in the regulation of MMP-2 in diabetes.

Experimental set-up

Encapsulation was performed during the synthesis of liposomes. Anti-miR-221-3p (cat. No. QG-339132_YI04100607-DFA, Qiagen), anti-miR-221-3p-FAM (cat. No. QG-339131_YI04100607 -DDC, Qiagen), and negative control (cat. No. QG-339137_YI00199006-DFA, Qiagen) were resuspended in TE buffer (Tris-EDTA buffer solution, cat. No. 93283-100ML, Sigma Aldrich) according to the manufacturer's protocol and stored in -20°C. Amount of encapsulated anti-miR-221-3p and the required amount of liposomes was calculated according to Tab.4. In order to encapsulate miRNA in liposomes, lipid thin films were hydrated with PBS with the appropriate concentration of miRNA. After hydration, liposomes were processed as described below.

3.1.4. Artificial exosomes synthesis

The freeze/thawing method is commonly used in liposomes production. The method is based on a series of repetitive cycles of fast freezing (usually in liquid nitrogen) and slow thawing. During this process liposomes membrane is disrupted and their composition becomes more homogenized. During freeze/thawing cycles the lamellarity of the liposomes decreases, which in turn increases the trapped volume [142]. Additionally, it has been

observed that the cargo of liposomes can be exchanged between them during the process [143].

Experimental set-up

For the synthesis, exosomes and liposomes were mixed in different ratios (Tab.2.) in eppendorf tubes and placed in liquid nitrogen for 5 minutes. Next, samples were transfer into a thermoblock (Thermomixer 5350, Eppendorf) and incubated for 10 minutes in 24°C with additional mixing (500 rpm). Cycles were repeated up to 10 times.

To establish the most efficient synthesis protocol, three factors were investigated:

a) liposomes composition
b) liposomes to exosomes ratio
c) number of freeze/thawing cycles

Factor	Tested conditions [mol%]	Justification
Liposome composition	SM (70:30) PS (70:30) DOPC (70:30)	Different lipids properties can affect membrane stability and process of fusion
Liposomes lipids to EVs proteins ratio	1 to 8 1 to 16 1 to 32 1 to 50 1 to 100	In theory, the best outcome should occur when a single liposome fuses with a single EV, so the different ratio between these particles were tested and compared with the calibration curve
Number of freeze/thawing cycles	1 - 10	Each freeze/thawing cycle improves mixing between lipids in lipids membrane, making the structure more homogenous

Tab. 2. Scheme of the experiment. *Different factors were investigated in order to establish the most efficient synthesis protocol. Liposomes to EVs ratio are presented as the amount of total lipids in liposomes divided by the amount of protein in EVs samples.*

Lipid mixing and fusion was monitored by means of Förster Resonance Energy Transfer (FTER), dynamic light scattering (DLS) and Nanoparticle Tracking Analysis (NTA), as well as Cryogenic Transmission Electron Microscopy (Cryo-EM). The methods and procedures are described in the following section.

3.1.5. Decoration of artificial exosomes with Del-1

Targeting of endothelial cells by aEx is based on the properties of developmental endothelial locus-1 (Del-1) protein, which is a 52-kDa glycoprotein secreted by endothelial cells [144]. Del-1 contains 3 epidermal growth factor–like (EGF-like) domains at the amino terminus and 2 discoidin I–like domains at the C-terminus. The second EGF–like repeat contains the Arg-Gly-Asp (RGD) motif, which is responsible for binding to the integrins αVβ3 and αVβ5 on the endothelial cells. The discoidin I–like domain enables binding to phosphatidylserine. It has been shown that Del-1 can act as a bridging molecule between integrins on endothelial cells and phosphatidylserine in the external surface of microparticles (MPs) and can mediate endothelial uptake of MPs [145]. The hypothesis of this work is that aEx covered by biologically active Del-1 would mediate efficient uptake of the cargo of aEx by the endothelial cells.

Experimental set-up

In order to cover aEx with Del-1 protein and target aEx towards endothelial cells, samples were incubated with the protein at 37°C for 1h. After incubation, unbound proteins were removed with centrifugation on the Amicon column (cat. No. UFC5100, Milipore) with MWCO = 100 kDa. The binding of Del-1 to aEx was confirmed by the western blot analysis.

3.2. Monitoring fusion between extracellular vesicles and liposomes – Förster Resonance Energy Transfer

Chromophores are molecules, which can absorb electromagnetic radiation of a specific wavelength (energy), exciting them from a ground state into an excited state (Fig.5.). The excited state is not stable, so the molecule re-emitts the photon of a longer wavelength (lower energy) [146]. If two fluorophores are present in a close distance, and when the emission spectrum from one of them (donor) overlaps with the absorption spectrum of the

second one (acceptor), the energy could be transferred between them in a non-radiative manner, and then emitted by the second molecule as a photon. This phenomenon was first described in 1948 by Theodor Förster [147].

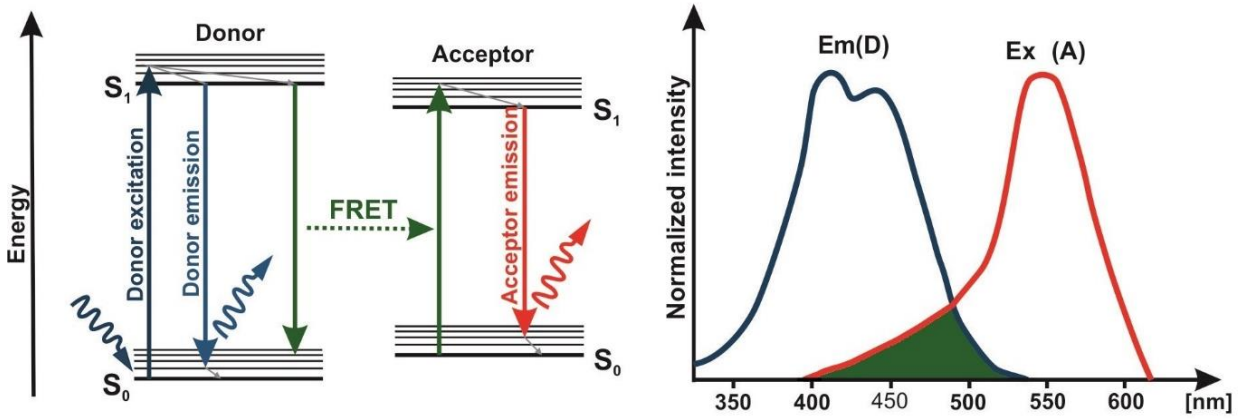

Fig. 5. Basic principles of Förster Resonance Energy Transfer (FRET) *[148]. A. Jablonski diagram illustrating the absorption and emission of energy and FRET between donor and acceptor . S_0 – ground state, S_1 – excited state, gray lines - relaxation. B. Overlapping spectrum of a donor and an acceptor molecule. Em (D) – emission spectrum of a donor, Ex (A) – absorption spectrum of an acceptor.*

Following requirements have to be met to observe energy transfer:

a) donor and acceptor need to have a strong electronic transition in the UV, visible, or IR range;

b) donor emission and acceptor absorbance spectra have to overlap;

c) a donor and an acceptor have to be physically close

d) orientation factor needs to be small

e) quantum yield of donor emission has to be efficient [149].

In this phenomenon, an excited donor, presented as an oscillating dipole, can exchange energy with having a similar resonance frequency second dipole (acceptor). Energy transfer manifests itself through the decrease or quenching of the donor fluorescence and a reduction of excited state lifetime accompanied by an increase in acceptor fluorescence intensity [150].

$$D + h\nu \rightarrow D^*$$

$$D^* + A \overset{K_T}{\rightarrow} D + A^*$$

$$A^* \rightarrow A + h\nu'$$

D(D) – donor (excited state)*

A(A) – acceptor (excited state)*

K_T – rate of energy transfer

This process is limited by the rate of energy transfer (Eq.1) which is connected to the lifetime of the donor excited state in the absence of the acceptor (τ_D), Förster critical distance (R_0) and distance between donor and acceptor molecule (*R*).

$$K_T = \frac{1}{\tau_D}\left(\frac{R_0}{R}\right)^6 \qquad \textit{(Eq. 1.)}$$

The Förster critical distance (R_0) describes the distance at which the probability of the emission of fluorescence from the excited donor is equal to the probability of a non-radiative transfer of energy to the acceptor. R_0 takes different values for different donor-acceptor pairs and usually is in range of 1 to 10 [nm]. R_0 depends on: a) an orientation factor – relative orientation in space of the transition dipoles of the donor and acceptor (κ), b) quantum yield of the donor fluorescence in the absence of acceptor (Φ_D), c) overlapped integral in the region of the donor emission and acceptor absorbance spectra (wavelength expressed in nanometers) (J) and the reflective index of the medium (*n*). It is given as:

$$R_0^6 = \frac{9\,(ln\,10)\,\kappa^2\,\Phi_D J}{128\pi^5 n^4 N_A} \qquad \textit{(Eq. 2.)}$$

N_A – Avogadro number

The efficiency of energy transfer is linked with R_0 and depends on the intermolecular distance between the two fluorophores:

$$E = \frac{R_0^6}{R^6 + R_0^6} \qquad \textit{(Eq. 3.)}$$

[149]

E – transfer efficiency between a donor and an acceptor,
R – distance between a donor and an acceptor,
R_0 – Förster critical distance that results in a 50% energy transfer efficiency.

The biggest changes in transfer efficiency, leading to the highest sensitivity of FRET on the changes in distance, are observed between 0.5 R_0 to 1.5 R_0 (Fig.6.). Below and above these values, the sensitivity decreases because of the flattening of the transfer efficiency curve.

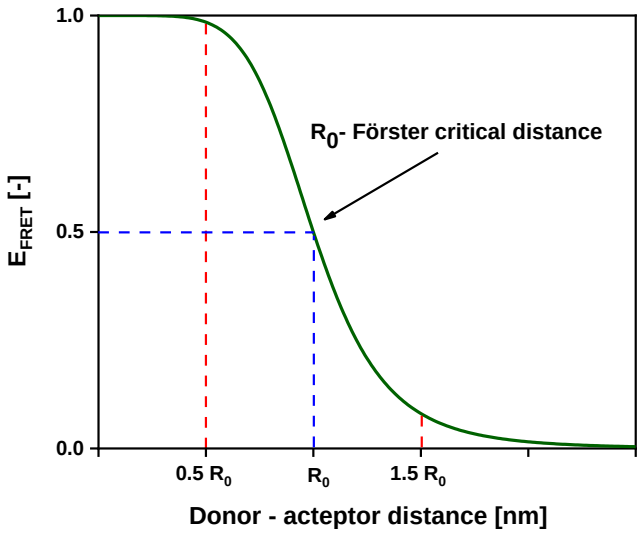

Fig. 6. The dependency of FRET efficiency (E_{FRET}) on the donor acceptor distance [149].

Due to the strong dependency of FRET on the distance between a donor and an acceptor, this method is widely used in studying molecular interactions (e.g. lipid interaction, membrane fusion, protein folding) in their natural environment. In my research, I used FRET to confirm and monitor the fusion of liposomes with EVs.

Liposomes for FRET experiments were labeled with 1 mol% of fluorescent FRET pairs: rhodamine B (cat. No. 810157C, Avanti Polar Lipids) and NBD (cat. No. 810143C, Avanti Polar Lipids). Both probes were conjugated with PE (Fig.7.). During the fusion, liposomes containing lipids conjugated with fluorescent probes, were diluted by the lipids in the membrane of nonfluorescent EVs. As a result, the distance between NBD and rhodamine increased which caused the decrease in fusion efficiency. This could be measured as a decrease in fluorescence intensity in the rhodamine maximum (583 nm) and increase in the fluorescent intensity in the NBD maximum (530 nm).

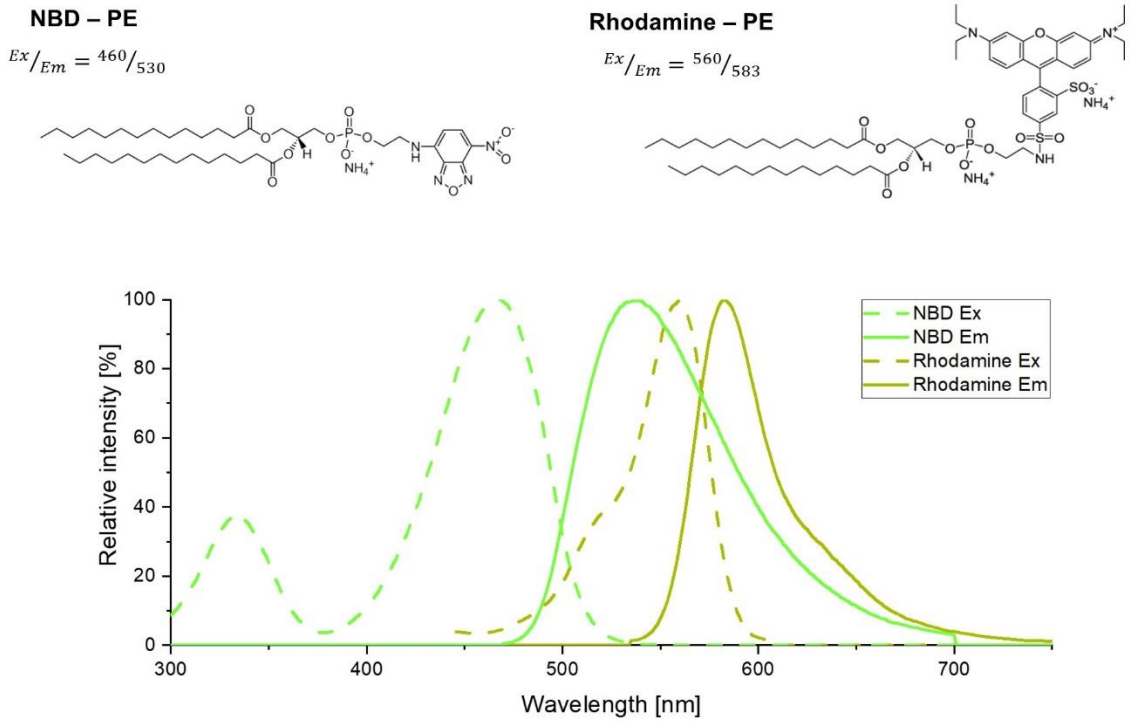

Fig. 7. Structure and spectra of NBD and rhodamine dye conjugated with PE.

Experimental set-up

The fluorescent probes, in the 1:1 ratio, were added to the lipid mixture before organic solvent evaporation and processed according to the protocol described in subsection 5.1.2. Fluorescent liposomes for three tested liposomes' compositions (DOPC, SM and PS) were mixed with EVs in the different ratios (Tab.2) and underwent series of freeze/thawing cycles

(up to ten cycles). Before the first, and after every second cycle, the fluorescence spectra in a range of 500 nm to 700 nm were measured, with the excitation wavelength of 460 nm on a spectrometer (Infinite 200 Pro plate reader, Tecan). Fusion efficiency was calculated, as an increase in intensity of fluorescence in the NBD maximum range according to the following equation:

$$fusion\ efficiency = \frac{I_{530}}{I_{530}+I_{580}} \qquad \textit{(Eq. 4.)}$$

I_{530} *– maximum fluorescence intensity for NBD component in the recorded spectra,*
I_{580} *- maximum fluorescence intensity for rhodamine component in the recorded spectra.*

In parallel to the FRET experiment, calibration curve for lipid dilution was prepared. Liposomes containing 1.00, 0.750, 0.500, 0.375 and 0.250 mol% of NBD-DMPE and rho-DMPE in 1:1 ratio were prepared according to the protocol described in subsection 5.1.2. These concentrations represent the lipid dilution ratio of 0.5, 1.0, 1.5 and 2.0, respectively. The spectra for calibration samples were measured after 10th cycle of freeze/thawing, fusion efficiency was calculated according to Eq.4. and plotted against lipid dilution.

3.3. Physical characteristics

3.3.1. Cryogenic Electron Microscopy

Cryogenic electron microscopy (cryo-EM) is a microscopic technique utilizing electron beam, in which samples in aqueous solution are preserved for observation by plunge-freezing in liquid ethane, or a mixture of liquid ethane and propane. In this method, samples are embedded within a thin amorphous ice film. Next, the samples are observed with a low dose transmission electron microscope operating at a liquid nitrogen temperature or below. The biggest advantage of this method is preserving the samples in near native state, in contrast to the traditional TEM microscopy where sample undergo dehydration, which influences the structure of molecules in the sample.

Experimental set-up

Samples for cryo-EM were prepared using Vitrobot (Thermofisher Inc.). Samples in a volume of 4 µl, with concentrations given in Tab.3., were placed on quantifoil holey carbon copper 400 mesh grids (cat. No. AGS173-3, Quantifoil®) in the Vitrobot chamber with 100% humidity at 24°C. Samples were left on the grid for 30 s, blotted with force settings set to 2 for 1 s, and then plugged into liquid ethane. Frozen samples were stored in liquid nitrogen before the imaging. Observations were performed on the JEOL JEM2100HT (Jeol Ltd) electron microscope in the cryo-mode, with the accelerating voltage equal to 80 kV.

Type of sample	Concentration
EVs	2.5 mg EVs protein /ml
Liposomes	2 µmol of lipids /ml
aEx	2.5 mg EVs protein /ml

Tab. 3. Concentration of samples prepared for Cryo-EM imaging. *The concentrations were calculated for the EVs proteins (EVs and aEx samples), and for the concentration of lipids in liposomes samples.*

3.3.2. Zeta-potential measurement

Every particle in the electrolyte is surrounded by ions which create an electric double layer. This layer consists of two parts: an inner region where the ions are strongly bound – called a Stern layer and an outer region with loosely bounded ions – called a diffuse layer. Between those layers, a slipping plane is present and the potential which exists at this boundary is called zeta potential or an electrokinetic potential.

The zeta potential can be measured by determining the electrophoretic mobility (Eq.5.). During the measurements, electric field is applied across the electrolyte and the charged particles move towards the electrode of opposite charge. Knowing the electrophoretic mobility value, zeta potential can be calculated based on Henry's equation:

$$\zeta = \frac{3\eta\mu_e}{2\epsilon f(\kappa a)} \qquad \textit{(Eq. 5)}$$

ζ – zeta potential,
η – viscosity,
μ_e – electrophoretic mobility,
ϵ – dielectric constant,
$f(\kappa a)$ – Henry's function.

By measuring the value of the zeta potential, it is possible to predict stability of particles in the colloidal system. When the zeta potential is higher than +30 mV or lower than -30 mV, the system is considered as stable.

Experimental set-up

Zeta potential measurements were performed using Malvern Nano ZS light scattering apparatus (Malvern Instrument Ltd., Worcestershire, UK). Zeta potential was measured using the technique of laser Doppler velocimetry (LDV). For the measurements, samples were diluted in PBS buffer filtered through a filter containing pores with a diameter of 50 nm. Each sample was measured 5 times and 100 scans were collected during a single measurement. Data were analyzed using Malvern Zetasizer 7.12 and OriginPro 2020 software.

3.3.3. Nanoparticle tracking analysis

Nanoparticle tracking analysis (NTA) is used for visualization and determination of the size distribution of nanoparticles, based on the measurement of light scattering and Brownian motions. During measurements, laser beam illuminates particles in a suspension. Particles scatter light which is recorded by a CCD camera for the chosen period of time. The software analyzes video sequence, tracks particles, and calculates the mean square displacement (MSD) in two dimensions. Based on that, the hydrodynamic diameter is calculated using Stokes - Einstein equation (Eq. 6). Because the volume in which Brownian motions are recorded is known, the software also calculates the concentration of particles in the suspension. Additionally, by using fluorescent probes, NTA can be used for phenotyping biological samples like EVs.

$$d_h = \frac{\kappa T}{3\pi\eta D_t} \qquad \textit{(Eq. 6)}$$

d_h – hydrodynamic diameter,
κ – the Botlzmann's constant,
T – temperature of the solvent (in Kelvins),
η – viscosity of the solvent,
D_t – translational diffusion coefficient.

The method has some limitations. A typical diameter of the particles which can be detected is in the range of 50 nm to 1000 nm, and the lower limit of detection strongly depends on the refractive index of the sample. Additionally, proper dilution of the sample is important, because having both high and low concentrations of particles can strongly influence the results calculation.

Experimental set-up

The measurements of the size distribution and concentration of liposomes, EVs and aEX were performed using NanoSight LM 10 (Malvern Panalytical), coupled with a 405 nm laser. For the NTA analysis, each sample was diluted to the appropriate concentration with PBS filtered through the filter with 50 nm pores. All samples were prepared in triplicates and measured in five independent records for 30 s. The measurements were analyzed and normalized to the starting sample volume using the OriginPro 2020 Software.

3.3.4. Western blot – extracellular vesicles

Western blot consist of two steps. In the first step, denatured proteins are separated in polyacrylamide gel according to the length of the peptide (SDS-PAGE type). In the second step, proteins are transferred in the electric field to the polyvinylidene difluoride (PVD) or nitrocellulose membrane where they can be recognized by specific primary antibodies. To visualize the proteins on the membrane, secondary antibody link with biotin or reporter enzyme (alkaline phosphatase or horseradish peroxidase) is used. More than one secondary antibody can bind to the primary antibody whereby the signal is enhanced. The signal is developed by the incubation with a substrate for enzyme, creating colored or luminescent product of reaction.

Experimental set-up

For western blot experiments, protein extracts (15 µg per sample) were diluted in a 1:1 ratio in the Laemmli Sample buffer (cat. No. 161-0737, Bio-Rad Laboratories Inc.) with 5% β-mercaptoethanol (cat. No. 161-0710, Bio-Rad Laboratories Inc), denatured in 95°C for 10 minutes, and then separated by electrophoresis on the 4-15% gradient Mini-PROTEAN TGX Stain-Free Protein Gels (cat. No. 4568085, Bio-Rad Laboratories Inc.). Afterwards, the samples were transferred to PVDF membranes using the Mini-Protean 3 system (Bio-Rad Laboratories Inc.).

Western blot analysis was performed using Lumi-Light^{PLUS} Western Blotting Kit (Mouse/Rabbit) (cat. No. 12015218001, Roche). The blots were blocked overnight in 1 % BSA in TBS/Tween buffer (0.05 M Tris-HCl, 0.15 M NaCl, 0.1% Tween 20, pH 7.5, Lumi-Light^{PLUS} Western Blotting Kit (Mouse/Rabbit) and incubated for 1h with specific primary antibodies against Arf-6 (dilution 1:200, cat. No. sc-7971, Santa Cruz Biotechnology), CD63 (dilution 1:500, cat. No. CBL553, Sigma Aldrich) and Del-1 (dilution 1:500, cat. No. SAB1406924, Sigma Aldrich). After incubation with the primary antibody, the membranes were washed three times with Tween/TBS buffer and incubated for 1h with a HRP-conjugated secondary antibody (Lumi-Light^{PLUS} Western Blotting Kit (Mouse/Rabbit)) diluted 1:250 in 1% BSA in TBS/Tween buffer. Afterwards, membranes were washed three times in the TBS/Tween Buffer and three times in the TBS buffer (0.05 M Tris-HCl, 0.15 M NaCl, 0.1%). Immunopositive bands were visualized using Lumi-Light Reagent (Roche) and ChemiDoc™ XRS^{+} System (Bio-Rad Laboratories Inc.). The relative levels of protein expression were determined using Lab Image software. Individual protein levels were normalized to the total intensity of the bands on a given line, detected in the gel after electrophoresis.

3.3.5. Encapsulation efficiency

The assay is based on the self-quenching properties of calcein. When calcein is entrapped in liposomes at high concentrations (50 mM), its fluorescence intensity is low. Once calcein is released from the liposomes, the fluorescence intensity increases due to the dilution of

calcein in the surrounding media. 0.1% Triton X-100 is used to solubilize the liposome membranes and release calcein. The entrapment efficiency can be calculated as the fluorescence quench according to Eq. 7.

$$\%\ quench = \left(1 - \frac{F}{F_T}\right) \times 100 \qquad \textit{(Eq. 7)}$$

F – fluorescence of the sample prior to the addition of 0.1% Triton X-100
F_T – fluorescence of the sample after the addition of Triton X-100

Experimental set-up

Calcein (cat. No. C0875, Sigma Aldrich), in the final concentration of 50mM, was added to PBS buffer and used to hydrate thin lipid films. After hydration, liposomes were prepared according to the subsection 5.1.2. Unencapsulated calcein was removed from the liposomes suspension using size exclusion chromatography (SEC) on Sepharose CL-4B (cat. No. CL4B200, Sigma Aldrich). Purified liposomes were fused with EVs in the 1:100 ratio.

As a reference method for calcein encapsulation, a modified calcium transfection method was used [151]. 50 µg of EVs were incubated with calcein solution in PBS (50 mM final concentration) and $CaCl_2$ in (0.1 M final concentration). The final volume was adjusted to 300 µl. The mixture was placed on ice for 30 min, then for heat shock at 42°C for 60 s, and finally on ice for additional 5 min.

Encapsulation efficiency was determined fluorometrically at the excitation and emission wavelengths of 490 and 515 nm, respectively, using a fluorescence spectrophotometer (Infinite 200 Pro plate reader, Tecan).

3.4. Biological tests

For all biological tests, HUVECs were seeded in different cell culture flasks, depending on the test, 48h before samples' collection (Tab.4). After 24h of culturing, cell culture media were changed to fresh ones (mixture of SFM and 199 media in a ratio 1:1, without serum) and HUVECs were stimulated with the tested factors for the following 14h. Samples were then collected and proceeded in a way suitable for further tests. To ensure reproducible

conditions of experiment the amount of EVs and the amount of anti-miR or negative control was calculated according to Tab.4..

Type of flask	Flask I	Flask II	6-well plate	24- well plate	96-well plate
Type of experiment	EVs isolation	Western blot/qPCR	Western blot/qPCR/ up-take	Wound healing assay /zymography	Cytotoxicity
Area/area of one well [cm^2]	75	25	9.6	1.9	0.3
Medium volume [ml]	10	3	1.5	0.25	0.1
Number of seeded cells	1 000 000	300 000	150 000	25 000	4 000
Density of seeded cells per cm^2	13 333	12 000	15 625	13 158	13 333
Amount of EVs protein [mg/ml]	1	0.3	0.15	0.025	0.01
Concentration of EVs proteins per ml of cell culture media [mg/ml]	0.1	0.1	0.1	0.1	0.1
Amount of anti-miR or negative control per well [pm]	-	-	150	25	5
Amount of miRNA per cell [fm/cell]	-	-	1	1	1.25

Tab. 4. Cells seeding density for all types of performed tests with the amount of EVs, anti-miR/negative control used in the performed experiments.

For all experiments (unless otherwise stated) eight different conditions were investigated. Symbols used for them are described below:

- NG – refers to HUVEC cells cultured in normoglycemic conditions (5 mmol of glucose) without any additional factors
- HG – refers to HUVEC cells cultured in hyperglycemic conditions (25 mmol of glucose) without any additional factors
- NG + EVs – refers to HUVEC cells cultured in normoglycemic conditions (5 mmol of glucose) stimulated with EVs
- HG + EVs – refers to HUVEC cells cultured in hyperglycemic conditions (25 mmol of glucose) stimulated with EVs
- HG + aEx - refers to HUVEC cells cultured in hyperglycemic conditions (25 mmol of glucose) stimulated with aEx, with encapsulated anti-miR
- HG + aEx_Del-1 - refers to HUVEC cells cultured in hyperglycemic conditions (25 mmol of glucose), stimulated with aEx with encapsulated anti-miR and decorated with Del-1 protein
- HG + Nc - refers to HUVEC cells cultured in hyperglycemic conditions (25 mmol of glucose), stimulated with aEx with encapsulated negative control (Nc)
- HG + anti-miR - refers to HUVEC cells cultured in hyperglycemic conditions (25 mmol of glucose), stimulated with anti-miR added to the cell culture media, without encapsulation in aEx or any other carrier.

3.4.1. Cytotoxicity tests

Influence of the synthesized particles on endothelial cells was assessed using ApoTox-Glow Triplex Assay (cat. No. G6321, Promega). ApoTox-Glo Triplex Assay applies simultaneous measurement of the activity of two proteases. The first one is a cell viability marker and second one is a cytotoxicity marker. Additionally, caspase activity, which is a hallmark of apoptosis, is measured.

Experimental setup

All assays were performed according to the manufacturers' protocols. In brief, 20 µl of the mixture of proteases substrates was added to each well and incubated for 30 minutes in 37°C. Then the fluorescence was measured on the Infinite 200 Pro F Plex plate reader (Tecan Inc.) at two wavelengths: $400_{Ex}/505_{Em}$ for viability and $485_{Ex}/520_{Em}$ for cytotoxicity. In the next step, caspase substrate in the volume of 100 µl was added to each well and cells were incubated at room temperature. After 30 minutes, the luminescence was measured on the same plate reader as fluorescence. The results were analyzed with OriginPro Software.

3.4.2. Cellular up-take – confocal microscopy

Staining of EVs for microscopic studies is very challenging. They are two strategies of staining isolated EVs, EVs-specific and non-EVs specific. In the first approach, probe recognizes a specific motif on the EVs surface (i.e. a protein or a glycoprotein). This interaction is strong, there is no leaking of the dye to the surrounding structures, but unfortunately it can influence EVs' up-take. In the second approach - non-specific EVs staining, lipophilic dyes such as PKH26 dye are widely used. In that approach it is crucial to prepare appropriate control due to the possible dye desorption from EVs to other compounds in the samples. On the other hand, this strategy does not interfere with EVs up-take [152].

Experimental set-up

To label EVs and aEx, a PKH26 dye (PKH26 Red Fluorescent Cell Linker Kit for General Cell Membrane Labeling, Sigma Aldrich, cat. No. PKH26GL) was used. EVs samples, containing

1 mg of proteins, were incubated with 0.4 µl of PKH26 in 200 µl of diluent C at room temperature for 30 min. Then, samples were blocked with 200 ul of 1% BSA solution. To remove unbound dye, samples were placed on an Amicon column (cat. No. UFC5100, Milipore), centrifuged and then washed with additional centrifugation in 400 µl of PBS. After staining, the PKH26-labeled carriers were resuspended in 1 ml of the cell culture medium. For imaging of aEx, anti-miR-221-3p labeled with FAD was used. Samples were prepared according to protocol described in section 5.1.4.

For confocal up-take experiments, HUVECs were cultured on glass slides. After 14 h of incubation, cells were washed three times with PBS and fixed with 3.7% formalin solution in PBS. Cells were dyed with phalloidine conjugated with Alexa Fluor™ 647 (cat. No. A22287, Invitrogen) to visualize the cytoskeleton and Hoechst dye (Hoechst 333342, cat. No. H1399 Invitrogen) to visualize nucleus, according to the manufacturers' protocols. Cellular uptake of the endothelial EVs was observed and recorded using Zeiss LSM 710 confocal laser microscope with an oil-immersion Plan-Apochromat 40x NA 1.4 objective (Carl Zeiss Microscopy GmbH), 633 nm (phalloidine), 561 nm (PKH26), 405 nm (Hoechst), and 488 nm (FAD) lasers.

3.4.3. qPCR

Quantitative Polymerase Chain Reaction (qPCR), is a widely used method for the assessment of the amount of a specific cDNA fragments in the sample. During the reaction, in every cycle n^2 new copies of specific cDNA matching to used primers are synthesized. Temperature changes during the cycle determine the steps of the procedure and the number of cycles. Due to the presence of a dye in the rection mixture, which exhibits fluorescence only after interaction with the double-stranded DNA, the method allows for the monitoring of the amount of the reaction product in real-time. With temperature changes, double-stranded DNA desaturates, the fluorescent signal disappears, and single-stranded DNA copies anneals with primers to synthesize n^2 new copies of DNA. Typical qPCR reaction consists of around 40 cycles.

Experimental set-up

qPCR analysis was performed to evaluate the level of mRNA for TIMP-3 after stimulation with EVs and aEx. Total RNA was isolated with Total RNA Mini Plus Concentrator (cat. No. 036-25C, A&A Biotechnology,) according to the manufacturer's protocol. Concentration of isolated RNA was evaluated on NanoDrop 2000 (Thermo Fisher Scienitific, Waltham, Massachusetts, USA) and the quality of isolated material was assessed based on ratio of

absorbance 260nm/280nm and 260nm/230nm. The value for both ratios over 1.8 was considered as acceptable for further analysis.

cDNA was synthesized with TranScriba Kit (cat. No. 4000- 20, A&A Biotechnology) according to the manufacturer's protocol; 0.5 μg of RNA template was used. The amplification reaction was performed using 3color Sensitive RT HS-PCR Mix SYBR® (cat. No. 2000- 250SM, A&A Biotechnology) according to the manufacturer's protocol. Primers for TIMP – 3 (cat. No. 10041595) and candidates for housekeeping genes – RPLP0 (ribosomal protein lateral stalk subunit P0, cat. No. 10041595), AKTB (β-actin, cat. No. 10025636) and TFRC (Transferrin receptor 1, cat. No. 10025636) were purchased from Bio-Rad (Bio-Rad Laboratories Inc.). Amplification was performed using QuantStudio 6 Flex Real-Time PCR System (Applied Biosystems, Foster City, California, USA). All samples were prepared with three biological replicates and three technical replicates.

In order to choose the most stable housekeeping gene, an analysis with NormFinder software was performed. According to the software, the most suitable gene is RPLP, with the calculated stability value of 0.033. RPLP was used to perform further results calculation as a housekeeping gene. ΔΔCt method was used to analyze the results and data was normalized to the NG+EVs samples.

3.4.4. Western blot – HUVEC cells

Western blot experiments and results analysis was performed as described in the subsection 5.3.4. Protein extracts (15 ug per sample) from HUVEC cells were denatured, separated on the electrophoresis gel, transferred to the PVDF membrane and incubated for 1h at RT with a primary antibody against TIMP-3 (dilution 1:100, cat. No. sc-373839, Santa Cruz Biotechnology). After incubation for 1h with a HRP-conjugated secondary antibody, immunopositive bands were visualized using ChemiDoc™ XRS$^+$ System. Relative levels of TIMP-3 expression were determined using Lab Image software. Individual protein levels were normalized to the total intensity of the bands in a given line, detected in the gel after electrophoresis.

3.4.5. Zymography

Zymography is a method which allows for the assessment of the activity of matrix metalloproteinases in cells, tissues, or cell culture media. It is a variation of the SDS-PAGE electrophoresis, in which the gel additionally contains protease substrate – gelatin – which is digested by active gelatinases (MMP-2 and MMP-9). The assay was used to assess MMP-2 and MMP-9 activity in cell culture media which were collected from HUVEC cell cultures dedicated for western blot analysis. After stimulation with investigated factors, as described in previous section, cell culture media were centrifuged (400g, 5 min, 4°C) to remove cell debris and stored for further analysis.

Gels containing 0.1% of gelatin (cat. No. G6650, Sigma Aldrich) were prepared according to the previously described protocol [153]. Briefly, separating gel was prepared by mixing: 10 ml of separation gel buffer stock (1.88 M Tris-HCl, pH = 8.8) with 17.8 ml dH_2O, 5ml of 1% gelatin, 16.6 ml of acrylamide-bis-acrylamide stock (cat. No. 1610158, Bio-Rad Laboratories Inc.), 0.25 ml of 20% SDS, 150 µl of 10% APS and 30 µl of TEMED. Immediately after adding TEMED, around 5 ml of gel was placed between the electrophoresis glass plates, covered with a 5 mm layer of water and left for 1h to polymerize at RT. Stacking gel was prepared by mixing: 2 ml of stacking gel buffer stock (1.88 M Tris-HCl, pH = 6.8) with 11 ml dH_2O, 2 ml of acrylamide-bis-acrylamide stock, 0.1 ml of 20% SDS and 75 µl of 10% APS and 10 µl of TEMED. After gel polymerization, water was decanted and the separating gel was overlayed with the stacking gel. Gels were left for 1h in room temperature to polymerize.

Cell culture media samples (20 µl per sample) were diluted 3:1 in the Laemmli Sample buffer (cat. No. 161-0747, Bio-Rad Laboratories Inc.) and loaded to the previously prepared zymography gels. Samples were separated with electrophoresis and washed twice with 2.5% Triton X-100 for 15 min, rinsed with miliQ water, and incubated in a developing buffer (50mM Tris-HC, pH 7.8, 15 mM NaCl, 5 mM $CaCl_2$) for 15 min in RT. The developing buffer was then exchanged for the fresh one and the gels were incubated overnight at 37°C with gentle agitation. They were then stained with Coomesie Blue (cat. No. 200-107, Kucharczyk

Techniki Elektroforetyczne) for 1h at RT and incubated in a destaining solution (10% methanol, 5% acetic acid in dH_2O) until areas of gelatinolytic activity appeared as clear sharp bands. Images of the stained gels were recorded using UVtec camera and analyzed with ImageLab software.

3.4.6. Wound healing assay

Wound healing assay was performed in order to evaluate cell migration and their ability to perform wound healing, after stimulation with the investigated factors. During wound healing assays, confluent cells migrate to the artificially crated wound (space without cells) in order to fill the empty space and close the wound. To evaluate the results, the degree of wound closure can be calculated as a confluency index (CI). CI is defined as a percentage of an area covered by cells after a given time of incubation, compared to the area of the wound at time t = 0 h (Eq. 8).

$$CI = \left(1 - \frac{area\ uncovered\ by\ cells\ after\ 14\ h}{area\ of\ the\ wound}\right) \times 100\% \quad \textit{(Eq. 8)}$$

Experiment set-up

HUVECs were seeded in Ibidi inserts (cat. No. 80209, Culture Inserts 2-Well Ibidi) on 12-well plates at a density of 44,000 cells/cm^2 (Tab.4.). For all tested conditions, samples were prepared in triplicates. After 24 h of culturing in standard media, inserts were removed, cells were washed twice with PBS and placed in fresh culture media containing tested carriers. Immediately after the removal of the inserts (t = 0 h) and after 14 h of incubation in experimental conditions (t = 14 h) four microscopic images of each wound area were recorded. A confluence index (CI) was chosen as a parameter to assess cell migration. Results were analyzed using Image J software.

2.5. Statistics and graph design

All statistical analyses and graph designs were performed with the OriginPro 2020 software (OriginLab Corporation, Northampton, USA). The distribution types of different datasets were validated using the Shapiro-Wilk normality test. For the data with normal distribution, t-student test was used to compare the differences between two independent groups. In case of non-normally distributed data, Mann-Whitney U test was used for the same purpose. Statistical analysis for these biological test was performed only between chosen pairs which correspond to the aims of the project and chosen research questions. The studied pairs were: HG+aEx *vs* HG+EVs, HG+aEx *vs* NG+EVs, HG+aEx *vs* HG+aEx_Del-1, HG+aEx *vs* HG+Nc*,* HG+aEx *vs* HG+anti-miR*,* NG+Evs *vs* HG+EVs*,* NG *vs* NG+EVs, and HG *vs* HG+EVs. When non-parametric comparisons between more than two groups were performed, Kruskal-Wallis Anova, followed by Dunn's multiple comparison test was used.

Data on the graphs for biological tests was normalized to the level of the investigated factor: NG+EVs, as these conditions were considered the closest to the physiological.

4. Results

4.1. Monitoring fusion efficiency – FRET experiments

FRET experiments were performed in order to establish the most efficient synthesis protocol and to confirm, that the fusion between EVs and liposomes can occur. They were performed for the three types of liposomes: DOPC, SM, and PS (containing given lipid in the concentration of 70 mol%). Liposomes were mixed in the different ratios, between the lipids in liposomes and proteins in EVs (1:8, 1:16, 1:32, 1:50, and 1:100 ratios, as described in detail in section 2.2). The emission spectra of the samples were measured before the first freeze/thawing cycle and after every second cycle, for the continuous monitoring of the progress of fusion.

In this experimental set-up, when the fusion occurs between liposomes and EVs, a decrease in the fluorescence intensity near 580 nm (NBD emission maximum) and a simultaneous increase in fluorescence intensity near 530 nm (rhodamine emission maximum) should be observed. This is a result of increasing the distance between the two used fluorophores, which decreases the efficiency of the non-resonant energy transfer between the dyes. This can be attributed to the dilution of the dyed lipids in the liposomes' membrane with undyed proteins and lipids, coming from the membrane of EVs.

Examples of the fluorescence spectra recorded after subsequent freeze/thawing cycles, obtained for two mixing ratios: 1:8 and 1:100, are shown in Fig.8A (for the DOPC-based liposomes), Fig.9A (for the SM-based liposomes) and Fig.10A (for the PS-based liposomes). Changes between subsequent freeze/thawing cycles were more prominent if the samples were mixed in higher ratios (e.g. 1:100), for all studied systems.

The most distinguishable changes in the intensity maxima were observed for the DOPC-based liposomes, mixed with the EVs in the 1 to 100 ratio (Fig.8A). Changes in the characteristic emission maxima of the two fluorescent dyes are clearly visible on the graphs, and the corresponding intensities gradually change with the freeze/thawing cycle number. For the SM- and PS- based samples, some changes were observed. However, the

simultaneous change in the two characteristic fluorescence maxima, characteristic for the fusion process, was observed only for PS-based liposomes, mixed with EVs in the 1 to 100 ratio.

For the analysis of recorded emission spectra, fusion efficiency was calculated (described in detail in Eq.4., section 2.2). The results show, that the fusion efficiency gradually increases with the number of performed freeze/thawing cycles for all types of liposomes (Fig.8B, Fig.9B, and Fig. 10B). For the DOPC-based samples, fusion is more efficient if the liposomes and EVs are mixed in higher ratios, with the highest fusion efficiency obtained for the 1 to 100 ratio.

DOPC-based liposomes, which were subjected to the freeze/thawing procedure without the addition of EVs, showed only a very slight increase in the calculated fusion efficiency parameter. This is expected, because this experiments serves as a negative control for the actual fusion experiments.

In case of PS-based liposomes, subjected to the freeze/thawing procedure without EVs, a significant increase in the calculated fusion efficiency after every second cycle was observed. It has to be stressed, that this doesn't correspond to the actual fusion processes, since no EVs were present during freeze/thawing procedure, but rather describes internal changes in the system affecting the efficiency of the non-radiative energy transfer between the dyes.

SM-based samples were characterized by the strongly fluctuating values of the calculated fusion efficiency. This was especially notable for the samples freeze/thawed without the addition of EVs.

The values of the final fusion efficiencies, and calculated lipid dilutions after 10^{th} freeze/thawing cycle are shown in Tab. 5. Lipid dilutions were calculated based on the calibration curves (described in detail in section 2.2) . When the parameter of lipid dilution has a value of 1, this corresponds to the situation, when, on average, a single liposome has completely fused with a single EV. Alternatively, this means that exactly half of the material in the artificial exosome comes from the liposome, while the other half comes from the EV.

This result was obtained for the samples containing DOPC-based liposomes (1.04 ± 0.11) mixed with EVs in the 1 to 100 ratio. Additionally, DOPC-based liposomes were characterized by the lowest value of lipid dilution, if the sample underwent freeze/thawing cycles without addition of EVs (0.35 ± 0.06).

The largest difference in the lipid dilution ratio was observed for the PS-based samples. The value, in case of the samples which underwent freeze/thawing procedure without the addition of EVs was equal to 0.80 ± 0.04. In case of liposomes fused with EVs in the 1 to 100 ratio, it was equal to 1.99 ± 0.24, which is over two times higher than in case of the original liposomes.

For the SM samples, little differences in the lipid dilution ratios were observed, regardless of the chosen ratio between liposomes and EVs. In case of the samples subjected to the freeze/thawing procedure without the addition of EVs lipid dilution ratio was equal to 0.47 ± 0.02, while for the ones mixed with EVs in the 1 to 100 ratio it was equal to 0.57 ± 0.09.

Type of sample	**Parameter**	**0**	**1 to 8**	**1 to 16**	**1 to 32**	**1 to 50**	**1 to 100**
DOPC	Fusion efficiency	0.19 ± 0.01	0.08 ± 0.00	0.11 ± 0.00	0.19 ± 0.03	0.22 ± 0.04	0.28 ± 0.02
	Lipid dilution	0.35 ± 0.06	-0.53 ± 0.02	-0.29 ± 0.00	0.33 ± 0.21	0.59 ± 0.31	1.04 ± 0.11
PS	Fusion efficiency	0.28 ± 0.01	0.20 ± 0.05	0.27 ± 0.08	0.32 ± 0.06	0.32 ± 0.05	0.44 ± 0.03
	Lipid dilution	0.80 ± 0.04	0.15 ± 0.34	0.72 ± 0.60	1.03 ± 0.30	1.09 ± 0.35	1.99 ± 0.24
SM	Fusion efficiency	0.47 ± 0.02	0.40 ± 0.04	0.42 ± 0.03	0.45 ± 0.02	0.45 ± 0.02	0.49 ± 0.01
	Lipid dilution	0.47 ± 0.02	-0.03 ± 0.29	0.10 ± 0.19	0.30 ± 0.15	0.34 ± 0.11	0.57 ± 0.09

Tab. 5. The average fusion efficiency for the measurement performed after 10th freeze/thawing cycle and corresponding lipid dilutions calculated based on the calibration curve equation.

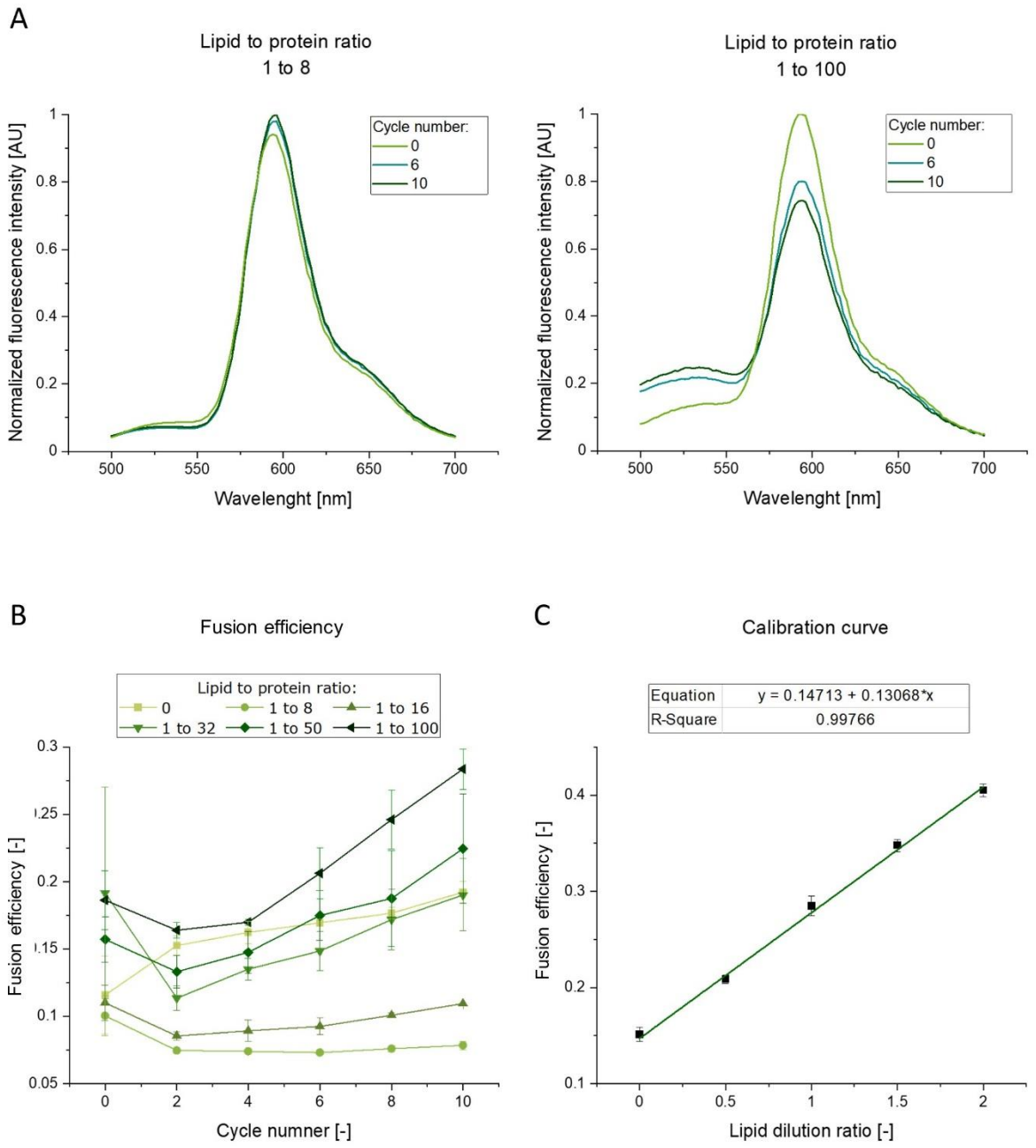

Fig. 8. Results of the FRET experiments for the liposomes containing 70 mol% of DOPC and 30 mol% of DC-Cholesterol. *A - an example of the emission spectra of samples mixed in 1 to 8 ratio and 1 to 100 ratio with EVs. The presented spectra were recorded before the first freeze/thawing cycle (cycle 0) and after 6^{th} and 10^{th} cycle. B - dependence of the fusion efficiency on the cycle number. The graph presents five different mixing ratios (1 to 8, 1 to 16, 1 to 32, 1 to 50, and 1 to 100) and the results calculated for sample of liposomes without EVs. C - calibration curve of the fusion efficiency and corresponding lipid dilution ratio.*

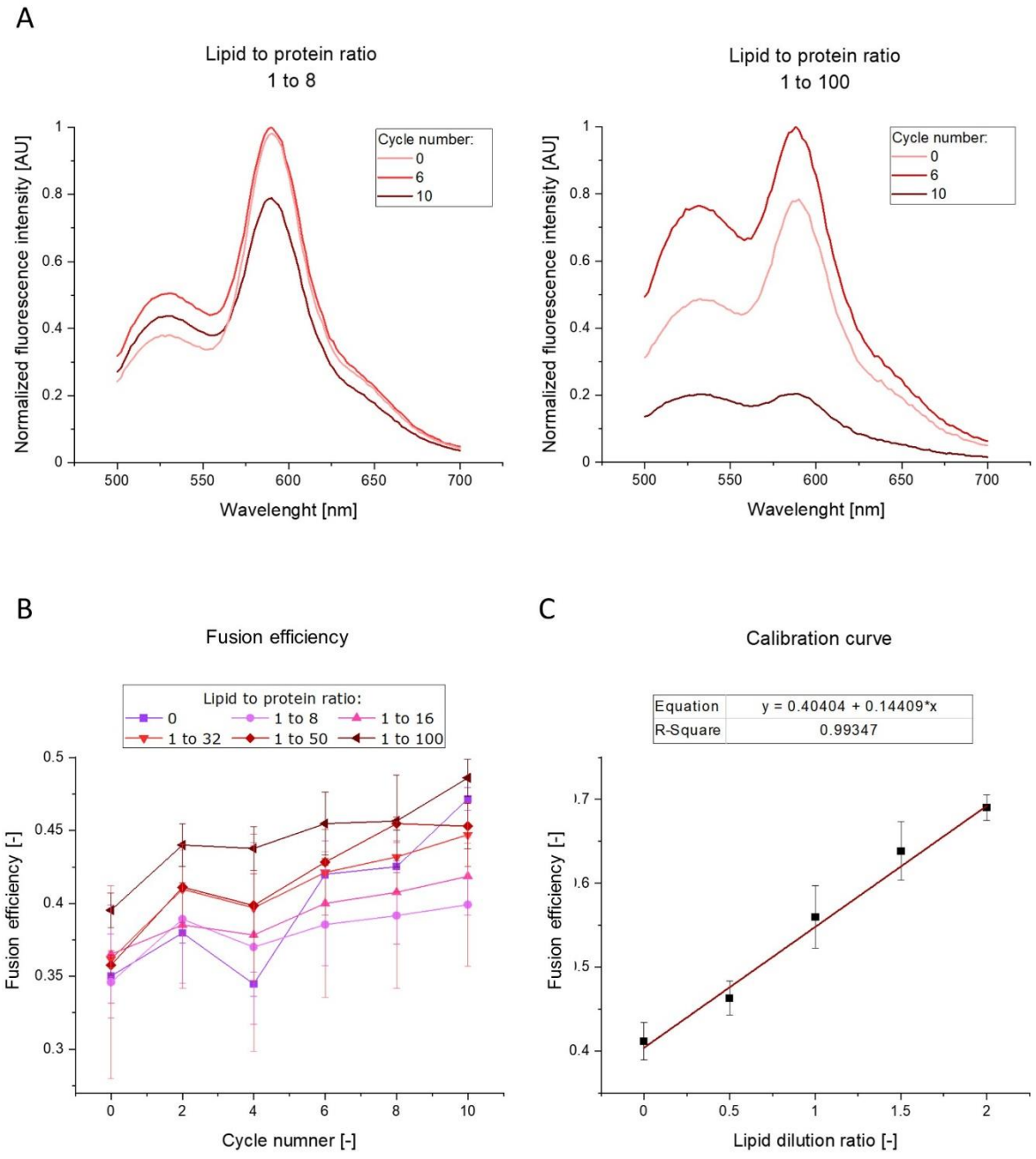

Fig. 9. Results of the FRET experiments for the liposomes containing 70 mol% of SM and 30 mol% of DC-Cholesterol. *A - an example of the emission spectra of samples mixed in 1 to 8 ratio and 1 to 100 ratio with EVs. The presented spectra were recorded before the first freeze/thawing cycle (cycle 0) and after 6^{th} and 10^{th} cycle. B - dependence of the fusion efficiency on the cycle number. The graph presents five different mixing ratios (1 to 8, 1 to 16, 1 to 32, 1 to 50, and 1 to 100) and the results calculated for sample of liposomes without EVs. C - calibration curve of the fusion efficiency and corresponding lipid dilution ratio.*

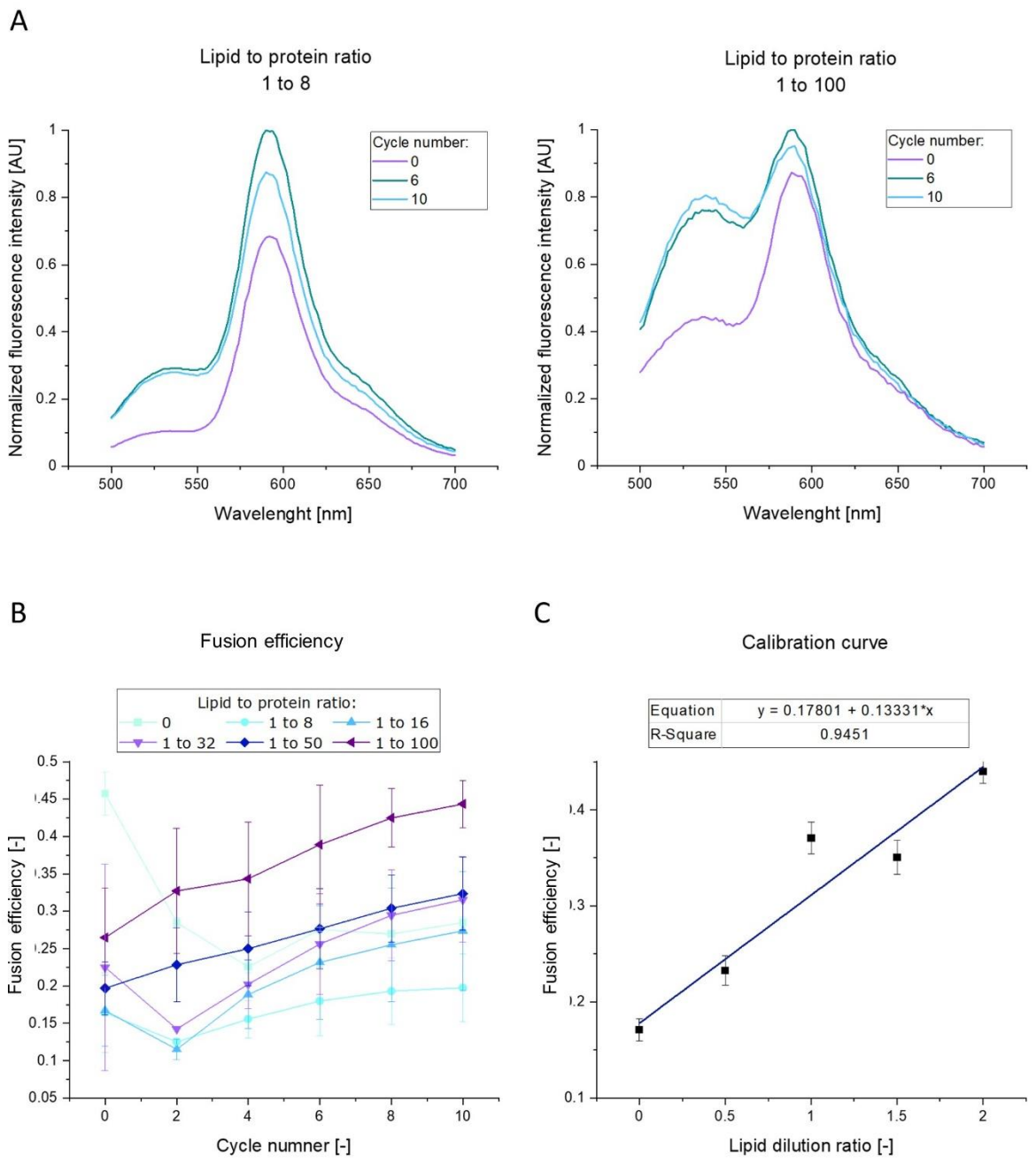

Fig. 10. Results of the FRET experiments for the liposomes containing 70 mol% of PS and 30 mol% of DC-Cholesterol. *A - an example of the emission spectra of samples mixed in 1 to 8 ratio and 1 to 100 ratio with EVs. The presented spectra were recorded before the first freeze/thawing cycle (cycle 0) and after 6th and 10th cycle. B - dependence of the fusion efficiency on the cycle number. The graph presents five different mixing ratios (1 to 8, 1 to 16, 1 to 32, 1 to 50, and 1 to 100) and the results calculated for sample of liposomes without EVs. C - calibration curve of the fusion efficiency and corresponding lipid dilution ratio.*

4.2. Physical characterization of the extracellular vesicles, liposomes and artificial exosomes

FRET experiments, described in section 3.1, confirmed that the fusion between liposomes and EVs can occur. From this section, the particles created by this process will be referred to as the artificial exosomes (aEx). The subscript in the abbreviation will refer to the type of the liposomes, which underwent fusion with the EVs. For example, aEx_{DOPC}, will refer to the artificial exosomes, created by fusing EVs with the DOPC-based liposomes.

Additionally, because FRET experiments showed that the samples mixed in the 1 to 100 ratio had the highest fusion efficiency, this dilution was chosen as an optimal one to synthesize aEx. All the following experiments were performed for the liposomes mixed with EVs in 1 to 100 ratio.

4.2.1. Cryo-TEM

Cryo-TEM imaging was performed in order to visualize liposomes, aEx and EVs (representative micrographs are shown in Fig.11.). DOPC-based liposomes were characterized by the highest homogeneity. The particles were around 150 nm in diameter, mostly unilamellar and were present in high concentration. The SM-based liposomes were visible in lower numbers, with a larger variation in size (70 nm to 400 nm). Additionally, the membrane of particles was often pleated and some multilamellar particles were visible. PS-based liposomes were visible in the lowest amount (only several objects in the field of view). Their membranes were smooth, and they diameter was equal to around 130 nm.

EVs were clearly visible during characterization, with several objects in the field of view. Their diameter varied strongly (60 nm to 350 nm) and both unilamellar and multilamellar particles were observed. $aEx_{DOPC,}$ similarly to the DOPC-based liposomes were observed in high concentration, with the diameter of around 150 nm. Their membranes were smooth and an area with high electron density was observed in the particles' centers. Unfortunately, for aEx_{SM} and aEx_{PS} no objects were detected, despite the fact that several attempts have been made and several modifications were introduced to the sample preparation protocols (for example, increasing the concentration of liposomes and EVs).

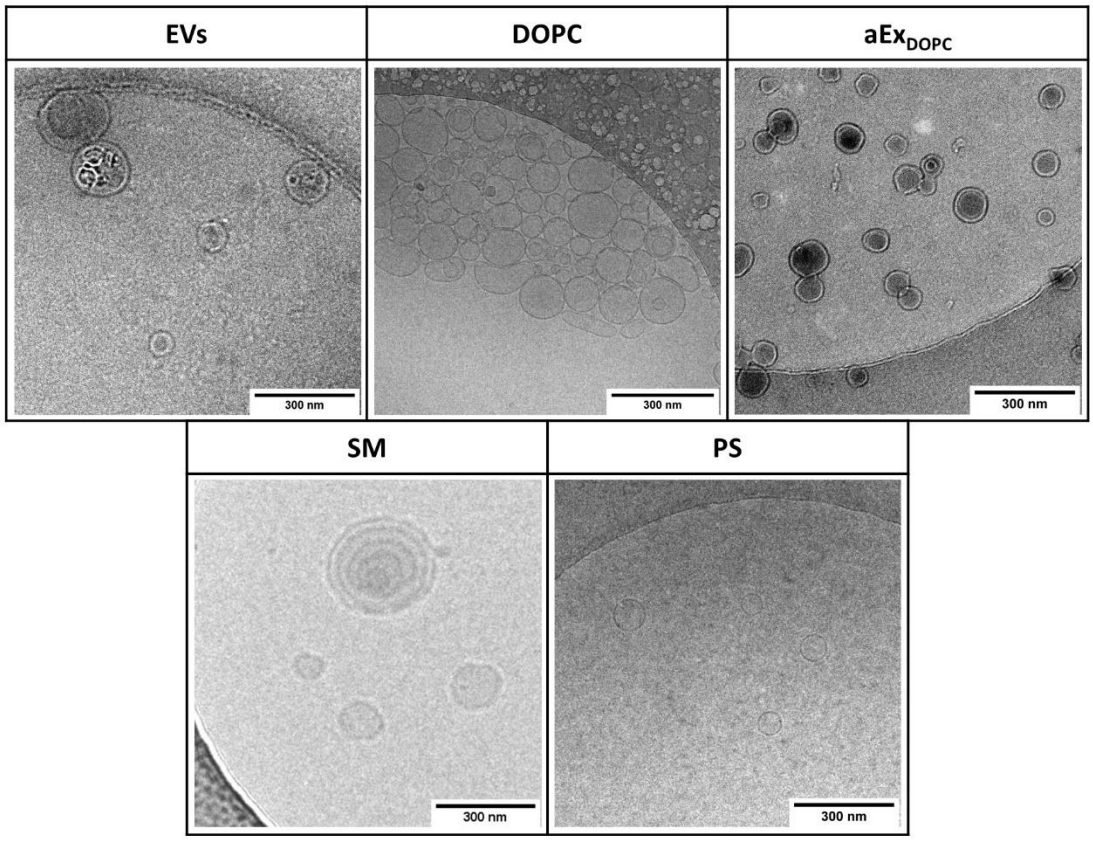

Fig. 11. Cryo-TEM images of the liposomes (DOPC, SM, and PS), aEx$_{DOPC}$, and EVs.

4.2.2. Changes in the zeta-potential

Dynamic light scattering measurements were performed in order to evaluate the zeta-potential of EVs, liposomes (DOPC, SM, and PS), and corresponding aEx (aEx$_{DOPC}$, aEx$_{SM,}$ aEx$_{PS}$). In order to ensure that the observed differences in measured parameters are not a an artificial effect, related to the mixing of two different samples, but the result of the fusion process, additional samples were measured. They consisted of liposomes mixed with EVs in the same ratio as in the aEx samples (in 1 to 100 ratio), but they didn't undergo freeze/thawing procedure (DOPC+EVs, SM+EVs, PS+EVs). The distributions of zeta potential for all the tested samples are presented in Fig.12.

The results show, that EVs have a negative value of zeta-potential (see Tab.6.). The DOPC and SM liposomes had a positive zeta-potential value, while the PS liposomes were characterized by the negative value of zeta-potential.

Comparison of the zeta-potentials of liposomes mixed with EVs (without performing freeze-thawing procedure), and aEx, show that for all the tested samples there was a change in zeta-potential values. However, only in case of the liposomes composed of DOPC and aEx_{DOPC}, the change was statistically significant.

	ζ_{EVs} [mV]	$\zeta_{liposomes}$ [mV]	$\zeta_{liposomes+EVs}$ [mV]	ζ_{aEx} [mV]	P
DOPC	-12.3 ± 3.0	30.6 ± 4.0	-27.7 ± 5.6*	-19.2 ± 6.0*	0.009
SM		30.5 ± 4.4	-18.5 ± 8.1	-23.4 ± 6.1	0.242
PS		-14.6 ± 4.5	-18.2 ± 6.0	-16.1 ± 4.1	0.450

Tab. 6. Mean absolute values of the zeta potential (ζ) calculated for EVs, liposomes, aEx, and mixture of EVs with liposomes (liposomes + EVs).

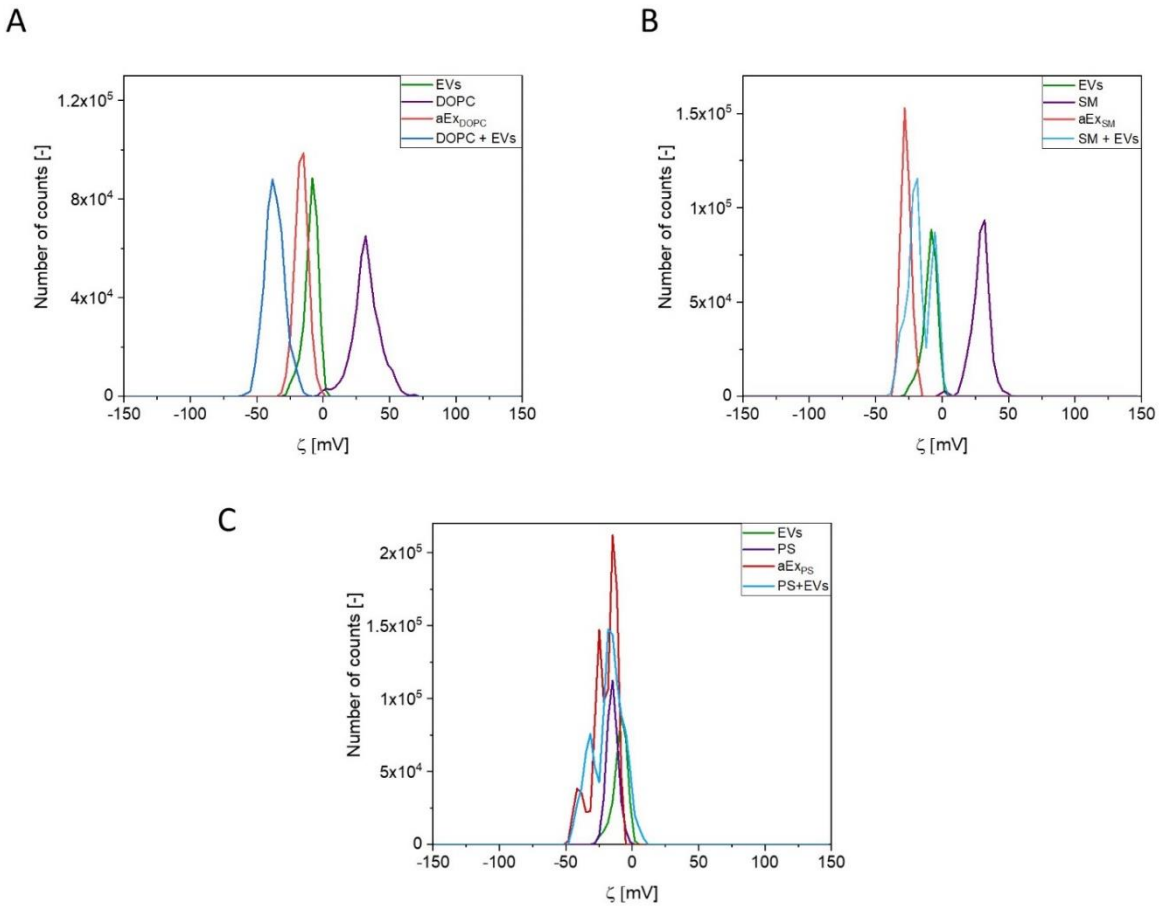

Fig. 12. Representative graphs of zeta-potential. *The graphs presents results of measurement for EVs samples, DOPC (A), SM (B), PS (C) liposomes, corresponding aEx as well as mixture of liposomes and EVs before freeze/thawing cycles.*

4.2.3. Diameter and concentration measurements – NTA analysis

NTA measurements were performed in order to evaluate a mean diameter, size distribution and concentration of the samples (Fig.13.) The analysis was performed for the three types of liposomes (DOPC, SM, and PS) and the corresponding types of aEx (aEx_{DOPC}, aEx_{SM}, aEx_{PS}). Similarly, to the DLS experiments, measurements were conducted also for the mixture of liposomes and EVs before freeze/thawing cycles, in order to ensure that the observed changes are a result of the fusion of EVs and liposomes. All the measured concentrations were normalized to the starting volume of the sample.

The results show that the size of EVs used in the experiments had multimodal distribution, with an average diameter of 111.1 ± 13.0 nm and the mode value equal to 77.6 ± 8.1 nm (Tab.7.). The samples of liposomes were characterized by an unimodal size distribution, regardless of the type of liposomes. The average diameter of liposomes was also similar from 107.5 ± 4.6 nm for the DOPC liposomes, to 131.3 ± 4.4 nm, for the SM liposomes. The mode values for the liposomes were a few nm lower than the mean diameter.

Statistical analysis showed, that for all liposomes types, the average diameter of aEx was significantly lower, than for the mixture of liposomes and EVs without freeze-thawing cycles. Similarly, the mode value was lower, but the difference was statistically significant only in case of the DOPC and PS samples.

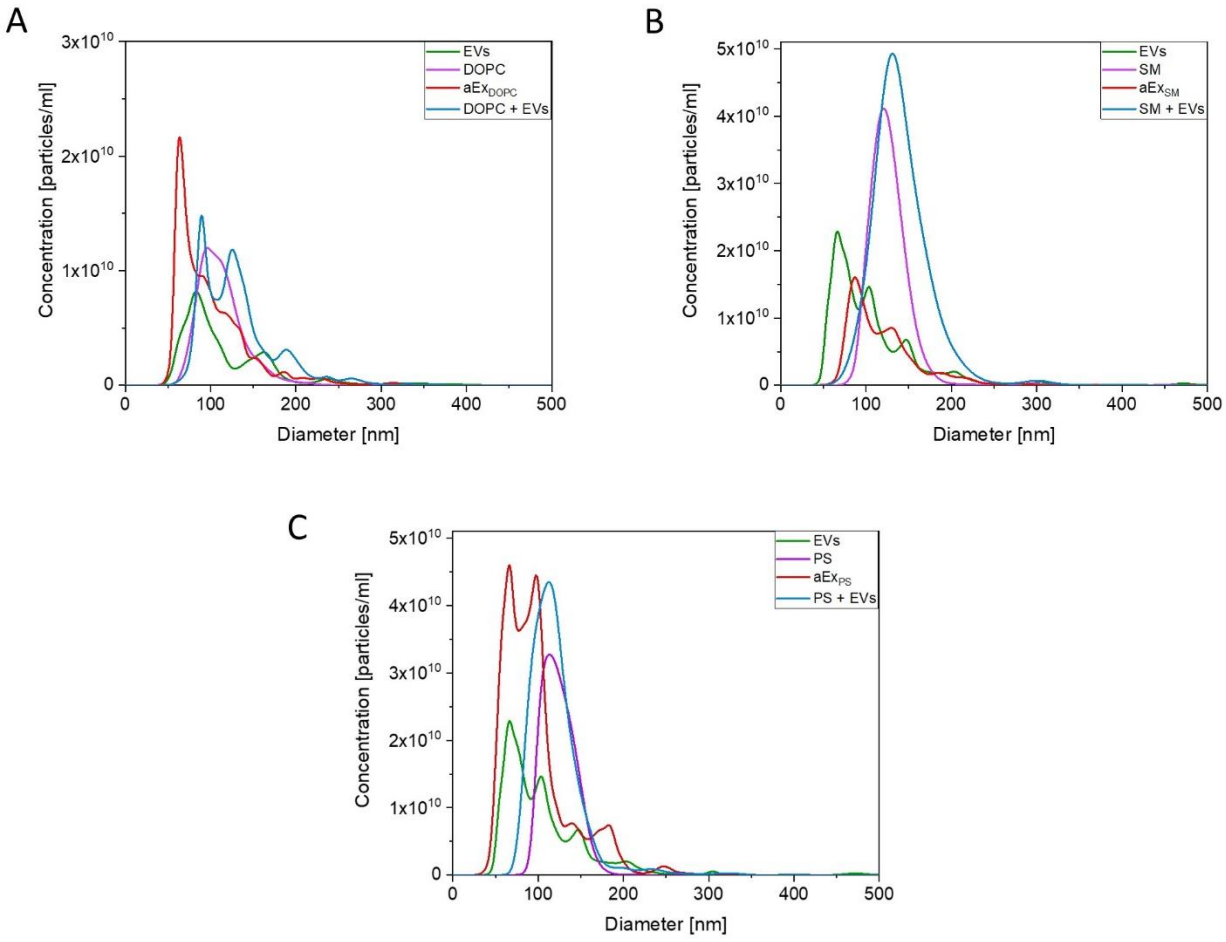

Fig. 13. Size distribution of the EVs, liposomes, aEx and mixture of liposomes and aEx before performing freeze/thawing cycles for the three different types of liposomes: DOPC (A), SM (B), and PS (C).

Concentration measurements showed, that the concentration of EVs and liposomes, prepared for the freeze/thawing procedure, are within the same order of magnitude. For aEx_{DOPC} and aEx_{PS} samples, concentration of artificial exosomes was higher than the concentration of the corresponding samples of liposomes and EVs. However this difference was not statistically significant. For the aEx_{SM}, opposite dependency was observed: the concentration of artificial exosomes was significantly lower than the concentrations of the corresponding samples of liposomes and EVs.

DOPC	EVs	DOPC	aEx_{DOPC}	DOPC+EVs	P
Concentration [particles/ml]	$9.18 \times 10^{11} \pm 8.77 \times 10^{10}$	$5.57 \times 10^{11} \pm 3.22 \times 10^{10}$	$7.41 \times 10^{11} \pm 2.80 \times 10^{10}$	$1.21 \times 10^{11} \pm 2.95 \times 10^{10}$	0.38
Diameter [nm]	111.1 ± 13.0	107.5 ± 4.6	96.1 ± 6.5*	121.7 ± 8.0*	<0.001
Mode [nm]	77.6 ± 8.1	98.7 ± 6.9	73.3 ± 6.0*	106.0 ± 4.1*	0.013
SM	EVs	SM	aEx_{SM}	SM +EVs	P
Concentration [particles/ml]	$9.18 \times 10^{11} \pm 8.77 \times 10^{10}$	$2.57 \times 10^{11} \pm 8.64 \times 10^{9}$	$7.50 \times 10^{11} \pm 5.18 \times 10^{10}$ *	$3.27 \times 10^{12} \pm 1.48 \times 10^{11}$ *	0.028
Diameter [nm]	111.1 ± 13.0	131.3 ± 4.4	116.4 ± 10.4*	141.7 ± 2.5*	0.001
Mode [nm]	77.6 ± 8.1	125.5 ± 6.3	87. ± 10.7	129.1 ± 4.5	0.052
PS	EVs	PS	aEx_{PS}	PS + EVs	P
Concentration [particles/ml]	$9.18 \times 10^{11} \pm 8.77 \times 10^{10}$	$3.33 \times 10^{11} \pm 8.42 \times 10^{9}$	$1.82 \times 10^{12} \pm 1.64 \times 10^{11}$	$6.26 \times 10^{11} \pm 1.44 \times 10^{10}$	0.052
Diameter [nm]	111.1 ± 13.0	126.9 ± 0.7	103.9 ± 7.1*	122.5 ± 3.8*	<0.001
Mode [nm]	77.6 ± 8.1	118.0 ± 3.2	85.5 ± 6.6*	111.4 ± 3.1*	0.001

Tab. 7. Results of the NTA measurements: concentrations. mean diameter and mode presented as a mean value of three independent measurements with SD. *Differences between subgroups were tested with Mann Whitney Test ($p<0.05$). * indicates significance in comparison between aEx and liposomes mixed with EVs (DOPC+EVs, SM+EVs, PS+EVs).*

4.2.4. Analysis of the presence of the typical EVs markers

Western blot experiments were performed to evaluate whether characteristic markers of EVs (CD63 and Arf-6) are detectable in the samples after the fusion procedure (after synthesizing aEx). Analysis was based on the measured intensities of the bands, which were normalized to the total protein band intensities detected on the gel after electrophoresis.

Western blot analysis showed a clear presence of both markers in case of the samples of pure EVs. Additionally, results confirmed that after the fusion of EVs with liposomes the CD63 and Arf-6 remain detectable in the AEx samples, regardless of the type of the used liposomes. No statistically significant differences were observed between the analyzed samples. (Fig.14.).

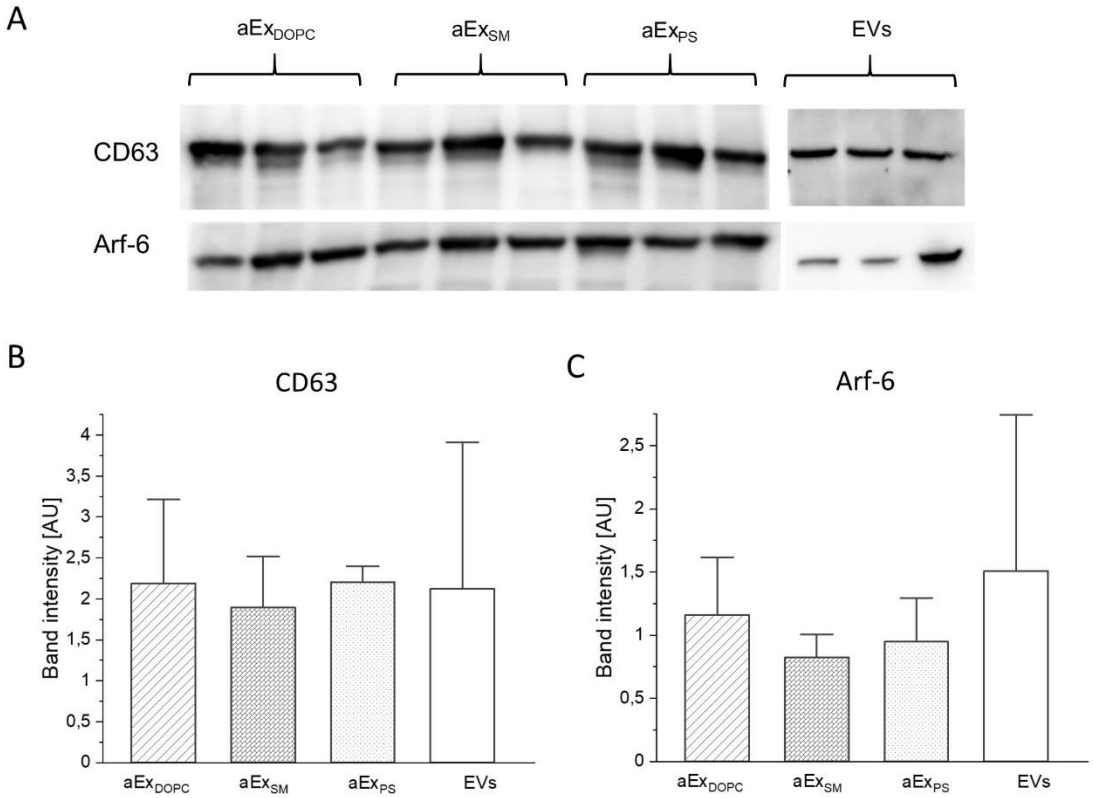

Band intensity [-]	CD63	Arf-6
aEx$_{DOPC}$	2.11 ± 0.68	1.16 ± 0.30
aEx$_{PS}$	2.20 ± 0.13	0.95 ± 0.23
aEx$_{SM}$	1.89 ± 0.42	0.82 ± 0.12
EVs	2.13 ± 1.19	1.51 ± 0.82

Fig. 14. The results of the analysis of the presence of CD63 and Arf-6 in EVs and aEx samples*. A – the images of the PVDF membrane with the visible bands, B - analysis of the band intensities for CD63, C - analysis of the band intensities for Arf-6. Results were normalized to the total band intensities on the gel after electrophoresis and presented as the average values with standard deviation [whiskers]. The statistical analysis was performed with Kruskal-Wallis Anova, comparison among the groups was performed with Dunn's post-hoc test($p<0.05$). Because there was no statistically significant differences between the samples, p values are not presented in the table.*

4.2.5. Decoration of aEx and EVs with Del-1 protein

Western blot experiments were performed in order to confirm the successful decoration of aEx with the Del-1 protein. Del-1 protein is present in the samples of natural EVs, which was confirmed by the experiments. Incubation with Del-1 protein increases its amount for the samples of EVs and aEx. However, statistically significant difference was observed only between the samples of incubated aEx and non-incubated EVs.

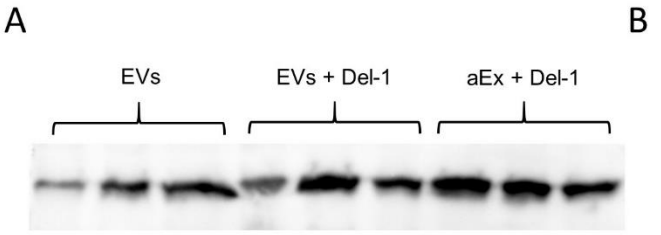

	Average normalized band intensity [-]	p sample
EVs	0.38 ± 0.04	0.032 aEx+Del-1
EVs + Del-1	0.63 ± 0.15	0.093 Evs
aEx + Del-1	0.85 ± 0.38	1.000 EVs+Del-1

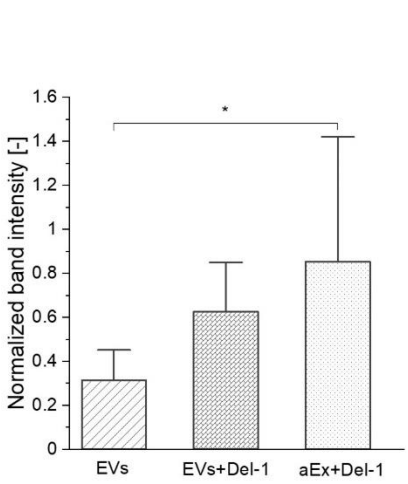

Fig. 15. The results of the western blot for the presence of Del-1 protein. *A – the images of the PVDF membrane with visible bands, B - analysis of the band intensities. Results were normalized to the total band intensities on the gel after electrophoresis and presented as the average values with standard deviation [whiskers]. The statistical analysis was performed with Kruskal-Wallis Anova, comparison among the groups was performed with Dunn's post-hoc test ($p<0.05$).*

4.2.6. Evaluation of encapsulation efficiency

Encapsulation efficiency (EE) measurements were performed using calcein probe, in order to assess the possible differences between encapsulation by two methods. The first one, used for encapsulation of cargo inside the liposomes and aEx, includes the hydration of thin lipid film with the calcein solution. It is followed by the fusion of the liposomes formed from the film with EVs. An alternative method, commonly used to encapsulate cargo in EVs, is based on the modified transfection, which introduces calcein directly to the EVs. This method isn't used in case of the liposomes, or aEx.

The samples of liposomes, formed using all studied lipids were characterized by a very similar value of EE, which was close to 80% (Fig. 16A). Comparison of the EE for the DOPC-based liposomes, $aEx_{DOPC,}$ and EVs showed that aEx_{DOPC} had the highest value of EE. Additionally, EE for both the DOPC samples and aEx_{DOPC} was significantly higher than EE for EVs (Fig.16.B).

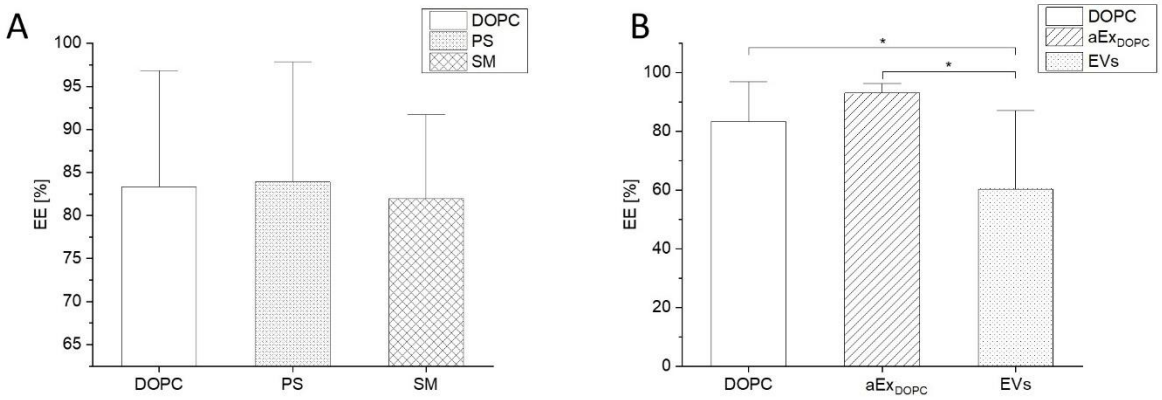

	EE [%]	p sample
DOPC	83.4 ± 9.00	0.988 PS
PS	83.9 ± 9.32	0.877 SM
SM	82.0 ± 6.51	0.932 DOPC

	EE [%]	p sample
DOPC	83.4 ± 9.00	<0.001 EVs
aEx_{DOPC}	93.1 ± 2.20	0.148 DOPC
EVs	60.4 ± 17.86	<0.001 aEx DOPC

Fig. 16. The results of the encapsulation efficiency measurement*. A – comparison of the encapsulation efficiency for the liposomes samples, B - comparison of the encapsulation efficiency for the aExDOPC, DOPC and EVs samples. Results are presented as the average values with standard deviation [whiskers]. The statistical analysis was performed with Kruskal-Wallis Anova, comparison among the groups was performed with Dunn's post-hoc test (p<0.05).*

4.3. Biological tests

4.3.1. Cytotoxicity

The ApoTox-Glow test was performed, in order to evaluate viability, cytotoxicity and caspase activity. In the first part of experiment, HUVECs were cultured after the incubation with liposomes (DOPC, SM, PS) and corresponding aEx (aEx_{DOPC}, aEx_{SM}, aEx_{PS}), in the normoglycemic conditions (Fig.17). The calculated results were normalized to the value of the NG sample, which represents HUVECs cultured in the physiological conditions (without any additional factors in the cell culture media).

In case of almost all tested samples, both viability and cytotoxicity was significantly increased, in comparison to the HUVECs cultured without additional factors in the cell culture media (NG). The only exception were the samples of HUVECs which were cultured with liposomes composed of DOPC (NG+DOPC). In this case, cytotoxicity was not significantly higher than for the NG samples. Analysis of caspase activity showed some changes in the activity, however none were statistically significant.

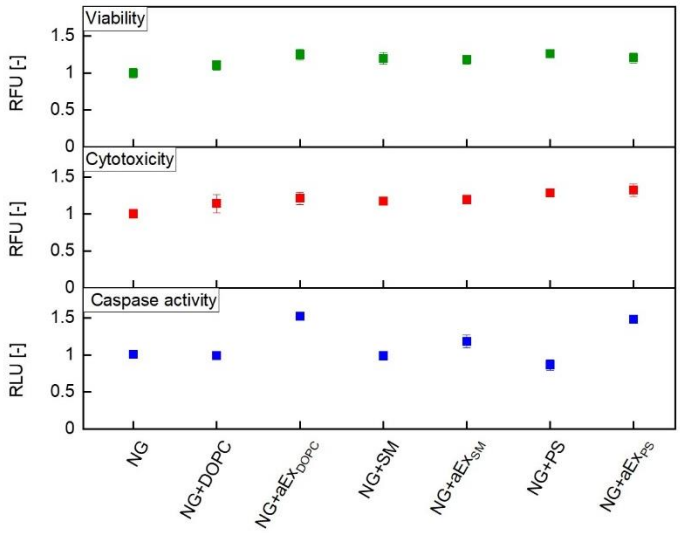

	Viability [-]	P ^{NG}	Cytotoxicity [-]	P ^{NG}	Caspase activity [-]	P ^{NG}
NG	1.00 ± 0.07	-	1.00 ± 0.05	-	1.00 ± 0.04	-
NG+DOPC	1.10 ± 0.06	**0.037**	1.14 ± 0.12	0.403	0.99 ± 0.03	1.000
NG+aEx$_{DOPC}$	1.25 ± 0.07	**0.012**	1.21 ± 0.08	**0.037**	1.52 ± 0.04	0.095
NG+SM	1.20 ± 0.08	**0.012**	1.17 ± 0.05	**0.012**	0.98 ± 0.03	1.000
NG+aEx$_{SM}$	1.18 ± 0.06	**0.012**	1.19 ± 0.04	**0.037**	1.18 ± 0.09	0.144
NG+PS	1.26 ± 0.06	**0.012**	1.28 ± 0.05	**0.037**	0.86 ± 0.07	0.296
NG+aEx$_{PS}$	1.20 ± 0.06	**0.012**	1.32 ± 0.08	**0.060**	1.48 ± 0.02	0.095

Fig. 17. Results of ApoTox-Glo triplex assay for liposomes cultured in normoglycemia and normalized to the NG samples. *Results are presented in relative fluorescence units (RFU) and relative luminescence unit (RLU). Data are presented as mean values (quad) with the standard deviation (whiskers).*

In the second part of the experiment, similar tests were performed for HUVECs cultured with the addition of EVs and aEx, both decorated and non-decorated with the Del-1 protein. For these samples, results were normalized to the values obtained for NG+EVs sample, which represents HUVECs cultured with an addition of EVs in the cell culture media, in the normoglycemic conditions (Fig.18.). The highest viability was observed for the cells cultured in the hyperglycemic conditions, without an addition of EVs to the cell culture media (HG). Additionally, the viability of these cells was significantly higher than the cells cultured in the normoglycemic conditions with EVs (NG+EVs). High viability was also observed for the samples cultured with an addition of aEx, covered with the Del-1 protein. The viability of these cells was significantly higher than the viability of NG+EVs samples. For the other samples, the viability was decreased, but only in case of the NG samples, this change was statistically significant. The cytotoxicity was higher in all tested samples, in comparison to the NG+EVs samples, but only for two samples (HG+aEx and HG+Nc), this difference was statistically significant. Analysis of caspase activity showed, that in all tested conditions the activity was significantly decreased in comparison to the NG+EVs samples.

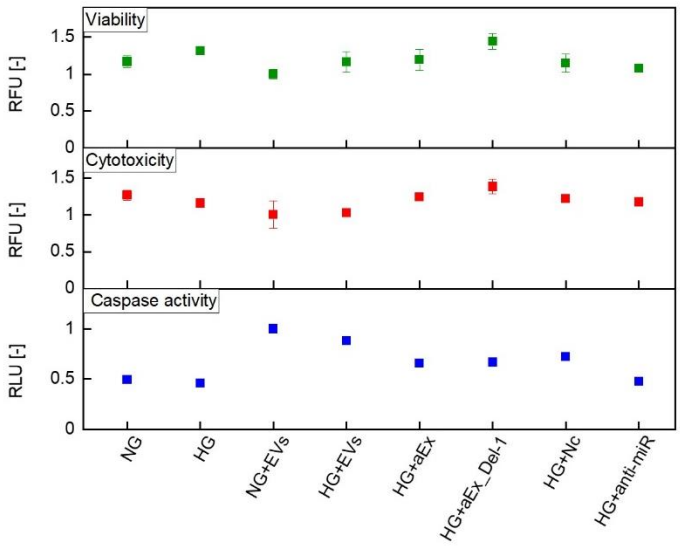

	Viability [-]	P NG	Cytotoxicity [-]	P NG	Caspase activity [-]	P NG
NG	0.83 ± 0.05	**0.022**	1.27 ± 0.07	0.060	0.50 ± 0.02	**0.012**
HG	1.13 ± 0.04	**0.012**	1.16 ± 0.03	0.144	0.46 ± 0.02	**0.012**
NG+Evs	1.00 ± 0.07	-	1.00 ± 0.18	-	1.00 ± 0.02	-
HG+EVs	1.00 ± 0.12	**0.037**	1.03 ± 0.04	1.000	0.88 ± 0.04	**0.012**
HG+aEx	0.94 ± 0.09	0.095	1.44 ± 0.15	**0.012**	0.66 ± 0.02	**0.012**
HG+aEx_Del-1	1.23 ± 0.09	**0.012**	1.24 ± 0.05	0.095	0.67 ± 0.02	**0.012**
HG+Nc	0.98 ± 0.10	**0.037**	1.38 ± 0.10	**0.022**	0.72 ± 0.01	**0.012**
HG+anti-miR	0.92 ± 0.11	0.210	1.21 ± 0.03	0.144	0.48 ± 0.03	**0.012**

Fig. 18. Results of ApoTox-Glo triplex assay for aEx samples. *The results were normalized to the NG+EVs samples and are presented in relative fluorescence units (RFU) and relative luminescence unit (RLU). Data are presented as mean values (quad) with the standard deviation (whiskers).*

4.3.2. Confocal microscopy – up-take of EVs

Confocal microscopy experiments were performed in order to assess the uptake of EVs and aEx by the HUVECs. Representative images are shown in Fig. 19. Prior to the experiments with EVs and aEx, control experiment with blank samples was performed. Blank samples included pure PKH26 and anti-miR without any carriers, processed (dyed) in the same way

as the EVs and aEx. No signal coming from PKH or FAM dye was detected in both control experiments.

Experiments with EVs and aEx confirmed that both types of particles are internalized by the HUVEC cells. In the images of HUVECs incubated with EVs, which were stained with PKH26, signal coming from EVs was clearly visible, as small dots located mostly near the nucleus region. Images obtained both in normoglycemic and hyperglycemic conditions were very similar and no differences in the up-take were observed. aEx were also internalized by HUVEC cell. aEx were mostly located near the nucleus region and clearly visible as separated small dots. Additionally, the colocalization of aEx and anti-miR-221-3p (FAM dye) was observed (red arrow). When aEx were covered with Del-1 protein, up-take was on a level similar to aEx not covered with the protein. However, in this case the colocalization was not observed.

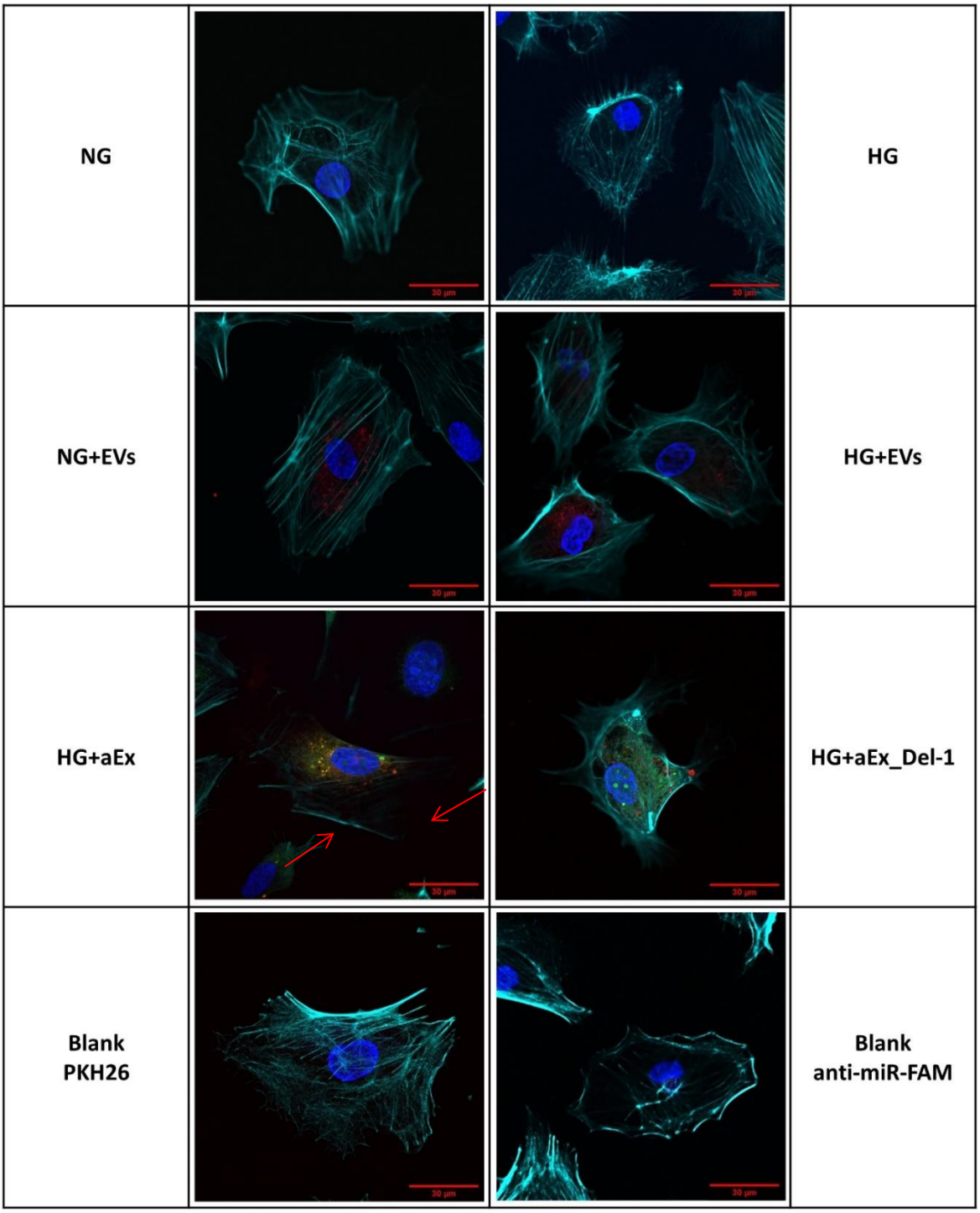

Fig. 19. Representative images form confocal microscopy of EVs up-take experiments. *Blue – cell nucleus (Hoechst 333342 dye), - turquoise cytoskeleton (Phalloidin conjugated with Alexa Fluor 647), red – EVs (PHK26), green – anti-miR-221-3p (FAM).*

4.3.3. Expression of mRNA and TIMP-3 protein

qPCR and western blot analyses were performed, in order to evaluate the expression of mRNA for TIMP-3 and TIMP-3 protein (which is the target of the anti-miR cargo of the aEx). In order to determine the physiological level of mRNA, samples collected from HUVECs cultured with, and without EVs, in the normoglycemic and hyperglycemic conditions, were additionally tested. Results showed that in the hyperglycemic culture conditions, expression of mRNA for TIMP-3 was decreased. However, this difference was statistically significant only if the cells ware cultured with the additional presence of EVs.

Incubation with aEx significantly increased the level of mRNA for TIMP-3, as compared to both the HG+EVs and NG+EVs samples (Fig.20.). Moreover, there was no statistically significant difference in the mRNA expression, regardless of the Del-1 decoration of aEx.

In these experiments, two controls were evaluated. The analysis showed that the negative control (HG+Nc), did not influence the level of mRNA for TIMP-3 and it is significantly different from the value obtained for aEx. The second control, pure miR-221-3p, added directly to the cell culture media without any carrier, induced the largest change in the expression of mRNA. However, these changes were not statistically significant from the NG+EVs samples and the measurement results within this group were characterized by very high variability.

Analysis of the protein expression levels showed some differences in the TIMP-3 levels, but none of them was statistically significant.

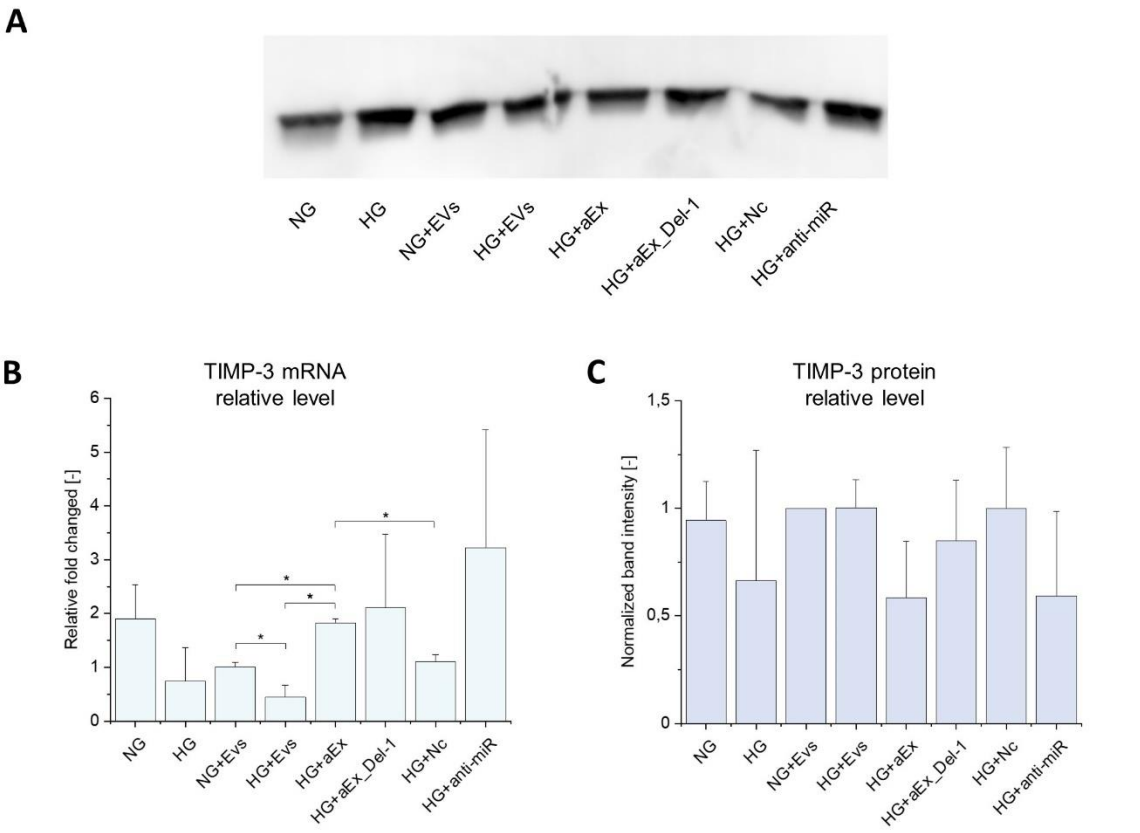

	Relative fold change ± SD [-]	p aEx	p other
NG	1.90 ± 0.64	-	0.131 NG+EVs
HG	0.75 ± 0.62	-	0.492 HG+EVs
NG+Evs	1.00 ± 0.09	**<0.001**	**0.015 HG+EVs**
HG+Evs	0.45 ± 0.22	**<0.001**	-
HG+aEx	1.82 ± 0.08	-	-
HG+aEx_Del-1	2.10 ± 1.37	0.756	-
HG+Nc	1.10 ± 0.13	**0.001**	-
HG+anti-miR	3.22 ± 2.19	0.384	-

	Normalized band intensity ± SD [-]	p aEx	p other
NG	0.94 ± 0.18	-	0.645 NG+EVs
HG	0.66 ± 0.61	-	0.398 HG+EVs
NG+Evs	1.00 ± 0.00	0.111	0.979 HG+EVs
HG+Evs	1.00 ± 0.13	0.069	-
HG+aEx	0.58 ± 0.26	-	-
HG+aEx_Del-1	0.85 ± 0.28	0.298	-
HG+Nc	1.00 ± 0.28	0.136	-
HG+anti-miR	0.59 ± 0.39	0.973	-

Fig. 20. TIMP-3 expression analysis*. A - the image of the PVDF membrane with visible bands for TIMP-3 protein, B - results of the analysis of TIMP-3 expression on the level of mRNA) and protein (C). Results were normalized to the NG+EVs samples and presented as the average values with standard deviation [whiskers]. The statistical analysis was performed with t-student test (p<0.05).*

4.3.4. Metalloproteinases activity

Metalloproteinases activity was assessed in a zymography assay, which can detect the activity of gelatinases – MMP-2 and MMP-9. Assay detects an active form of MMP, as well as the activity of pro-enzymes (zymogens). It is possible because of the intrinsic activity of autocatalytic cleavage of MMP-2 and MMP-9 [154]. In the tested conditions, the activity of pro-enzymes was higher than the activity of the active enzyme.

In order to determine the physiological level of the studied enzymes, cell culture media form HUVECs cultured both with and without the addition of EVs, in the normoglycemic or hyperglycemic conditions were tested.

When the EVs were added to the cell culture media, activity of pro-MMP-9 and active-MMP-9 was increased, both in the normoglycemic (NG+EVs) and hyperglycemic (HG+EVs) culture conditions (Fig.21.B). However, the only statistically significant difference between the two groups cultured with the addition of EVs was found in the activity of pro-MMP-9, which was higher in hyperglycemic conditions, compared to the normoglycemic conditions.

The level of pro-MMP-9 after stimulation with aEx was not changed, as compared to the NG+EVs and HG+EVs samples. No statistically significant differences were observed regardless of whether aEx were decorated with the Del-1 protein.

Different results were obtained in case of the active-MMP-9. Stimulation with aEx significantly reduced the activity of active-MMP-9, as compared to the samples cultured in the NG+EVs and HG+EVs conditions. Similarly to the case of pro-MMP-9, decoration with Del-1 did not have the influence on the activity of active-MMP-9.

In comparison to the negative control (HG+Nc), and anti-miR-221-3p directly added to the cell culture media (HG+anti-miR), the influence of aEx was statistically significant for pro-MMP-9 and induced a decrease in the activity of both enzymes. The activity of active-MMP-9 was decreased in case of the HG+anti-miR samples and increased for the HG+Nc samples. Both changes were statistically significant, in comparison to the changes induced by aEx.

A

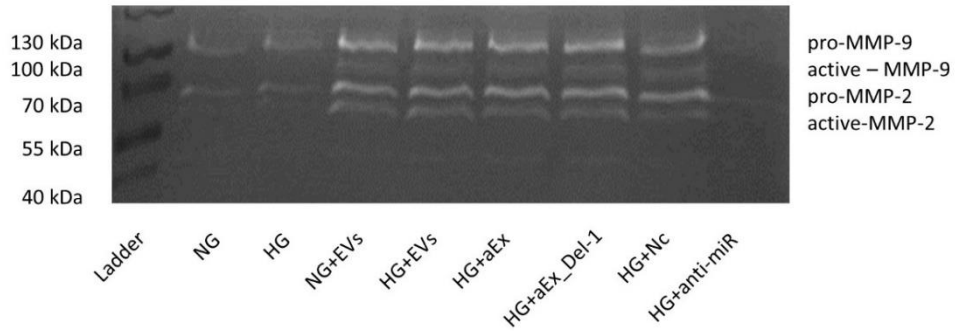

B

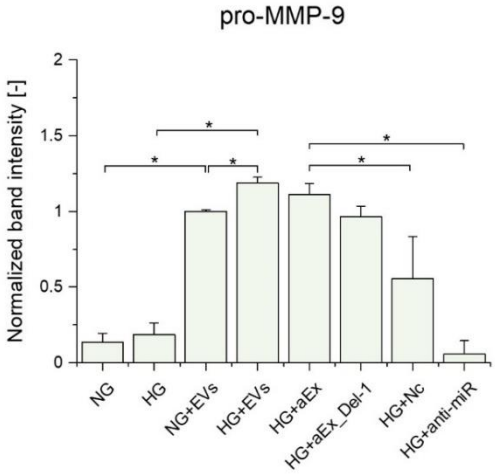

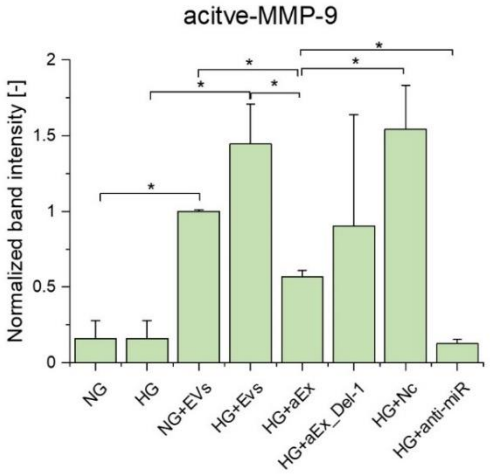

	Relative fold change ± SD [-]	p aEx	p other
NG	0.14 ± 0.06	-	**<0.001** NG+EVs
HG	0.18 ± 0.08	-	**0.001** HG+Evs
NG+Evs	1.00 ± 0.00	0.125	**0.001** HG+Evs
HG+EVs	1.19 ± 0.04	0.180	-
HG+aEx	1.11 ± 0.07	-	-
HG+aEx_Del-1	0.96 ± 0.07	0.071	-
HG+Nc	0.56 ± 0.28	**0.028**	-
HG+anti-miR	0.06 ± 0.09	**<0.001**	-

	Relative fold change ± SD [-]	p aEx	p other
NG	0.16 ± 0.13	-	**0.006** NG+EVs
HG	0.16 ± 0.12	-	**0.043** HG+EVs
NG+Evs	1.00 ± 0.01	**<0.001**	0.099 HG+EVs
HG+EVs	1.44 ± 0.26	**0.005**	-
HG+aEx	0.57 ± 0.04	-	-
HG+aEx_Del-1	0.90 ± 0.73	0.509	-
HG+Nc	1.54 ± 0.29	**0.027**	-
HG+anti-miR	0.13 ± 0.03	**<0.001**	-

C

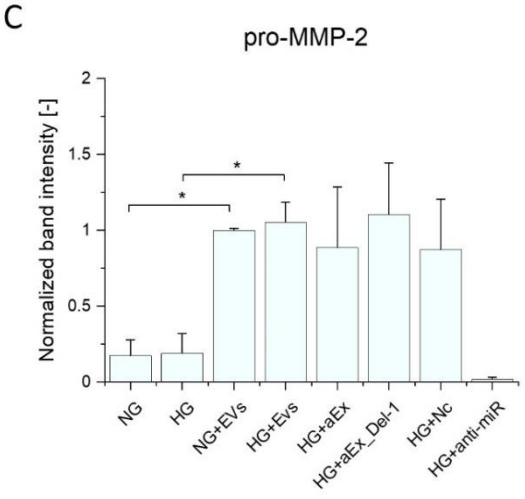

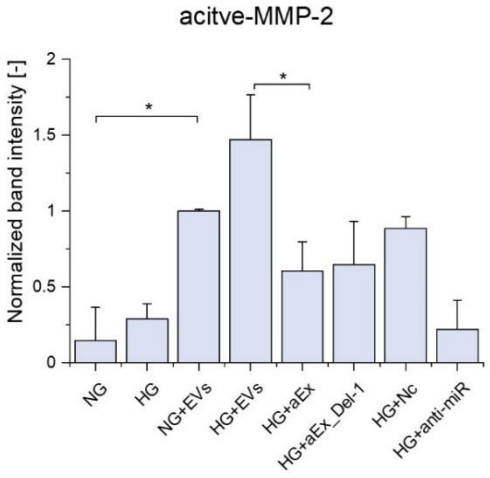

	Relative fold change ± SD [-]	p aEx	p other
NG	0.17 ± 0.11	-	**0.005** NG+Evs
HG	0.19 ± 0.13	-	**0.001** HG+Evs
NG+Evs	1.00 ± 0.01	0.669	0.556 HG+Evs
HG+EVs	1.05 ± 0.13	0.529	-
HG+aEx	0.89 ± 0.40	-	-
HG+aEx_Del-1	1.10 ± 0.34	0.511	-
HG+Nc	0.87 ± 0.33	0.963	-
HG+anti-miR	0.02 ± 0.02	0.064	-

	Relative fold change ± SD [-]	p aEx	p other
NG	0.15 ± 0.22	-	**0.021** NG+Evs
HG	0.29 ± 0.11	-	0.051 HG+Evs
NG+Evs	1.00 ± 0.00	0.069	0.109 HG+Evs
HG+EVs	1.47 ± 0.29	**0.013**	-
HG+aEx	0.61 ± 0.19	-	-
HG+aEx_Del-1	0.65 ± 0.29	0.856	-
HG+Nc	0.88 ± 0.08	0.078	-
HG+anti-miR	0.22 ± 0.19	0.068	-

Fig. 21. Summary of the metalloproteinases activity tests. *A - the image of the stained gel with visible bands for MMP-2 and MMP-9 with pro-from and active form. B - Analysis of activity of the MMP-2 and MMP-9 (C). Results were normalized to the NG+EVs samples and presented as the average values with the standard deviation [whiskers]. Statistical analysis was performed with the t-student test (p<0.05).*

In addition to the MMP-9, the physiological levels of pro- and active-MMP-2 were determined. The results showed, that in the presence of EVs in cell culture media, the activity of both pro-MMP-2 and active-MMP-2 was significantly increased in normoglycemic (NG+EVs) and hyperglycemic culture conditions (Fig.21.C). There were no statistically significant differences between the samples collected form HUVECs stimulated with EVs regardless of whether they were cultured in the normo- or hyperglycemic conditions.

The level of pro-MMP-2 after stimulation with aEx did not significantly change, in comparison to the NG+EVs and HG+EVs samples. There were also no statistically significant differences regardless of whether aEx were decorated with Del-1 protein. There were also

no statistically significant differences between aEx samples and both negative controls: HG+Nc and HG+anti-miR. Similar results were obtained by the analysis of the activity of active-MMP-2. The only observed statistically significant difference was the decrease of active-MMP-2 activity in aEx samples, in comparison to HG+EVs.

4.3.5. Wound healing assay

Wound healing assay was performed in order to assess the ability of HUVECs to perform wound healing after stimulation with different factors. The results were calculated as the confluence index (CI) – the percentage of the wound area, after 14h stimulation with the investigated factor, compared to the area of the wound at the beginning of the test. The lowest CI was observed for the HUVECs cultured in the hyperglycemic conditions, with the addition of EVs (HG+EVs). The highest value of CI was observed for the cells cultured in hyperglycemic conditions stimulated with aEx (HG+aEx). This value was significantly higher than in case of the HG+EVs sample. AEx covered with Del-1 were also characterized by higher CI, compared to HG+EVs sample, however the difference between aEx decorated and not decorated with Del-1 protein was not statistically significant. Additionally, CI of negative control (HG+Nc) was significantly lower than CI for the aEx samples. Second control, anti-miR-221-3p which was added directly to the cell culture media resulted in the higher CI, which was not statistically significant from value obtained for aEx-stimulated samples.

The results confirmed that the EVs can stimulate cell migration both in normoglycemic and hyperglycemic conditions. Moreover, the CI was significantly lower for HUVECs stimulated with EVs but cultured in hyperglycemic conditions, as compared to the ones cultured in normoglycemic conditions.

A

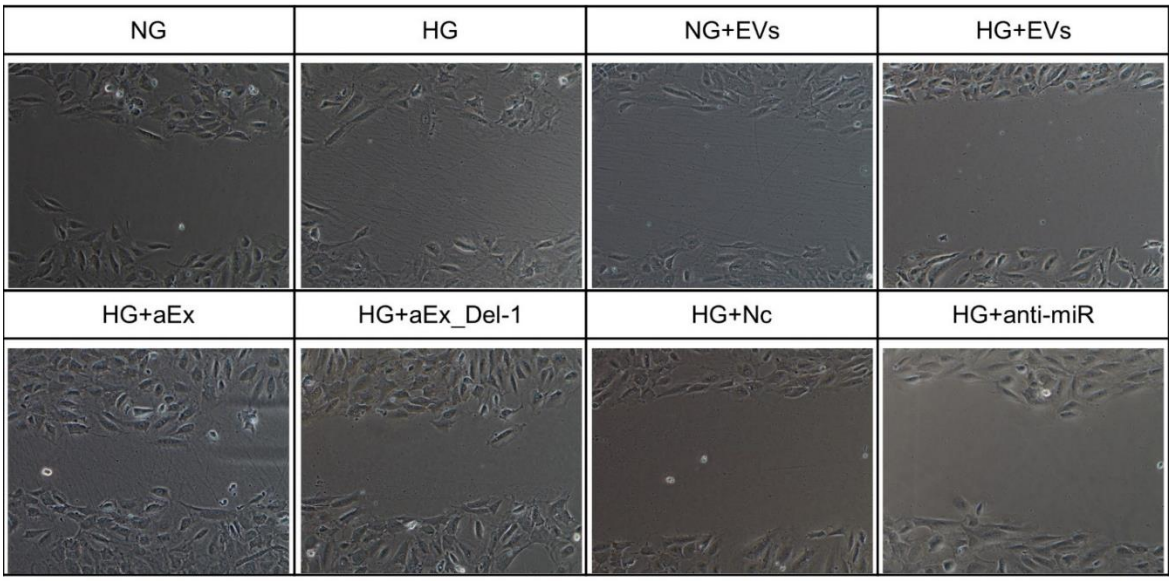

B

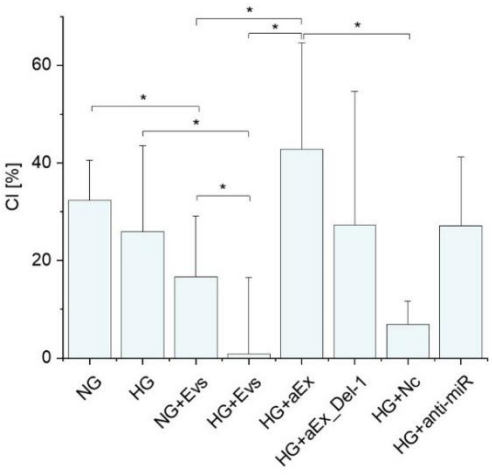

	CI [%]	p aEx	p other
NG	32.3 ± 8.2	-	**0.010** NG+EVs
HG	25.9 ± 17.6	-	**0.005** HG+EVs
NG+EVs	16.7 ± 12.5	**0.006**	**0.030** HG+EVs
HG+EVs	0.89 ±15.6	**0.001**	-
HG+aEx	42.8 ± 21.7	-	-
HG + aEx_Del-1	27.3 ± 27.4	0.397	-
HG+Nc	6.9 ± 4.7	**0.001**	-
HG + anti-miR	27.1 ± 14.2	0.112	-

Fig. 22. Wound healing results. Images were taken after 24h of incubation in tested conditions*. A – the examples of the microscopic images of wounds created in wound healing assay after 14h of incubation, B – statistical analysis of the results. Differences between subgroups were tested with Mann Whitney Test (p<0.05). * indicates significance in comparison between tested groups.*

5. Discussion

In this thesis, a new approach to the design and synthesis of biomimetic drug carriers is presented. The project focuses on one of the most prevalent disorders – diabetes, and addresses one of the main complications of diabetes - microangiopathy. In the project, I utilized the important features of natural messaging carriers – extracellular vesicles (EVs) and their synthetic equivalents – liposomes, in order to create hybrid vesicles – artificial exosomes (aEx). aEx are designed to deliver fragments of RNA (anti-miR) to the endothelial cells in order to block an overexpression of miR, which was previously liked to the endothelial cell dysfunction (ECD).

This thesis focuses on the two main aspects: 1) design of the carriers, development of the protocol of aEx synthesis and their physical characterization, 2) evaluation of the biological activity of aEx, in the context of restoring physiological characteristics of endothelial cells, and stimulation of cell migration in the wound healing processes.

5.1. Synthesis and physical characteristics of artificial exosomes

In the first part of the thesis, based on the literature research, the intended design of the carrier was developed and evaluated. The aim of the project was to create artificial exosomes for the nucleic acid delivery. The perfect carrier for this purpose should: (a) protect its cargo from degradation; (b) be effectively transported and internalized by the targeted cells; (c) promote the release of the cargo in the specific cell compartment (i.e. in the cytoplasm for antisense oligonucleotides [ASO], siRNAs or miRNAs); (d) induce a therapeutic effect in low doses; (e) be non-cytotoxic and safe for the *in vivo* therapeutic applications; (f) be easy to produce, store and deliver on a large scale [155]. One of the proposed candidates for drug delivery systems serving these purposes are viral vector-based systems. However, because of the many challenges inherently connected with this approach [156], there is an urgent need to develop alternative, non-viral vectors. In the recent years a lot of research was performed on the development of liposomal formulas, which could be used in nucleic acid delivery and great focus was dedicated to the cationic liposomes.

Cationic liposomes contain cationic lipids, which usually consist of positively charged headgroups, which can electrostatically interact with negatively charged nucleic acids. This can be used to create, for example, liposome/DNA complexes (lipoplexes) and hydrophobic lipid anchors, which incorporate in the core of the liposomes [155].

DOSPA(2,3dioleyloxy-N-[2[sperminecarboxaminino]ethyl]-N,N-dimethyl-1 propanaminium trifluroacetate), DOTAP (1,2-dioleoyl-3-trimethylammonium propane), or DC-Cholesterol are some of the examples of frequently used cationic lipids. It has been shown that the effective delivery depends not only on the type of lipids used for the synthesis of liposomes, but also on the ratio between the amount of encapsulated nucleic cargo and cationic lipid [136]. Moreover, these two factors are also responsible for the toxicity of cationic liposomes [157] which is one of the most important obstacles to overcome, before introducing these types of carriers to the therapy.

The interest of the research community in the extracellular vesicles has grown rapidly since their first description in 1971. Extracellular vesicles are unique carriers of various bioactive molecules (DNA, RNA, proteins). Their biocompatible characteristics, small size, long circulation time, presence of multiple adhesive molecules on their surface, and the ability to cross physical barriers make them promising conveyors for biotherapeutics delivery. Unfortunately, in past years, the possibility of using EVs in therapy was very limited, due to challenges in the isolation, upscaling the EVs production, and lack of guidelines for the appropriate storage [158].

Due to aforementioned challenges, it seems that instead of using natural EVs for the delivery, a promising approach would be to synthesize artificial liposomes, with the composition similar to the lipid composition of the EVs. Up to this moment several groups have tried to synthesize exosomes-mimicking liposomes or exoliposomes. Beloribi et. al. [159] showed that artificial liposomes, with the lipid composition inspired by the exosomes secreted by human SOJ-6 pancreatic tumor cells, were able to induce cell death *via* an inhibition of the Notch pathway. Observed effect was similar to the effect induced by the natural exosomes. The efficiency of inhibition depended on the ratio of cholesterol and

sphingomyelin to other phospholipids. Authors concluded that the lipids may alter the lipid composition of the microdomains, where the Notch partners are located, and influence Notch-1 functionality. Another study showed that exosome-mimicking liposomes, composed of DOPC/SM/Chol/DOPS/DOPE, can be used for the delivery of VEGF siRNA to the A549 and HUVEC cells. Delivery efficiency and other key characteristics of the system were compared to the Lipo 2000, DOTAP and PC-Chol liposomes. Results showed that exosome-mimicking liposomes were less cytotoxic, had higher cellular uptake, as well as higher silencing efficiency than PC-Chol liposomes. However, the uptake and the silencing efficiency of exosomes-mimicking liposomes was lower than the cationic Lipo 2000 and DOTAP liposomes [160].

In the project I decided to use synergistic approach and synthesize hybrids of EVs and EVs-inspired liposomes, in order to create new carrier, with a mixed characteristic. I used the metanalysis of the different lipidomic studies performed by Skotland in 2017 [133 and Tab.1.], in order to evaluate which lipids were present in the EVs. The analysis showed that cholesterol is the most abundant lipid in the EVs obtained from the different cells. Cholesterol content ranges from 15%, for the mast cells-derived EVs, to 63%, for the urine-derived EVs. The second most abundant type of lipids in EVs is sphingomyelin (up to 28.6% for prostasomes), as well as two phospholipids: phosphatidylcholine and phosphatidylserine (up to 28% for the EVs derived from mast cells and 20.3% for the EVs isolated form B-lymphocytes). Based on these results, I decided to use three lipids for the liposome synthesis: DOPC, SM and PS which were mixed in 70 mol% of the chosen lipid and 30 mol% of DC-Cholesterol. DC-Cholesterol, as mentioned before, is one of the cationic lipids widely used in liposomes dedicated to the delivery on nucleic acids.

Studies of Piffoux et .all [123] and Sato et. all [122] showed that freeze/thawing method can be used to synthesize hybrid or artificial exosomes, *via* the fusion of EVs with liposomes. In this thesis, I characterized the efficiency of fusion between the three types of liposomes and EVs isolated form HUVEC cells. I confirmed that the fusion can occur between DOPC, SM, PS liposomes and EVs. Fusion efficiency depends on the ratio between the amount of lipids in the liposomes and the total amount of proteins in EVs (Tab.7.). The highest

efficiency was obtained, when the samples were mixed in the 1 to 100 ratio. Additionally, fusion efficiency increased with the number of freeze/thawing cycles, which reflects the progress of the fusion over time. The highest ratio was obtained for the PS liposomes and DOPC liposomes. In case of the DOPC liposomes, the lipid dilution was close to 1. This means that, on average, a single liposome has completely fused with a single EV, which could be a good prognosis factor for the high encapsulation efficiency values. These samples should also be more similar to the EVs, than the samples with higher lipid dilution, due to the fact that higher lipid dilution parameter means that aEx contain fewer material from the natural EVs.

AEx synthesis by the fusion of DOPC, PS, and SM, with EVs in the 1 to 100 ratio were chosen for the further analysis. In the study of Rayamajhi et al. [161], following parameters were used to characterize hybrid exosomes: zeta potential, size (measured with DLS), micrographs form cryo-TEM microscopy, presence of the typical EVs markers and encapsulation efficiency. I have adopted similar approach for the characterization in this project, as it provides the complete picture of the physical properties of the synthesized carriers.

Zeta-potential measurements and NTA analysis was performed not only for the liposomes, EVs and aEx, but also for the mixture of EVs and liposomes without performing freeze/thawing process (before the fusion of the two particles). I decided to use this strategy to ensure, that the changes observed in the zeta-potential, size and size-distribution are not an additive effect, resulting simply from mixing of two samples, but are indeed the results of the fusion.

Zeta-potential of all three types of aEx was negative, and for the aEx_{DOPC} and aEx_{PS} had an unimodal distribution. This can indicate that the fusion between EVs and liposomes occurred with high efficiency (Tab.6. and Fig. 12). Only in case of aEx_{DOPC}, zeta potential was significantly different than the zeta potential of the mixture of DOPC liposomes and EVs. Unfortunately, none of aEx type had zeta-potential value over or below 30 mV, which would be a good prognosis for their stability.

The average size of the particles (aEx) observed by the NTA method was significantly reduced after the fusion process, as compared to the average size of the mixture of liposomes and EVs before the fusion (Tab.7. and Fig. 13).

Moreover, the comparison of the size distribution of the mixture of DOPC liposomes and EVs before the fusion and the aEx_{DOPC} synthesized in the process, showed the change in size distribution from bimodal to the right-skewed unimodal. This is a clear signature of the fusion process, wherein particles with two average sizes undergo fusion, and create a new, more homogenous population. However, in case of aEx_{SM} and aEx_{PS}, no changes from bimodal to unimodal size distribution were observed.

Western blot analysis confirmed that the EVs markers (CD63 and Arf-6) were present in the samples of all tested types of aEx and that there were no statistically significant differences between them. These results confirmed, that the fusion process occurs without losing the EVs proteomic signature and is consistent with the results obtained by Rayamajhi et. al. [161].

Using Cryo-TEM imaging I confirmed that aEx are present in the samples after the fusion process of EVs with the DOPC liposomes. Similarly to the results of the Rayamajhi group [161], observed objects were characterized by a very high electron density in the center. Unfortunately, I was not able to observe any objects in case of the aEx_{SM} and aEx_{PS} samples. This could be a result of an initially low amount of visible particles of the samples of liposomes, or a different affinity of the different samples to the cryo-TEM grid (perhaps due to the differences in the zeta potential). Because only the aEx_{DOPC} were observed in the Cryo-TEM imaging, and significant changes in the zeta-potential values and size distribution were observed only for this type of aEx, they were chosen for the further studies of the encapsulation efficiency and their biological effects.

Measured encapsulation efficiency was high (around 85%) for all three types of tested liposomes (Fig.6.). The measurements of encapsulation efficiency for aEx were performed only for the $aEx_{DOPC,}$ because of the reasons explained above. Encapsulation of calcein in EVs, using the modified transfection method, had significantly lower efficiency, than

encapsulation in aEx using lipid hydration method. In multiple theoretical studies, challenges in the encapsulation processes were identified as some of the most important obstacles, hindering EVs applications as drug delivery systems [158]. Up to this moment, several strategies of drug loading after EVs isolation were tested such as: incubation of the molecule with isolated EVs [117], electroporation [119] or drug loading during extrusion [117]. It is difficult to compare the efficiency of these strategies, because all authors used different approaches to measure drug loading efficiency. Nevertheless, loading of drugs, by the fusion of drug-containing liposomes with EVs seems to be a very promising strategy. Additionally, utilization of liposomes gives an opportunity for further modifications of aEx. This could be realized, for example, by incorporating compounds which specific properties, such as PEGylated lipids, into the membranes of liposomes, in order to increase their circulation time in blood and reduce their uptake by the mononuclear phagocytes [122].

5.2. Interaction of exosomes with HUVEC cells

Before functional experiments, the interaction of aEx and tested liposomes with HUVEC cells was evaluated, in order to assess the toxicity of carriers and to confirm their internalization.

The viability of HUVECs stimulated with all tested kinds of liposomes and corresponding aEx, was increased in comparison to the unstimulated cells. Surprisingly, in all samples the cytotoxicity was slightly increased, without any significant changes in the caspase activity. These results are consistent with literature, which described potential cytotoxicity of cationic lipids [162]. On the other hand, moderate increases in the proteases activity, accompanied by the increased viability, could be caused by natural changes in cell culture. This would mean that they are a result of apoptosis, and not by the necrosis induced by the investigated liposomes and aEx.

In contrast to the experiments described above, tests for the aEx with encapsulated anti-miR-221-3p were performed in the hyperglycemic conditions, in order to assess synergic influence of two factors: hyperglycemia and tested carriers. The results showed that aEx in hyperglycemic conditions were cytotoxic, but the same samples, covered with Del-1 were

not. Interestingly, when negative control was encapsulated in aEx, the viability of HUVECs was decreased. This change was accompanied by an increase in the cytotoxicity.

For all the tested samples, the decreased activity of caspase was detected. While the observed changes were significant, their magnitude was very small and doesn't impact the interpretation of other results. It is possible that some unknown, outside factor has contributed to these outcomes. While this is not the main goal of this work, further studies are needed to study these effects.

Confocal microscopy imaging showed, that aEx ware internalized by the HUVECs, on the level similar to EVs. The most important observation was the colocalization of the signal from PHK26 dye (EVs membrane staining) and FAM probe, which was conjugated to miR-221-3p encapsulated in aEx. These results confirmed, that aEx can deliver miR-221-3p to the target cells. However, I didn't observe an increased internalization of aEx, after covering them with Del-1 protein. Del-1 is responsible for EVs internalization through the interaction between PS in the EVs membrane and integrins αVβ3 and αVβ5 on endothelial cells. In the western blot analysis I confirmed that Del-1 is present in the aEx samples, on the level higher than in EVs but it was not able to facilitate the up-take of aEx. Further studies of the interaction between Del-1 and aEx are required, especially with regard to the minimal amount of the Del-1 protein required to induce biological changes in the system.

5.3. Biological activity of the artificial exosomes

To investigate the influence of aEx with encapsulated anti-miR-221-3p on the TIMP-3 expression and cell migration, four different tests were performed: qPCR, western blot, analysis of the activity of metalloproteinases, and wound healing assay.

In the literature, several miRs targeting TIMP-3 have been identified, which include: miR-17, miR-21, miR-205, miR-221, miR-222, and miR-770 [163]. Among them, miR-221 seems to be particularly interesting in the context of diabetes and hyperglycemia-included ECD. Not only is miR-221 level increased in the serum of the patients suffering from diabetes, but it also correlates with the severity of diabetic retinopathy [164]. In the

microarray analysis, it has been shown that the expression of ten miRNAs (including miR-221) elevates gradually with an increasing concentration of glucose in endothelial cell cultures [22]. Seven of them (including miR-221-3p) can be linked to the endothelial cell apoptosis. Another study confirmed, that exposure of HUVECs to high levels of glucose, increases the expression of miR-221 and impairs cell migration. Blocking the activity of miR-221, with antisense nucleotides, can reverse this effect in case of the cells cultured in hyperglycemic conditions [165]. These results indicate, that miR-221 is could be a promising therapeutic target.

To investigate the influence of aEx loaded with anti-miR-221-3p on the TIMP-3 levels, two types of experiments were performed: qPCR and western blot. The results of qPCR showed significant differences in the mRNA expression among the samples. Cells cultured in hyperglycemia, both in the EVs-depleted cell culture media, and in the presence of EVs, had a decreased level of mRNA for TIMP-3, in comparison to the normoglycemic conditions. Study of Cardellini et al. [166] showed that mRNA level for TIMP-3 was reduced in the samples of carotid atherosclerotic plaques, collected form patients suffering from diabetes, as compared to the level of healthy patients. Additionally, diabetic retinopathy could be associated with the elevated levels of miR-221 and a downregulation of TIMP-3 expression [167]. The level of mRNA for TIMP-3 could be connected not only with glucose levels, but also with the oxidative stress. It has been shown that mRNA for TIMP-3 in the samples of human retinal pericytes, after stimulation with heavily oxidized and glycated LDL (HOG-LDL) for 24 h, is also downregulated [168]. These changes can be reversed after incubation with the mixture of normal LDL and HOG-LDL. These results shows, that TIMP-3 could also be used as a possible treatment target.

qPCR results showed that the incubation of the cells with aEx loaded with anti-miR-221-3p led to the increased level of mRNA for TIMP-3, both for aEx decorated and undecorated with Del-1. To the best of my knowledge, it is the first time when this link was observed and measured in HUVECs. This effect was described on other types of cells, such as hepatocellular carcinoma cell line HepG2 [169]. In this study, cells were incubated with liposomes with encapsulated anti-miR-221-3p, leading to the increased level of mRNA for

TIMP-3 after the stimulation. Similar results were obtained by Gan *et. al* [170]. Researchers used anti-miR-221 and anti-miR-222 to block the activity of these miRNAs in two lines of breast cancer cells. They also observed, that the expression of TIMP-3 significantly increased in both tested cell lines.

On the level of protein expression, I did not observe any significant differences in the TIMP-3 content. Western blot experiments were performed after 14 h of culture. It is possible that prolonging the time of incubation of HUVECs with aEx could give enough time to induce more significant changes on the level of proteins, which would be consistent with observed mRNA levels. Another reason of the lack of changes on the protein level could be, that free TIMPs or, TIMPs complexes with MMP, are secreted to the extracellular matrix [163]. This would mean that the significant differences could be difficult to detect in the western blot analysis, but should be easily distinguishable in zymography.

The zymography assay showed that activity of MMP-2 and MMP-9 is increased in the hyperglycemic conditions in the presence of EVs, but this increase was not statistically significant. Interestingly, there was no difference in the activity of MMP-2 and MMP-9 for the cells cultured in the EVs-depleted conditions. It was shown, that EVs contain metalloproteinases [171], and because of this we can assume that the observed activity can be a result of the combined activity of the enzymes secreted by cells, and those contained in the EVs.

Nevertheless, after stimulation with aEx, the activity of both enzymes significantly decreased, in comparison to the activity observed for the hyperglycemic cultures in the presence of EVs. Additionally, the activity was lower than in case of the normoglycemic cells cultured in the presence of EVs. These results show, that aEx can effectively block the activity of metalloproteinases, possibly by affecting TIMP-3 activity, through the delivery of anti-miR-221-3p. The link between a decreased level of TIMP-3 and an increased activity of MMP-2 and MMP-9 has been previously described. The investigation of the carotid atherosclerotic plaques from patient with type 2 diabetes showed that expression of TIMP-3 was significantly reduced, leading to MMP-9 hyperactivity [158].

There is a correlation between TIMPs, MMP and wound healing. In the ulcers wounds fluids from the diabetic patients, a dysregulated ratio between MMP-9 and TIMP-1 was shown to correlate with poor healing prognosis [172]. The changes in the level of TIMP-3 and MMP-2 and MMP-9 activity can also be associated with dysregulated wound healing processes. In the biopsy samples, collected form the ischemic diabetic foot ulcers, a decreased level of mRNA for TIMP-3 and an elevated activity of MMP-9 was observed. The authors of the study concluded, that ischemic non-healing ulcers can be caused by an increased proteolytic activity and that the treatment of this kind of wound, aimed at increasing the activity of TIMP-3 could be a new therapeutic strategy [173]. It was shown that there is a link between a downregulation of miR-221, an upregulation of TIMP-3 and an enhanced migration and proliferation of pulmonary arterial smooth muscle cells [174].

The results of wound healing assay presented in this thesis confirmed that targeting TIMP-3 could have beneficial effects on wound healing. aEx with encapsulated miR-221-3p can stimulate migration and wound healing processes. In the wound healing assay, samples incubated with aEx showed the highest value of CI (CI = 42.8 ± 21.7%) among all tested samples, indicating their positive effect on wound healing. Additionally, this value was significantly higher than the CI of the samples stimulated with EVs, as well as the negative control samples.

6. Conclusions

In this thesis, a new protocol of the synthesis of artificial exosomes was developed and evaluated. FRET was used to monitor the process of fusion between EVs and liposomes and the results confirmed that the fusion occurs. The most beneficial lipid-to-protein ratio was also identified. Synthesized artificial exosomes are characterized by a high encapsulation efficiency and are internalized effectively by endothelial cells. Although artificial exosomes still need some modifications, in order to reduce their cytotoxicity, obtained results are very promising and could lead to the new therapeutic strategies.

Additionally, it was confirmed that the encapsulated anti-miR-221-3p can increase the expression of TIMP-3 in HUVECs cultured in hyperglycemia, which decreases MMP-2 and MMP-9 activity. All these changes showed a positive influence on cell migration and facilitated wound healing processes. This confirmed a suggestion made by other scientists, that targeting TIMP-3 is a good therapeutic strategy for the treatment of the macroangiopathic complications of diabetes.

The results presented in this thesis confirmed that artificial exosomes are promising candidates for a drug delivery platform, which could be used in the future in a number of different diseases. The Author hopes, that they will be useful for a wider audience, and that they will find real-life applications.

List of figures

List of tables

References

1. Stępien E. Acceleration of new biomarkers development and discovery in synergistic diagnostics of coronary artery disease. In: Baskot B editor. Coronary angiography—advances in noninvasive imaging approach for evaluation of coronary artery disease. London: InTech; 2011.

2. World Health Organization. Global Report on Diabetes. [Internet]. 2016. [cited 2021 Oct 04]. Available from: https://www.who.int/publications/i/item/9789241565257.

3. Hohendorff J, Drożdż A, Borys S, et al. Effects of Negative Pressure Wound Therapy on Levels of Angiopoetin-2 and Other Selected Circulating Signaling Molecules in Patients with Diabetic Foot Ulcer. J Diabetes Res. 2019;2019:1756798.

4. Engerman RL, Kern TS. Progression of incipient diabetic retinopathy during good glycemic control. Diabetes. 1987;36(7):808–12.

5. Ihnat MA, Thorpe JE, Kamat CD, Szabó C, Green DE, Warnke LA, et al. Reactive oxygen species mediate a cellular "memory" of high glucose stress signalling. Diabetologia. 2007;50(7):1523–31.

6. Félétou M. The Endothelium: Part 1: Multiple Functions of the Endothelial Cells—Focus on Endothelium-Derived Vasoactive Mediators. San Rafael: Morgan & Claypool Life Sciences; 2011.

7. Cines BDB, Pollak ES, Buck CA, Loscalzo J, Zimmerman GA, Mcever RP, et al. Endothelial Cells in Physiology and in the Pathophysiology of Vascular Disorders. J Am Soc Hematol. 1998;91(10):3527–61.

8. Ido Y, Carling D, Ruderman N. Hyperglycemia-Induced Apoptosis in Human Umbilical Vein Endothelial Cells. Diabetes. 2002;51(22):159–67.

9. Kolluru GK, Bir SC, Kevil CG. Endothelial Dysfunction and Diabetes: Effects on Angiogenesis, Vascular Remodeling, and Wound Healing. Int J Vasc Med. 2012;2012:918267.

10. Kaneto H, Katakami N, Matsuhisa M, Matsuoka TA. Role of reactive oxygen species in the progression of type 2 diabetes and atherosclerosis. Mediators Inflamm. 2010;2010:453892.

11. Cherian S, Roy S, Pinheiro A, Roy S. Tight glycemic control regulates fibronectin expression and basement membrane thickening in retinal and glomerular capillaries of diabetic rats. Investig Ophthalmol Vis Sci. 2009;50(2):943–9.

12. Roy S, Ha J, Trudeau K, Beglova E. Vascular basement membrane thickening in diabetic retinopathy. Curr Eye Res. 2010;35(12):1045–56.

13. Giebel SJ, Menicucci G, McGuire PG, Das A. Matrix metalloproteinases in early diabetic retinopathy and their role in alternation of the blood-retinal barrier. Lab Investig. 2005;85(5):597–607.

14. Stepien E, Costa MC, Kurc S, Drozdz A, Cortez-Dias N, Enguita FJ. The circulating non-coding RNA landscape for biomarker research: Lessons and prospects from cardiovascular diseases review-article. Acta Pharmacol Sin. 2018;39(7):1085–99.

15. Castaño C, Novials A, Párrizas M. Exosomes and diabetes. Diabetes Metab Res Rev. 2019;35(3):1–10.

16. Seyhan AA, Nunez Lopez YO, Xie H, Yi F, Mathews C, Pasarica M, et al. Pancreas-enriched miRNAs are altered in the circulation of subjects with diabetes: a pilot cross-sectional study. Sci Rep. 2016;6:1–15.

17. Lin YCD, Huang HY, Shrestha S, Chou CH, Chen YH, Chen CR, et al. Multi-omics profiling reveals microRNA-mediated insulin signaling networks. BMC Bioinformatics. 2020;21(Suppl 13):1–19.

18. Zampetaki A, Kiechl S, Drozdov I, Willeit P, Mayr U, Prokopi M, et al. Plasma MicroRNA profiling reveals loss of endothelial MiR-126 and other MicroRNAs in type 2 diabetes. Circ Res. 2010;107(6):810–7.

19. Párrizas M, Brugnara L, Esteban Y, González-Franquesa A, Canivell S, Murillo S, et al. Circulating miR-192 and miR-193b are markers of prediabetes and are modulated by an exercise intervention. J Clin Endocrinol Metab. 2015;100(3):E407–15.

20. Garcia-Contreras M, Shah SH, Tamayo A, Robbins PD, Golberg RB, Mendez AJ, et al. Plasma-derived exosome characterization reveals a distinct microRNA signature in long duration Type 1 diabetes. Sci Rep. 2017;7(1):1–10.

21. Stępień EŁ, Durak-Kozica M, Kamińska A, Targosz-Korecka M, Libera M, Tylko G, et al. Circulating ectosomes: Determination of angiogenic microRNAs in type 2 diabetes. Theranostics. 2018;8(14):3874–90.

22. Silambarasan M, Tan JR, Karolina DS, Armugam A, Kaur C, Jeyaseelan K. MicroRNAs in Hyperglycemia Induced Endothelial Cell Dysfunction. Int J Mol Sci. 2016 Apr;17(4):518.

23. Wu JH, Gao Y, Ren AJ, Zhao SH, Zhong M, Peng YJ, et al. Altered microRNA expression profiles in retinas with diabetic retinopathy. Ophthalmic Res. 2012;47(4):195–201.

24. Fiorentino L, Cavalera M, Mavilio M, Conserva F, Menghini R, Gesualdo L, et al. Regulation of TIMP3 in diabetic nephropathy: A role for microRNAs. Acta Diabetol. 2013;50(6):965–9.

25. Chyrchel B, Drożdż A, Długosz D, Stepień EŁ, Surdacki A. Platelet reactivity and circulating platelet-derived microvesicles are differentially affected by P2Y12 receptor antagonists. Int J. Med. Sci. 2019;16(2):264-275.

26 . Wang S, Kojima K, Mobley JA, West AB. Proteomic analysis of urinary extracellular vesicles reveal biomarkers for neurologic disease. EBioMedicine. 2019;45:351–61.

27. Cheng Y, Pereira M, Raukar N, Reagan JL, Queseneberry M, Goldberg L, et al. Potential biomarkers to detect traumatic brain injury by the profiling of salivary extracellular vesicles. J Cell Physiol. 2019;234(8):14377–88.

28. Welton JL, Loveless S, Stone T, von Ruhland C, Robertson NP, Clayton A. Cerebrospinal fluid extracellular vesicle enrichment for protein biomarker discovery in neurological disease; multiple sclerosis. J Extracell Vesicles. 2017;6(1): 1369805.

29. Leiferman A, Shu J, Upadhyaya B, Cui J, Zempleni J. Storage of Extracellular Vesicles in Human Milk, and MicroRNA Profiles in Human Milk Exosomes and Infant Formulas. J Pediatr Gastroenterol Nutr. 2019;69(2):235–8.

30. Sekuła M, Janawa G, Stankiewicz E, Stepień E. Endothelial microparticle formation in moderate concentrations of homocysteine and methionine in vitro. Cell Mol Biol Lett. 2011;16(1):69–78.

31. Théry C, Witwer KW, Aikawa E, Alcaraz MJ, Anderson JD, Andriantsitohaina R, et al. Minimal information for studies of extracellular vesicles 2018 (MISEV2018): a position statement of the International Society for Extracellular Vesicles and update of the MISEV2014 guidelines. J Extracell vesicles. 2018;7(1):1535750.

32. Harding C, Heuser J, Stahl P. Receptor-mediated endocytosis of transferrin and recycling of the transferrin receptor in rat reticulocytes. J Cell Biol. 1983;97(2):329–39.

33. Huotari J, Helenius A. Endosome maturation. EMBO J. 2011;30(17):3481–500.

34. Ostrowski M, Carmo NB, Krumeich S, Fanget I, Raposo G, Savina A, et al. Rab27a and Rab27b control different steps of the exosome secretion pathway. Nat Cell. 2010;12(1):19–30.

35. Savina A, Vidal M, Colombo MI. The exosome pathway in K562 cells is regulated by Rab11. J Cell Sci. 2002;115(12):2505–15.

36. Hsu C, Morohashi Y, Yoshimura SI, Manrique-Hoyos N, Jung SY, Lauterbach MA, et al. Regulation of exosome secretion by Rab35 and its GTPase-activating proteins TBC1D10A-C. J Cell Biol. 2010;189(2):223–32.

37. Loomis RJ, Holmes DA, Elms A, Solski PA, Der CJ, Su L. Citron kinase, a RhoA effector, enhances HIV-1 virion production by modulating exocytosis. Traffic. 2006;7(12):1643–53.

38. Laulagnier K, Motta C, Hamdi S, Roy S, Fauvelle F, Pageaux JF, et al. Mast cell- and dendritic cell-derived exosomes display a specific lipid composition and an unusual membrane organization. Biochem J. 2004;380(1):161–71.

39. Quinn PJ. Plasma membrane phospholipid asymmetry. Subcell Biochem. 2002;36:39–60.

40. Scott S, Pendlebury SA, Green C. Lipid organization in erythrocyte membrane microvesicles. Biochem J. 1984;224(1):285–90.

41. Bevers EM, Comfurius P, Zwaal RFA. Changes in membrane phospholipid distribution during platelet activation. BBA - Biomembr. 1983;736(1):57–66.

42. Llorente A, Skotland T, Sylvänne T, Kauhanen D, Róg T, Orłowski A, et al. Molecular lipidomics of exosomes released by PC-3 prostate cancer cells. Biochim Biophys Acta - Mol Cell Biol Lipids. 2013;1831(7):1302–9.

43. Buschow SI, Liefhebber JMP, Wubbolts R, Stoorvogel W. Exosomes contain ubiquitinated proteins. Blood Cells, Mol Dis. 2005;35(3):398–403.

44. Katzmann DJ, Babst M, Emr SD. Ubiquitin-dependent sorting into the multivesicular body pathway requires the function of a conserved endosomal protein sorting complex, ESCRT-I. Cell. 2001;106(2):145–55.

45. Trajkovic K, Hsu C, Chiantia S, Rajendran L, Wenzel D, Wieland F, et al. Ceramide triggers budding of exosome vesicles into multivesicular endosomes. Science. 2008;319(5867):1244–7.

46. Buschow SI, Nolte-'t Hoen ENM, van Niel G, Pols MS, ten Broeke T, Lauwen M, et al. MHC II In dendritic cells is targeted to lysosomes or t cell-induced exosomes via distinct multivesicular body pathways. Traffic. 2009;10(10):1528–42.

47. Fang Y, Wu N, Gan X, Yan W, Morrell JC, Gould SJ. Higher-order oligomerization targets plasma membrane proteins and HIV Gag to exosomes. PLoS Biol. 2007;5(6):1267–83.

48. Gibbings DJ, Ciaudo C, Erhardt M, Voinnet O. Multivesicular bodies associate with components of miRNA effector complexes and modulate miRNA activity. Nat Cell Biol. 2009;11(9):1143–9.

49. Matsuo H, Chevallier J, Mayran N, Le Blanc I, Ferguson C, Fauré J, et al. Role of LBPA and Alix in Multivesicular Liposome Formation and Endosome Organization. Science. 2004;303(5657):531–4.

50. Jansen F, Yang X, Hoelscher M, Cattelan A, Schmitz T, Proebsting S, et al. Endothelial microparticle-mediated transfer of microRNA-126 promotes vascular endothelial cell repair via spred1 and is abrogated in glucose-damaged endothelial microparticles. Circulation. 2013;128(18):2026–38.

51. Wang L, Li Y, Guan X, Zhao J, Shen L, Liu J. Exosomal double-stranded DNA as a biomarker for the diagnosis and preoperative assessment of pheochromocytoma and paraganglioma. Mol Cancer. 2018;17(1):1–6.

52. Villarroya-Beltri C, Gutiérrez-Vázquez C, Sánchez-Cabo F, Pérez-Hernández D, Vázquez J, Martin-Cofreces N, et al. Sumoylated hnRNPA2B1 controls the sorting of miRNAs into exosomes through binding to specific motifs. Nat Commun. 2013;4:2980.

53. Perez-Hernandez D, Gutiérrez-Vázquez C, Jorge I, López-Martín S, Ursa A, Sánchez-Madrid F, et al. The intracellular interactome of tetraspanin-enriched microdomains reveals their function as sorting machineries toward exosomes. J Biol Chem. 2013;288(17):11649–61.

54. Shahul S,Tung A, Minhaj M, Nizamuddin J, Wenger J, Mahmood E, Mueller A,Shaefi S, Scavone B, Kociol R D, Talmor D, Rana S 2017. KRAS-MEK Signaling Controls Ago2 Sorting into Exosomes. Physiol Behav. 2017;176(10):139–48.

55. Shurtleff MJ, Temoche-Diaz MM, Karfilis K V, Ri S, Schekman R. Y-box protein 1 is required to sort microRNAs into exosomes in cells and in a cell-free reaction. Elife. 2016; 5:e19276.

56. Robbins PD, Morelli AE. Regulation of immune responses by extracellular vesicles. Nat Rev Immunol. 2014;14(3):195–208.

57. Colombo F, Bastoni M, Nigro A, Podini P, Finardi A, Casella G, et al. Cytokines Stimulate the Release of Microvesicles from Myeloid Cells Independently from the P2X7 Receptor/Acid Sphingomyelinase Pathway. Front Immunol. 2018;9:204.

58. Morel O, Jesel L, Freyssinet JM, Toti F. Cellular mechanisms underlying the formation of circulating microparticles. Arterioscler Thromb Vasc Biol. 2011;31(1):15–26.

59. Kelton JG, Warkentin TE, Hayward CPM, Murphy WG, Moore JC. Calpain activity in patients with thrombotic thrombocytopenic purpura is associated with platelet microparticles. Blood. 1992;80(9):2246–51.

60. Xu Y, Zhang Y, Wang L, Zhao R, Qiao Y, Han D, et al. MIR-200a targets Gelsolin: A novel mechanism regulating secretion of microvesicles in hepatocellular carcinoma cells. Oncol Rep. 2017;37(5):2711–9.

61. Li B, Antonyak MA, Zhang J, Cerione RA. RhoA triggers a specific signaling pathway that generates transforming microvesicles in cancer cells. Oncogene. 2012;31(45):4740–9.

62. Muralidharan-Chari V, Clancy J, Plou C, Romao M, Chavrier P, Raposo G, et al. ARF6-Regulated Shedding of Tumor Cell-Derived Plasma Membrane Microvesicles. Curr Biol. 2009;19(22):1875–85.

63. McConnell RE, Higginbotham JN, Shifrin DA, Tabb DL, Coffey RJ, Tyska MJ. The enterocyte microvillus is a vesicle-generating organelle. J Cell Biol. 2009;185(7):1285–98.

64. Van Niel G, D'Angelo G, Raposo G. Shedding light on the cell biology of extracellular vesicles. Nat Rev Mol Cell Biol. 2018;19(4):213–28.

65. Shen B, Fang Y, Wu N, Gould SJ. Biogenesis of the posterior pole is mediated by the exosome/microvesicle protein-sorting pathway. J Biol Chem. 2011;286(51):44162–76.

66. Bolukbasi MF, Mizrak A, Ozdener GB, Madlener S, Ströbel T, Erkan EP, et al. MiR-1289 and "zipcode"-like sequence enrich mRNAs in microvesicles. Mol Ther - Nucleic Acids. 2012;1(2):e10.

67. Coleman ML, Sahai EA, Yeo M, Bosch M, Dewar A, Olson MF, et al. cBioPortal cancer genomic AHR CMM1 melanoma. 2001;3:339–46.

68. Sebbagh M, Renvoizé C, Hamelin J, Riché N, Bertoglio J, Bréard J. Caspase-3-mediated cleavage of ROCK I induces MLC phosphorylation and apoptotic membrane blebbing. Nat Cell Biol. 2001;3(4):346–52.

69. Song Y, Hoang BQ, Chang DD. ROCK-II-induced membrane blebbing and chromatin condensation require actin cytoskeleton. Exp Cell Res. 2002;278(1):45–52.

70. Orlando KA, Stone NL, Pittman RN. Rho kinase regulates fragmentation and phagocytosis of apoptotic cells. Exp Cell Res. 2006;312(1):5–15.

71. Bilyy RO, Shkandina T, Tomin A, Muñoz LE, Franz S, Antonyuk V, et al. Macrophages discriminate glycosylation patterns of apoptotic cell-derived microparticles. J Biol Chem. 2012;287(1):496–503.

72. Beltramo E, Lopatina T, Berrone E, Mazzeo A, Iavello A, Camussi G, et al. Extracellular vesicles derived from mesenchymal stem cells induce features of diabetic retinopathy in vitro. Acta Diabetol. 2014 Dec;51(6):1055–64.

73. Wang X, Gu H, Huang W, Peng J, Li Y, Yang L, et al. Hsp20-Mediated Activation of Exosome Biogenesis in Cardiomyocytes Improves Cardiac Function and Angiogenesis in Diabetic Mice. Diabetes. 2016;65(10):3111–28.

74. Gasser O, Hess C, Miot S, Deon C, Sanchez JC, Schifferli JA. Characterisation and properties of ectosomes released by human polymorphonuclear neutrophils. Exp Cell Res. 2003;285(2):243–57.

75. Ayre DC, Pallegar NK, Fairbridge NA, Canuti M, Lang AS, Christian SL. Analysis of the structure, evolution, and expression of CD24, an important regulator of cell fate. Gene. 2016;590(2):324–37.

76. Tsutsui T, Kawahara H, Kimura R, Dong Y, Jiapaer S, Sabit H, et al. Glioma-derived extracellular vesicles promote tumor progression by conveying WT1. Carcinogenesis. 2020;41(9):1238–45.

77. Tripisciano C, Weiss R, Eichhorn T, Spittler A, Heuser T, Fischer MB, et al. Different Potential of Extracellular Vesicles to Support Thrombin Generation: Contributions of Phosphatidylserine, Tissue Factor, and Cellular Origin. Sci Rep. 2017;7(1):1–11.

78. Deregibus MC, Cantaluppi V, Calogero R, Iacono M Lo, Tetta C, Bruno S, et al. Angiogenic program in endothelial cells by a horizontal transfer of mRNA Endothelial progenitor cell – derived microvesicles activate an angiogenic program in endothelial cells by a horizontal transfer of mRNA. 2012;110(7):2440–8.

79. Tokarz A, Szuścik I, Kuśnierz-Cabala B, Kapusta M, Konkolewska M, Żurakowski A, et al. Extracellular vesicles participate in the transport of cytokines and angiogenic factors in diabetic patients with ocular complications. Folia Med Cracov. 2015;55(4):35–48.

80. Zhang J, Guan J, Niu X, Hu G, Guo S, Li Q, et al. Exosomes released from human induced pluripotent stem cells-derived MSCs facilitate cutaneous wound healing by promoting collagen synthesis and angiogenesis. J Transl Med. 2015;13(1):1–14.

81. Durak-Kozica M, Enguita FJ, Stępień E. Targeting uPAR in diabetic vascular pathologies. Postepy Hig Med Dosw. 2019;73:803–8.

82. Dachary-Prigent J, Pasquet JM, Fressinaud E, Toti F, Freyssinet JM, Nurden AT. Aminophospholipid exposure, microvesiculation and abnormal protein tyrosine phosphorylation in the platelets of a patient with Scott syndrome: A study using physiologic agonists and local anaesthetics. Br J Haematol. 1997;99(4):959–67.

83. Aharon A, Rebibo-Sabbah A, Tzoran I, Levin C. Extracellular Vesicles in Hematological Disorders. Rambam Maimonides Med J. 2014;5(4):e0032.

84. Ender F, Freund A, Quecke T, Steidel C, Zamzow P, von Bubnoff N, et al. Tissue factor activity on microvesicles from cancer patients. J Cancer Res Clin Oncol. 2020;146(2):467–75.

85. Mallat Z, Benamer H, Hugel B, Benessiano J, Steg PG, Freyssinet JM, et al. Elevated levels of shed membrane microparticles with procoagulant potential in the peripheral circulating blood of patients with acute coronary syndromes. Circulation. 2000;101(8):841–3.

86. Reid VL, Webster NR. Role of microparticles in sepsis. Br J Anaesth. 2012;109(4):503–13.

87. Tan KH, Tan SS, Ng MJ, Tey WS, Sim WK, Allen JC, et al. Extracellular vesicles yield predictive pre-eclampsia biomarkers. J Extracell Vesicles. 2017;6(1):1408390.

88. Lacroix R, Plawinski L, Robert S, Doeuvre L, Sabatier F, de Lizarrondo SM, et al. Leukocyte-and endothelial-derived microparticles: A circulating source for fibrinolysis. Haematologica. 2012;97(12):1864–72.

89. Brodsky S V., Malinowski K, Golightly M, Jesty J, Goligorsky MS. Plasminogen activator inhibitor-1 promotes formation of endothelial microparticles with procoagulant potential. Circulation. 2002;106(18):2372–8.

90. Sheldon H, Heikamp E, Turley H, Dragovic R, Thomas P, Oon CE, et al. New mechanism for Notch signaling to endothelium at a distance by delta-like 4 incorporation into exosomes. Blood. 2010;116(13):2385–94.

91. Taraboletti G, D'Ascenzo S, Borsotti P, Giavazzi R, Pavan A, Dolo V. Shedding of the matrix metalloproteinases MMP-2, MMP-9, and MT1-MMP as membrane vesicle-associated components by endothelial cells. Am J Pathol. 2002;160(2):673–80.

92. Lombardo G, Dentelli P, Togliatto G, Rosso A, Gili M, Gallo S, et al. Activated Stat5 trafficking Via Endothelial Cell-derived Extracellular Vesicles Controls IL-3 Pro-angiogenic Paracrine Action. Sci Rep. 2016;6(4):1–14.

93. Balkom BWM va., Jong OG d., Smits M, Brummelman J, Ouden K den, Bree PM d., et al. Endothelial cells require miR-214 to secrete exosomes that suppress senescence and induce angiogenesis in human and mouse endothelial cells. Blood. 2013;121(19):3997–4006.

94. Tokarz A, Konkolewska M, Kuśnierz-Cabala B, Maziarz B, Hanarz P, Żurakowski A, et al. Retinopathy severity correlates with RANTES concentrations and CCR 5-positive microvesicles in diabetes. Folia Med Cracov. 2019;59(3):95–112.

95. Ramakrishnan DP, Hajj-Ali RA, Chen Y, Silverstein RL. Extracellular Vesicles Activate a CD36-Dependent Signaling Pathway to Inhibit Microvascular Endothelial Cell Migration and Tube Formation. Arterioscler Thromb Vasc Biol. 2016;36(3):534–44.

96. Borges FT, Melo SA, Özdemir BC, Kato N, Revuelta I, Miller CA, et al. TGF-β1-Containing exosomes from injured epithelial cells activate fibroblasts to initiate tissue regenerative responses and fibrosis. J Am Soc Nephrol. 2013;24(3):385–92.

97. Vicencio JM, Yellon DM, Sivaraman V, Das D, Boi-Doku C, Arjun S, et al. Plasma exosomes protect the myocardium from ischemia-reperfusion injury. J Am Coll Cardiol. 2015;65(15):1525–36.

98. Shabbir A, Cox A, Rodriguez-Menocal L, Salgado M, Van Badiavas E. Mesenchymal Stem Cell Exosomes Induce Proliferation and Migration of Normal and Chronic Wound Fibroblasts, and Enhance Angiogenesis in Vitro. Stem Cells Dev. 2015;24(14):1635–47.

99. Freeman DW, Noren Hooten N, Eitan E, Green J, Mode NA, Bodogai M, et al. Altered extracellular vesicle concentration, cargo, and function in diabetes. Diabetes. 2018;67(11):2377–88.

100. Li S, Wei J, Zhang C, Li X, Meng W, Mo X, et al. Cell-Derived Microparticles in Patients with Type 2 Diabetes Mellitus: A Systematic Review and Meta-Analysis. Cell Physiol Biochem. 2016;39(6):2439–50.

101. Agouni A, Ducluzeau P-H, Benameur T, Faure S, Sladkova M, Duluc L, et al. Microparticles from Patients with Metabolic Syndrome Induce Vascular Hypo-Reactivity via Fas/Fas-Ligand Pathway in Mice. PLoS One. 2011;6(11):1–11.

102. Kamińska A, Platt M, Kasprzyk J, Kuśnierz-Cabala B, Gala-Błądzińska A, Woźnicka O, et al. Urinary Extracellular Vesicles: Potential Biomarkers of Renal Function in Diabetic Patients. J Diabetes Res. 2016:5741518.

103. Zhang Y, Mei H, Chang X, Chen F, Zhu Y, Han X. Adipocyte-derived microvesicles from obese mice induce M1 macrophage phenotype through secreted miR-155. J Mol Cell Biol. 2016;8(6):505–17.

104. Kranendonk MEG, Visseren FLJ, Van Herwaarden JA, Nolte-'t Hoen ENM, De Jager W, Wauben MHM, et al. Effect of extracellular vesicles of human adipose tissue on insulin signaling in liver and muscle cells. Obesity. 2014;22(10):2216–23.

105. Yu Y, Du H, Wei S, Feng L, Li J, Yao F, et al. Adipocyte-derived exosomal MiR-27a induces insulin resistance in skeletal muscle through repression of PPARγ. Theranostics. 2018;8(8):2171–88.

106. Cianciaruso C, Phelps EA, Pasquier M, Hamelin R, Demurtas D, Ahmed MA, et al. Primary human and rat β-Cells release the intracellular autoantigens GAD65, IA-2, and proinsulin in exosomes together with cytokine-induced enhancers of immunity. Diabetes. 2017;66(2):460–73.

107. Lakhter AJ, Pratt RE, Moore RE, Doucette KK, Maier BF, DiMeglio LA, et al. Beta cell extracellular vesicle miR-21-5p cargo is increased in response to inflammatory cytokines and serves as a biomarker of type 1 diabetes. Diabetologia. 2018;61(5):1124–34.

108. Park K. Controlled drug delivery systems: past forward and future back. J Control Release. 2014;190:3–8.

109. Luan X, Sansanaphongpricha K, Myers I, Chen H, Yuan H, Sun D. Engineering exosomes as refined biological nanoplatforms for drug delivery. Acta Pharmacol Sin. 2017;38(6):754–63.

110. Raza K, Kumar P, Kumar N, Malik R. 9 - Pharmacokinetics and biodistribution of the nanoparticles. In: Nimesh S, Chandra R, Gupta N, (eds.). Advances in Nanomedicine for the Delivery of Therapeutic Nucleic Acids. Woodhead Publishing; 2017. p. 165–86.

111. Boerman OC, Storm G, Oyen WJG, Van Bloois L, Van der Meer JWM, Claessens RAMJ, et al. Sterically stabilized liposomes labeled with Indium-111 to image focal infection. J Nucl Med. 1995;36(9):1639–44.

112. Chow TH, Lin YY, Hwang JJ, Wang HE, Tseng YL, Wang SJ, et al. Improvement of biodistribution and therapeutic index via increase of polyethylene glycol on drug-carrying liposomes in an HT-29/luc xenografted mouse model. Anticancer Res. 2009;29(6):2111–20.

113. Liu D, Yang F, Xiong F, Gu N. The smart drug delivery system and its clinical potential. Theranostics. 2016;6(9):1306–23.

114. Clayton A, Harris CL, Court J, Mason MD, Morgan BP. Antigen-presenting cell exosomes are protected from complement-mediated lysis by expression of CD55 and CD59. Eur J Immunol. 2003;33(2):522–31.

115. Pascucci L, Coccè V, Bonomi A, Ami D, Ceccarelli P, Ciusani E, et al. Paclitaxel is incorporated by mesenchymal stromal cells and released in exosomes that inhibit in vitro tumor growth: A new approach for drug delivery. J Control Release. 2014;192:262–70.

116. Zhang Y, Liu D, Chen X, Li J, Li L, Bian Z, et al. Secreted Monocytic miR-150 Enhances Targeted Endothelial Cell Migration. Mol Cell. 2010;39(1):133–44.

117. Fuhrmann G, Serio A, Mazo M, Nair R, Stevens MM. Active loading into extracellular vesicles significantly improves the cellular uptake and photodynamic effect of porphyrins. J Control Release. 2015;205:35–44.

118. Sun D, Zhuang X, Xiang X, Liu Y, Zhang S, Liu C, et al. A novel nanoparticle drug delivery system: The anti-inflammatory activity of curcumin is enhanced when encapsulated in exosomes. Mol Ther. 2010;18(9):1606–14.

119. Tian Y, Li S, Song J, Ji T, Zhu M, Anderson GJ, et al. A doxorubicin delivery platform using engineered natural membrane vesicle exosomes for targeted tumor therapy. Biomaterials. 2014;35(7):2383–90.

120. Yoon J, Jo W, Jeong D, Kim J, Jeong H, Park J. Generation of nanovesicles with sliced cellular membrane fragments for exogenous material delivery. Biomaterials. 2015;59:12–20.

121. Jang SC, Kim OY, Yoon CM, Choi DS, Roh TY, Park J, et al. Bioinspired exosome-mimetic nanovesicles for targeted delivery of chemotherapeutics to malignant tumors. ACS Nano. 2013;7(9):7698–710.

122. Sato YT, Umezaki K, Sawada S, Mukai SA, Sasaki Y, Harada N, et al. Engineering hybrid exosomes by membrane fusion with liposomes. Sci Rep. 2016;6(February):1–11.

123. Piffoux M, Silva AKA, Wilhelm C, Gazeau F, Tareste D. Modification of Extracellular Vesicles by Fusion with Liposomes for the Design of Personalized Biogenic Drug Delivery Systems. ACS Nano. 2018;12(7):6830–42.

124. Rana S, Yue S, Stadel D, Zöller M. Toward tailored exosomes: The exosomal tetraspanin web contributes to target cell selection. Int J Biochem Cell Biol. 2012;44(9):1574–84.

125. Munagala R, Aqil F, Jeyabalan J, Gupta RC. Bovine milk-derived exosomes for drug delivery. Cancer Lett. 2016;371(1):48–61.

126. Smyth T, Petrova K, Payton NM, Persaud I, Redzic JS, Graner MW, et al. Surface functionalization of exosomes using click chemistry. Bioconjug Chem. 2014;25(10):1777–84.

127. Drożdż A, Kamińska A, Surman M, Gonet-Surówka A, Jach R, Huras H, et al. Low-vacuum filtration as an alternative extracellular vesicle concentration method: A comparison with ultracentrifugation and differential centrifugation. Pharmaceutics. 2020;12(9):1–17.

128. Record M, Carayon K, Poirot M, Silvente-Poirot S. Exosomes as new vesicular lipid transporters involved in cell-cell communication and various pathophysiologies. Biochim Biophys Acta - Mol Cell Biol Lipids. 2014;1841(1):108–20.

129. Phuyal S, Skotland T, Hessvik NP, Simolin H, Øverbye A, Brech A, et al. The ether lipid precursor hexadecylglycerol stimulates the release and changes the composition of exosomes derived from PC-3 cells. J Biol Chem. 2015;290(7):4225–37.

130. Wubbolts R, Leckie RS, Veenhuizen PTM, Schwarzmann G, Möbius W, Hoernschemeyer J, et al. Proteomic and biochemical analyses of human B cell-derived exosomes: Potential implications for their function and multivesicular body formation. J Biol Chem. 2003;278(13):10963–72.

131. Vidal M, Sainte-Marie J, Philippot JR, Bienvenue A. Asymmetric distribution of phospholipids in the membrane of vesicles released during in vitro maturation of guinea pig reticulocytes: Evidence precluding a role for “aminophospholipid translocase.” J Cell Physiol. 1989;140(3):455–62.

132. Brouwers JF, Aalberts M, Jansen JWA, van Niel G, Wauben MH, Stout TAE, et al. Distinct lipid compositions of two types of human prostasomes. Proteomics. 2013;13(10–11):1660–6.

133. Skotland T, Ekroos K, Kauhanen D, Simolin H, Seierstad T, Berge V, et al. Molecular lipid species in urinary exosomes as potential prostate cancer biomarkers. Eur J Cancer. 2017;70:122–32.

134. Pienimaeki-Roemer A, Kuhlmann K, Böttcher A, Konovalova T, Black A, Orsõ E, et al. Lipidomic and proteomic characterization of platelet extracellular vesicle subfractions from senescent platelets. Transfusion. 2015;55(3):507–21.

135. Surman M, Drożdż A, Stępień E, Przybyło M. Extracellular Vesicles as Drug Delivery Systems - Methods of Production and Potential Therapeutic Applications. Curr Pharm Des. 2019;25(2):132–54.

136. Zhang Y, Li H, Sun J, Gao W, Liu W, Li B, et al. DC-Chol/DOPE cationic liposomes: A comparative study of the influence factors on plasmid pDNA and siRNA gene delivery. Int J Pharm. 2010;390(2):198–207.

137. Meyer O, Kirpotin D, Hong K, Sternberg B, Park JW, Woodle MC, et al. Cationic liposomes coated with polyethylene glycol as carriers for oligonucleotides. J Biol Chem. 1998;273(25):15621–7.

138. Chan C-L, Majzoub RN, Shirazi RS, Ewert KK, Chen Y-J, Liang KS, et al. Endosomal escape and transfection efficiency of PEGylated cationic liposome-DNA complexes prepared with an acid-labile PEG-lipid. Biomaterials. 2012 Jun;33(19):4928–35.

139. Gui B, Hsieh C-L, Kantoff PW, Kibel AS, Jia L. Androgen receptor-mediated downregulation of microRNA-221 and -222 in castration-resistant prostate cancer. PLoS One. 2017;12(9):1–15.

140. Griffiths-Jones S, Saini HK, van Dongen S, Enright AJ. miRBase: tools for microRNA genomics. Nucleic Acids Res. 2008 Jan 1;36(suppl_1):D154–8. Date of access: 15.04.20121

141.RNAcentral 2021: secondary structure integration, improved sequence search and new member databases. Nucleic Acids Res. 2021 Jan;49(D1):D212–20. Date of access: 15.04.2021].

142. Sriwongsitanont S, Ueno M. Effect of Freeze-Thawing Process on the Size and Lamellarity of PEG-Lipid Liposomes. Open Colloid Sci J. 2011;2(4):1–6.

143. Litschel T, Ganzinger KA, Movinkel T, Heymann M. Freeze-thaw cycles induce content exchange between cell-sized lipid vesicles Freeze-thaw cycles induce content exchange between cell-sized lipid vesicles. New J Phys. 2018;20: 055008.

144. Auerbach R, Quertermous T, Quertermous EE, Kawana M, Hidai C, Hogan BLM, et al. Cloning and characterization of developmental endothelial locus-1: An embryonic endothelial cell protein that binds the alpha vbeta 3 integrin receptor. Genes Dev. 2008;12(1):21–33.

145. Dasgupta SK, Le A, Chavakis T, Rumbaut RE, Thiagarajan P. Developmental endothelial locus-1 (del-1) mediates clearance of platelet microparticles by the endothelium. Circulation. 2012;125(13):1664–72.

146. Jaffé HH, Miller AL. The fates of electronic excitation energy. J Chem Educ. 1966;43(9):469–73.

147. Förster T, Zwischenmolekulare Energiewanderung und Fluoreszenz, Ann. Phys. 1948; 437 (2), 55- 75.

148. Skruzny M, Pohl E, Abella M. FRET microscopy in yeast. Biosensors. 2019;9(4):1–17.

149. Medintz I, Hildebrandt N, editors. FRET – Förster Resonance Energy Transfer: From theory to applications. Weinheim: Wiley-VCH Verlag GmbH; 2014. p. 23-42.

150. Hussain SA, Chakraborty S, Bhattacharjee D, Schoonheydt RA. Fluorescence Resonance Energy Transfer between organic dyes adsorbed onto nano-clay and Langmuir–Blodgett (LB) films. Spectrochim Acta Part A Mol Biomol Spectrosc. 2010;75(2):664–70.

151. Zhu Z, Jin Y, Zhang D, Minhas JK, Lee H. Enrichment of selective miRNAs in exosomes and delivery of exosomal miRNAs in vitro and in vivo. Am J Physiol Cell Mol Physiol. 2016;312(1):L110–21.

152. Simonsen JB. Pitfalls associated with lipophilic fluorophore staining of extracellular vesicles for uptake studies. J Extracell Vesicles. 2019;8(1):1582237.

153. Toth M, Fridman R. Assessment of Gelatinases (MMP-2 and MMP-9) by Gelatin Zymography. Methods Mol Med. 2001;57:163-174.

154. Frankowski H, Gu Y-H, Heo JH, Milner R, Del Zoppo GJ. Use of gel zymography to examine matrix metalloproteinase (gelatinase) expression in brain tissue or in primary glial cultures. Methods Mol Biol. 2012;814:221–33.

155. Faneca H, Cardoso AL, Trabulo S, Duarte S, de Lima MCP. Cationic Liposome-Based Systems for Nucleic Acid Delivery: From the Formulation Development to Therapeutic Applications. In: Coelho J, (edr). Drug Delivery Systems: Advanced Technologies Potentially Applicable in Personalised Treatment. Dordrecht: Springer Netherlands; 2013. p. 153–84.

156. Thomas CE, Ehrhardt A, Kay MA. Progress and problems with the use of viral vectors for gene therapy. Nat Rev Genet. 2003;4(5):346–58.

157. Lechanteur A, Sanna V, Duchemin A, Evrard B, Mottet D, Piel G. Cationic liposomes carrying siRNA: Impact of lipid composition on physicochemical properties, cytotoxicity and endosomal escape. Nanomaterials. 2018;8(5):270.

158. Elsharkasy OM, Nordin JZ, Hagey DW, de Jong OG, Schiffelers RM, Andaloussi S EL, et al. Extracellular vesicles as drug delivery systems: Why and how? Adv Drug Deliv Rev. 2020;159:332–43.

159. Beloribi S, Ristorcelli E, Breuzard G, Silvy F, Bertrand-Michel J, Beraud E, et al. Exosomal Lipids Impact Notch Signaling and Induce Death of Human Pancreatic Tumoral SOJ-6 Cells. PLoS One. 2012;7(10):e47480.

160. Lu M, Zhao X, Xing H, Xun Z, Zhu S, Lang L, et al. Comparison of exosome-mimicking liposomes with conventional liposomes for intracellular delivery of siRNA. Int J Pharm. 2018;550(1–2):100–13.

161. Rayamajhi S, Duong T, Nguyen T, Marasini R, Aryal S. Macrophage-derived exosome-mimetic hybrid vesicles for tumor targeted drug delivery. Acta Biomater. 2019;94:482–94.

162. Romøren K, Thu BJ, Bols NC, Evensen Ø. Transfection efficiency and cytotoxicity of cationic liposomes in salmonid cell lines of hepatocyte and macrophage origin. Biochim Biophys Acta. 2004;1663(1–2):127–34.

163. Fan D, Kassiri Z, Grant G. Biology of Tissue Inhibitor of Metalloproteinase 3 (TIMP3), and Its Therapeutic Implications in Cardiovascular Pathology. Front Physiol. 2020;11(June):1–16.

164. Liu H, Li X, Wu N, Tong M, Chen S, Zhu S, et al. Serum microRNA-221 as a biomarker for diabetic retinopathy in patients associated with type 2 diabetes. Int J Ophthalmol. 2018;11(12):1889–94.

165. Li Y, Song Y-H, Li F, Yang T, Lu YW, Geng Y-J. MicroRNA-221 regulates high glucose-induced endothelial dysfunction. Biochem Biophys Res Commun. 2009 Mar;381(1):81–3.

166. Cardellini M, Menghini R, Martelli E, Casagrande V, Marino A, Rizza S, et al. TIMP3 is reduced in atherosclerotic plaques from subjects with type 2 diabetes and increased by SirT1. Diabetes. 2009;58(10):2396–401.

167. Wang C, Lin Y, Fu Y, Zhang D, Xin Y. MiR-221-3p regulates the microvascular dysfunction in diabetic retinopathy by targeting TIMP3. Pflugers Arch. 2020;472(11):1607–18.

168. Barth JL, Yu Y, Song W, Lu K, Dashti A. Oxidised , glycated LDL selectively influences tissue inhibitor of metalloproteinase-3 gene expression and protein production in human retinal capillary pericytes. Diabetologia. 2007;50(10):2200–8.

169. Zhang W, Peng F, Zhou T, Huang Y, Zhang L, Ye P, et al. Targeted delivery of chemically modified anti-miR-221 to hepatocellular carcinoma with negatively charged liposomes. Int J Nanomedicine. 2015;10:4825–36.

170. Gan R, Yang Y, Yang X, Zhao L, Lu J, Meng QH. Downregulation of miR-221/222 enhances sensitivity of breast cancer cells to tamoxifen through upregulation of TIMP3. Cancer Gene Ther. 2014;21(7):290–6.

171. Dolo V, Ginestra A, Cassare D, Violini S, Lucania G, Torrisi MR, et al. Selective Localization of Matrix Metalloproteinase Lymphocyte Antigen Class I Molecules on

Membrane Vesicles Shed by 8701-BC Breast Carcinoma Cells1. Cancer Res. 1998;58(19):4468–74.

172. Liu Y, Min D, Bolton T, Nubé V, Twigg SM, Yue DK, et al. Increased Matrix Metalloproteinase-9 Predicts Poor Wound Healing in Diabetic Foot Ulcers. Diabetes Care. 2009;32(1):117–9.

173. Menghini R, Uccioli L, Vainieri E, Pecchioli C, Casagrande V, Stoehr R, et al. Expression of tissue inhibitor of metalloprotease 3 is reduced in ischemic but not neuropathic ulcers from patients with type 2 diabetes mellitus. Acta Diabetol. 2013;50(6):907–10.

174. Yan Y, Xu Y, Ni G, Wang S, Li X, Gao J, et al. MicroRNA-221 promotes proliferation and migration of pulmonary arterial smooth muscle cells (PASMCs) by targeting tissue inhibitor of metalloproteinases-3 (TIMP3). Cardiovasc Diagn Ther. 2020;3(4):646–57.